uOttawa

L'Université canadienne
Canada's university

FACULTÉ DES ÉTUDES SUPÉRIEURES ET POSTOCTORALES

uOttawa

L'Université canadienne
Canada's university

FACULTY OF GRADUATE AND POSDOCTORAL STUDIES

Alsdeg Alsari
AUTEUR DE LA THÈSE / AUTHOR OF THESIS

Ph.D. (Chemical Engineering)
GRADE / DEGREE

Department of Chemical Engineering
FACULTÉ, ÉCOLE, DÉPARTEMENT / FACULTY, SCHOOL, DEPARTMENT

Effect of Air Pressure on Gas Transport Properties and Physical Aging of Poly(Phenyleneoxide) (PPO) Membranes

TITRE DE LA THÈSE / TITLE OF THESIS

Takeshi Matsuura
DIRECTEUR (DIRECTRICE) DE LA THÈSE / THESIS SUPERVISOR

CO-DIRECTEUR (CO-DIRECTRICE) DE LA THÈSE / THESIS CO-SUPERVISOR

EXAMINATEURS (EXAMINATRICES) DE LA THÈSE / THESIS EXAMINERS

Pierre Côté

Jason Zhang

Christopher Lan (absent)

André Tremblay

Gary W. Slater
Le Doyen de la Faculté des études supérieures et postdoctorales / Dean of the Faculty of Graduate and Postdoctoral Studies

Effect of Air Pressure on Gas Transport Properties and Physical Aging of Poly(Phenyleneoxide) (PPO) Membranes

BY

Alsdeg Mohamad Alsari

Dissertation submitted to the Chemical engineering Department in partial fulfillment of the requirements for the degree of

DOCTOR OF PHILOSOPHY
In the Department of Chemical Engineering
University of Ottawa

2007

Your file Votre référence
ISBN: 978-0-494-41625-9
Our file Notre référence
ISBN: 978-0-494-41625-9

Abstract

The objective of this research work is to understand the molecular mechanism involved in physical aging of amorphous glassy polymers. Free volume and segmental mobility arguments are commonly used to explain both the gas transport process and the physical aging of glassy polymers. Hence, gas permeation through glassy polymeric membranes is considered as an attractive tool to detect any time dependent changes of polymer free volume. Especially, emphasis is placed, in this work, on determining whether or not an experimental routine affects the time dependent changes of glassy polymeric membranes.

In the first part (Chapter 5), permeability data of oxygen and nitrogen were obtained from air permeation experiments under different pressures using dense polyphenylene oxide (PPO) membranes of different thicknesses, after the membranes were almost fully stabilized. Opposite trends were observed with respect to oxygen and nitrogen as their permeabilities changed with changes in feed pressure and membrane thickness. Moreover, the pressure effect on oxygen permeability was reversed when the membrane was flipped upside down. Attempts were made to interpret the above experimental observations within a framework of entropy and enthalpy effect on the energy barrier for gas permeation and the change in void space in the cross-sectional direction of a dense PPO membrane.

In the second part (Chapter 6), resemblance of aging curves of gas separation membranes to visco-elastic response curves was observed for all the studied membranes. Membrane aging curves consist of elastic and viscous components. It was further concluded that the elastic component of polymer relaxation was enhanced when membranes were aged at lower pressures while the viscous component was

enhanced at higher gas pressures. The transition from the elasticity dominant to the viscosity dominant region occurred more quickly for thicker membranes

In the third part (Chapter 7), the effect of gas pressure on membrane aging was studied thoroughly by applying feed gas pressure continuously or by reducing the feed gas pressure intermittently. The effect of pressure on the physical aging of PPO membranes was demonstrated by monitoring the time dependence of the permeability and selectivity of the membranes. In general, gas pressure decelerated the physical aging process, especially in earlier stages of the membrane life. Also, the aging of thin membranes is greater than the aging of thick membranes, under all applied gas pressures. In some experiments, anti-trade-off effect, i.e. the decrease in the selectivity together with the decrease in permeability, was observed. A plausible explanation was proposed based on a dual gas permeation model.

Résumé

L'objectif de ce travail de recherches est de comprendre le mécanisme moléculaire mécanisme dans le vieillissement physique des polymères vitreux amorphes. Le volume libre et les arguments segmentaires de mobilité sont généralement employés pour expliquer tous les deux le procédé de transport de gaz et le vieillissement physique des polymères vitreux. Par conséquent, la perméation de gaz par les membranes polymères vitreuses est considérée pendant qu'un outil attrayant pour détecter les changements n'importe quand dépendants du polymère libèrent le volume. En particulier, l'accent est mis, dans ce travail, sur déterminer si une routine expérimentale affecte les changements dépendants de temps des membranes polymères vitreuses.

Dans la première partie (le chapitre 5), les données de perméabilité de l'oxygène et l'azote ont été obtenus à partir des expériences de perméation d'air sous différentes pressions à l'aide des membranes denses de l'oxyde de polyphénylène (PPO) de différentes épaisseurs, après que les membranes aient été presque entièrement stabilisées. On a observé des tendances opposées en ce qui concerne l'oxygène et l'azote comme leurs permeabilities changés avec des changements de pression d'alimentation et d'épaisseur de membrane. D'ailleurs, l'effet de pression sur la perméabilité à l'oxygène a été renversé quand la membrane était à l'envers renversé. Des tentatives ont été faites d'interpréter les observations expérimentales ci-dessus dans un cadre d'entropie et d'effet d'enthalpie sur la barrière d'énergie pour la perméation de gaz et du changement de l'espace vide dans la direction en coupe d'une membrane dense de PPO.

Dans la deuxième partie (on a observé le chapitre 6), ressemblance des courbes de vieillissement des membranes de séparation de gaz aux courbes de réponse visco-élastiques pour toutes les membranes étudiées. Les courbes de vieillissement de membrane se composent des composants élastiques et visqueux. On l'a encore conclu que le composant élastique de la relaxation de polymère a été augmenté quand des membranes ont été vieillies à de plus basses pressions tandis que le composant visqueux était augmenté à des pressions de gaz plus élevées. La transition de l'élasticité dominante à la région dominante de viscosité s'est produite plus rapidement pour des membranes plus épaisses.

Dans la troisième partie (le chapitre 7), l'effet de la pression de gaz sur le vieillissement de membrane a été étudié complètement en appliquant la pression de gaz d'alimentation sans interruption ou en réduisant la pression de gaz d'alimentation par intermittence. L'effet de la pression sur le vieillissement physique des membranes de PPO a été démontré en surveillant la dépendance de temps de la perméabilité et de la sélectivité des membranes. En général, la pression de gaz a ralenti le processus physique de vieillissement, particulièrement aux premières parties de la vie de membrane. En outre, le vieillissement des membranes minces est plus grand que le vieillissement des membranes épaisses, sous toutes les pressions de gaz appliquées. Quelques expériences, anti-commercez-au loin l'effet, c.-à-d. la diminution de la sélectivité ainsi que la diminution de la perméabilité, a été observée. On a proposé une explication plausible a basé sur un modèle duel de perméation de gaz.

ACKNOWLEDGMENTS

I would like to express my sincere thanks to the many individuals who helped me through my stay at University of Ottawa:

First and foremost, my advisor, Prof. T. Matsuura for his supervision and guidance and long hours he spent on the dissertation;

to the colleagues in my lab, for their patience and friendship;

to the friends of mine, who believed in me all the way;

to my brothers and sisters, for their unlimited support;

and to my wife and parents for their blessings.

Table of Contents:

List of tables:

List of Figures:

Symbols

A	Permeation area of the film (m^2)
A_i	Gas peak area
B	Hole affinity constant (1/Pa in SI system)
C	Concentration of a gas in polymer (mol/m^3)
C_D	Concentration in the Henry type-sites (mol/m^3)
C_H	Concentration in the Langmuir sites (mol/m^3)
C_H'	Hole saturation constant (mol/m^3 in)
CED	Cohesive energy density of the polymer (J/m^3)
D	Diffusion coefficient (m^2/s)
D_o	Exponential factor (m^2/s)
D_D	Diffusivity coefficients in Henry environment (m^2/s)
D_g	Diffusion coefficient for free volume holes at $f = f_g$ (m^2/s)
D_H	Diffusivity coefficients Langmuir environments (m^2/s)
D_k	Kinetic diameter of penetrant (m)
(dv_f/dt)	Rate of change in the free volume
E_d	Activation energy (J/mol)
f	Fractional free volume (-)
f_g	Bulk fractional free volume (-)
f_i	Initial fractional free volume (-)
$(f_i - f_D)$	Reduction in fractional free volume due to diffusion (-)
$(f_i - f_{LC})$	Reduction in fractional free volume due to lattice contraction (-)
H_s	Enthalpy of solution (J/mol)
H_t	Enthalpy at some time t (J/mol)
H_∞	Equilibrium enthalpy (J/mol)
L	Film thickness (m)
M	Segmental mobility of polymer chains
P	Permeability (Barrer = 10^{-10} cm^3 (STP) cm/cm^2 s cmHg)
P	Gas partial pressure (Pa)
p_g	Glass transition pressure (Pa in SI system)
Q	Steady state permeation rate (mol/s)
Q_{O_2}, Q_{N_2},	Permeate flow rate of O_2 and N_2 (mol/s)

$\dot{Q}'_{CH_4}$	Sweep flow rate of CH_4 (mol/s)
Q'	Apparent flow rate (mol/s)
R	Universal gas constant
S	Solubility coefficient factor (mol/m^3 Pa)
S	Henry's solubility constant (mol/m^3 Pa)
S_0	Pre-exponential factors (mol/m^3 Pa)
T	Absolute temperature (K)
T_m	Melting temperature (K)
T_g	Glass transition temperature (K)
V	Permeate side volume (m^3)
v_f	Free volume of the polymer (m^3)
v	Specific volume of polymer (m^3/kg)
v_o	Volume occupied by polymer chains (m^3)
t	Aging time (s)
x_i	Mole fraction of component i (-)
Z	Material constant (-)
ΔG	Difference of Gibbs free energy (J/mol)
ΔH	Differences of activation enthalpy (J/mol)
Δp	Pressure gradient across the film (Pa)
$\Delta S^{\pm}_{A,B}$	Differences of entropy (J/mol K)
α	Selectivity (-)
α_D	Diffusivity selectivity (-)
α_S	Solubility selectivity (-)
β_V	Volume relaxation rate (-)
β_H	Enthalpy relaxation rate (J/s in SI system)
M	Struik shift factor
δ	Relative departure from equilibrium (-)
δ_H	Excess enthalpy (J/mol)
λ_d	Jump length (m)
τ	Material relaxation time (s)

Abbreviations:

AFM	Atomic force microscopy
C-P	Constant pressure-variable volume
C-V	Constant volume-variable pressure
DSC	Differential scanning calorimetry
DMA	Dynamic mechanical analysis
F	Feed gas stream
FFV	Fraction free volume
GC	Gas chromatograph
MFC	Mass flow controller
MFM	Mass flow meter
MSV	Multi position valve
NV	Needle valve
PMP	Poly(4-methyl-2-pentyne)
PPO	Poly(2,6-dimethyl-1,4-phenylene oxide)
PPPO	Poly phenyl phenylene oxide
PS	Permeate and sweep stream
PT	Pressure transducer
PTMSP	Poly[1(trimethylsilyl)-1-propyne]
PVC	Polyvinyl chloride
PVT	Pressure, Volume, Temperature
R	Retentate stream
S	Sweep gas stream
TC	Thermocouple
TCD	Thermal conductivity detector
TCE	Trichloroethylene
TRF	Thermal response factor

Contributions

By the time this thesis submitted to the faculty of graduate studies, two journal papers have been published in the journal of Separation Science and Technology:

(1) **"Effect of Pressure and Membrane Thickness on the Permeability of Gases in Dense Polyphenylene Oxide (PPO) Membranes: Thermodynamic Interpretation"** Alsdeg Alsari; Boguslaw Kruczek; T. Matsuura Separation Science and Technology, Volume 42, Issue 10 January 2007 , pages 2143 - 2155

(2) **"Effect of Pressure on the Aging of Dense (PPO) Membranes"** Alsdeg Alsari; B. Kruczek; T. Matsuura Separation Science and Technology, Volume 42, Issue 12 September 2007 , pages 2567 - 2582

CHAPTER 1

Introduction

1.1 Introduction

Applications employing polymeric membranes range from production of pure gases to barrier protection against environmental effects in food industry. Their vast range of applications is a result of their durability, which in part is due to wide range of physical and chemical properties. In the field of gas separation, because of their simplicity and energy efficiency, membrane processes are a very attractive competitor to traditional established separation processes. Despite the fact that membranes have made many inroads in the field of gas separation, their market share in comparison with other competing technologies such as cryogenic distillation, absorption and pressure swing adsorption is rather limited. Moreover, the number of commercial applications of gas separation membranes is quite low in comparison with applications of reverse osmosis, ultrafiltration, and microfiltration membranes. One could use different arguments to

explain this definite underachievement of membrane gas separation. However, it appears that one of the reasons is the difficulty in predictability of membrane permeability.

Transport properties of gas separation membranes are affected by physical aging, which is a phenomenon that is common for all amorphous glassy materials. Physical aging affects all material properties that are related to the free volume by decreasing the free volume and hindering the segmental movement. The deterioration of permselective properties that is induced by the time dependent changes in the membrane physical properties, makes it more difficult to anticipate the life and performance of the used membrane. Therefore, it is important to understand the aging phenomena in order to predict the life service of gas separation membranes.

The phenomena of physical aging and gas diffusion in glassy polymers are not fully understood or explained. Both phenomena are explained using similar theories with specific modifications to these theories in each case. These theories and their facilitation in each case can namely fall into three categories, which are modifications of the free volume molecular theory:

(1) The "hole" vacancy theory, where the gas molecules are absorbed and diffuse through the polymer matrix. In the case of physical aging, diffusion of the same holes is believed to take place (free volume diffusion).

(2) The activation theory, which was developed on the assertion that gas molecules should overcome interchain energy. The same interchain energy is believed to be the driving force towards equilibrium in glassy polymers. Therefore, the energy of the gas molecule should be higher than the attraction energy between segments

for the diffusion to take place; and the segmental attraction energy should be higher for aging to occur.

(3) The fluctuation theory, which based on the thermal fluctuation of polymer segments, permits the passing of gas molecules. On the other hand, the segmental (movement) fluctuation is considered a driving force for physical aging.

Free volume as a concept has been of a great value for explaining gas separation and physical aging. Emerging aspects, from one phenomenon, are likely to help in a better understanding of the other. Any trial that tends to explain aging of glassy polymeric membranes should rely on real time experiments, where pressure, gas mixtures, and changes in selectivity values should be considered. The gas permeation through glassy polymeric membranes has been used as a tool to prove that the changes occur because of aging, while no advantage was taken of the knowledge of aging phenomena for better understanding of gas permeation phenomena. The gas permeation through polymeric membranes is usually treated in the physical aging study as a sieving process. Hence, the resistance to the permeation of gas molecules increases with physical aging. This effect is more on the molecules of the larger size, resulting in higher selectivity. The experiments with gas mixtures were rarely used in the study of physical aging since the selectivity is usually expected to decline in the gas mixture due to the interaction between the penetrating gases. Therefore, the selectivity is mostly calculated from single gases permeation data. In other words, separation data have never been employed in explaining or modeling the time dependent change of the gas permeability.

Applying pressure on the polymer membrane should result in volume decrease by pressing the polymer segments closer to each other and pushing the holes out of the bulk. In the related fields of reverse osmosis, ultrafiltration and microfiltration a decrease in membrane productivity with time is attributed to mechanical compaction of membranes. Mechanical compaction results from the high-pressure gradient to which membranes are exposed during separation applications. These membranes are porous membranes and the liquid passes from one side of the membrane to the other through pores in between the polymer material (Persson et al., 1994). Also, the lattice contraction mechanism, before it was extended to glassy polymers, was developed for volume changes in liquids due to pressure change. The presence of gas molecules in the polymer network is believed to decelerate the aging process (Struik, 1978). It is believed that gas molecules restrict the segmental movement responsible for the aging mechanism. A glassy polymeric membrane prepared in atmospheric environment should contain air in its free volume. Unless the size of the permeating gas matters, replacing the air with another gas should not decelerate the aging process compared to aging in atmospheric environment. Teimblo et al. 2000, found that, larger molecules decelerate aging more than smaller ones. Besides, the free volume is estimated by permeability but not every gas can have access to all the free volumes. Therefore, the permeability measurement does not necessarily allow complete estimation of the lost free volume. On the other hand, when the membrane is subjected to vacuum, the resistance for the movement of all gas molecules is decreased, which will cause faster aging for any gases. The hydrostatic pressure on the membrane surface might cause closeness in between the polymer segments that could result in lower

aging rate; but the gas molecules pressure inside the membrane should work in opposite direction.

The morphology of the used membranes has a very important effect on the gas transport and selectivity properties. However, only the thickness of the studied samples was considered as a factor for aging. Aging accelerates faster in thin films. Future studies should consider other features of morphology like symmetric versus asymmetric, and dense versus porous. It is important to emphasize that all practical membranes have generally asymmetric structures consisting of selective skin layer and porous sub-layer providing mechanical support for the skin layer. According to Koros and Chern (1987) the drift in membrane productivity, under applied pressure, can be either due to the compaction of the open cell of the support layer or the densification of the glassy polymeric material in the top layer, or both of them. Accordingly, the phenomenon of physical aging is generally associated with the skin layer, while mechanical compaction with the porous sub-layer. They both however lead to the decrease in free volume of membrane. Similar to physical aging, mechanical compaction does not alter membrane chemistry and also results in a decrease in T_g of the polymer (Chow, 1984). Consequently, although the phenomenon of physical aging has not yet been linked with mechanical compaction of membranes, it is postulated that what is known, as mechanical compaction, could be another mechanism contributing to physical aging of glassy films.

The above discussion leads to an important speculation that is, the effect of pressure on permselective properties of thin films should be different from its effect on thick films. At some point permeability of thick films will decrease, due to compaction of the sublayer, with no or very small change in selectivity. On the other hand, any change

in permeability in thin films should be coupled with more pronounced change in selectivity than in thick films. That is because, thin films are more symmetric and the change in morphology will affect the dense layer.

The effect of the experimental protocol, which is part of the history of the examined membrane, was considered briefly, and no conclusion or serious discussion was drawn from these trials. Gas permeation measurements on PPO membranes carried out in different set ups proved to result in different permeability and selectivity data (Kruczek and Matsuura, 2000). The literature has presented works that deal with the problem of physical aging in glassy polymers, but not in glassy polymeric membranes under facilitating conditions. Some works deal with thin films used gases permeability to prove the time dependent change in the free volume. In these previous works, membranes were aged in vacuum environment and separation and permeation data were evaluated from single gases permeation. Moreover, the pressure gradients applied to measure gas permeation rates were generally low. For example, Dorkenoo and Pfromm measured gas permeation rates under just 2 psia (1999 & 2000). These are not the practical operating conditions of a membrane separation process, and following this scenario in studying physical aging cannot evaluate the performance of the polymer during its anticipated service life, unless the operating conditions are considered ineffective.

The effect of vacuum, which is facilitated in the constant volume system, was never considered as a factor accelerating the aging rate. Opposite to the presence of gas molecules, vacuum results in more free chain movement and less gas resistance, and aging in vacuum should be, even, faster than aging in atmospheric pressure. McCaig et al, 2000, considered the middle plane between the film's both surfaces as the starting point

for free volume diffusion. This assumption is valid for their experimental routine, where membranes were aged, in most of their aging time, under vacuum. This assumption will be questioned in continuous measurement in constant volume system, where the vacuum is applied to the permeate side only, and the feed side is subjected to the gas feed pressure. The same argument can be applied for the constant pressure system.

Finally, membrane separation and permeation characteristics for a particular mixed gas system, is typically calculated from single-component transport parameters. Therefore, estimation of free volume change with time is also carried out using single gases. This technique raised question in the 90s that, it might lead to erroneous estimates of the membrane separation efficiency. Taking into consideration the fact that aging is monitored by relating the free volume to the membrane permeability, the same concern could be raised when it comes to quantifying physical aging of glassy polymers. Even if attempts to study the true transport phenomena during mixed gas permeation through membranes have been successfully carried out, aging was rarely considered with mixtures. And what is more deceiving is the evaluation of the separation factors from single gas measurements. Most of the aging studies resulted in an increase in separation factor, but there are also other studies involving polyethersulfone (PES) hollow fiber membranes where the selectivity decreased. The difficulty in explaining the reason behind these changes was due to lack of understanding of physical aging phenomena and gas permeation in glassy polymers.

1.2 Motivations and Objectives

1.2.1 Motivations

(1) The motivation of any work concerning membranes is their potential as a better alternative to traditional separation processes. A lot of research has been carried out on glassy polymers as membranes material due to their favorable separation properties. However, their physical properties change with time, altering a full characterization of their gas transport and separation properties. Although the amount of research on the effect of these changes on mechanical properties is large, the amount is considerably smaller for their effect on gas permeation.

(2) The gas transport properties of a polymer, is a very sensitive tool to be used for studying physical aging. It allows continuous monitoring of changes in free volume change with time, in a glassy polymer. Also, both physical aging and diffusivity of a gas in glassy polymers are explained using the concept of free volume theory.

(3) The effect of physical aging on gas permeation and separation properties of polymers will be better understood on the realization that segmental movement is the main feature that governs diffusion in glassy polymers.

(4) In pressure driven membrane separation processes, including membrane gas separation, membranes are usually exposed to a steep time-dependent pressure gradient. At such conditions the influence of the applied pressure gradient on the kinetics of physical aging is warranted. For example, Deng and Jean (1993), who studied free volume distribution in glassy polymers by positron annihilation, showed very strong dependence of the average size and size distribution of free

volume holes on the applied pressure (1993). Moreover, the applied pressure affects mobility of polymeric chains, and the glass transition can also be realized by isothermal pressurization of a rubbery sample.

1.2.2 Objectives

The main objective of this research is to understand and evaluate the physical aging developing and progressing in poly(phynelene oxide) membranes under real conditions. To achieve this objective, it is further divided into two sub-objectives. The first is to study the effect of the transmembrane gas pressure on the time-dependent changes of the membrane performance. This includes building a relation between the membrane morphology and the operating gas pressure, and physical aging of the membrane. To study the combination effect of pressure and morphology (thickness) on the separation factor, an experimental technique that permits simultaneous detection of concentration changes and gas permeation rate under mixed gas condition will be used. The second objective is to study the effect of different feed gas pressure on the physical aging of polymeric membranes. This includes developing of conceptual model for physical aging in gas separation membranes.

1.3 Outline:

This thesis is written in a form of chapters. As a collection, they deal with the objectives drawn for this research. Generally, they could be divided to three groups: introduction and concepts, experimental, and results and discussion.

Chapter two is a theoretical background on gas transport in polymer membranes. Transport parameters are introduced, developed models are described, and polymer structure effect is discussed. Experimental techniques used for gas permeation and separation measurements are also presented.

Chapter three, deals with theoretical background on the physical aging, and glass transition concepts are discussed. Historic developments of experimental techniques for gas permeation and separation experiments are outlined. Literature review for physical aging in membranes is presented. Also, some of the models developed for physical aging in the field of membranes are discussed.

Chapter four is devoted to the experimental techniques used in this work. Those include membrane preparation and thickness control, detailed description of the constant pressure system, and the data collection and analysis breakdown.

Chapter five deals with experimental results and discussions of the effect of gas pressure on the gas transport properties of membranes with different thicknesses. Also, it discusses the end effect of physical aging on membranes with different structure irregularities.

Chapter six is a theoretical modeling for the aging behavior with relation to the viscoelastic behavior of solid materials.

Chapter seven discusses the effect of feed gas pressure on the physical aging of membranes with different thicknesses; and how that affects the membrane permselective properties.

Finally, conclusions from this work are summarized in chapter eight. More literature review devoted to the sub-subjects in each of these chapters is provided whenever it is needed.

CHAPTER 2

Theory of Gas Transport through Polymeric Membranes

2.1 Introduction

Glassy polymeric membranes for gas separation have been the focus of intense research because of favorable separation properties observed with these polymers (Kesting and Fritzsche, 1993). However, full characterization of the gas transport and separation properties of a glassy polymer is limited due to the time dependent changes of the polymer's physical properties. These changes are important in evaluating the performance of the polymer during its anticipated service life. Attempts have been made to explain the observed time-dependent transport behavior at different levels, macroscopic (solution diffusion), microscopic (free volume) and molecular (activation theory) (Stern, 1994).

2.2 Transport Mechanisms of Gases in Polymers

Solution diffusion model

The efficiency of a membrane gas separation process is exclusively characterized by the permselectivity of gases through the membrane. Gases will be separated on the basis of the difference in their permeation rates. The permeation rate of gases through polymeric membranes is measured by the permeability (P), which is a pressure-and-thickness-normalized gas flux. If a gas permeates at steady state conditions through a homogeneous polymeric film of uniform thickness, permeability can be calculated from:

$$P = \frac{Ql}{A\Delta p} 10^{10} \tag{2.1}$$

where Q is the steady state permeation rate (mL(STP)/s), l (cm) is the films thickness, A (cm^2) is a permeation area of the film, and Δp (cmHg) is a pressure difference across the film. Permeability calculated from Eq. (2.1) has units of Barrer, which is defined as:

$$1 \text{ Barrer} = 10^{-10} cm^3(STP)\ cm/(cm^2 s\ cmHg) \tag{2.2}$$

Barrers are widely used in the field of gas separation membranes in recognition of the major contributions of R.M. Barrer to this field.

The solution diffusion model describes the transport of gases through a membrane as a three step process: sorption of gas in the membrane, diffusion through the membrane due to an applied concentration gradient, and desorption of the gas [Koros and Chern, (1987) and Kesting and Fritzsche (1993)]. Both the sorption/desorption and diffusion steps are dependent on the characteristics of the membrane material and the gases.

In the solution-diffusion model, permeability is written as a product of the solubility coefficient factor, S, and a kinetic parameter, D, called the diffusion coefficient [Koros and Fleming, 1993]

$$P = SD\,. \tag{2.3}$$

The ideal selectivity (α_o), which is the ratio of permeabilities of species A and B, can be written as a product of solubility selectivity (α_S) and diffusivity selectivity (α_D)

$$\alpha_o = \frac{P_A}{P_B} = \frac{S_A}{S_B}\frac{D_A}{D_B} = \alpha_S \alpha_D\,. \tag{2.4}$$

Separation of gases in the solution-diffusion mechanism is based on both solubility and mobility factors. Solubility selectivity favours the most condensable molecule, while mobility selectivity favours the smallest molecule. The study of gas transport and separation through polymer membranes is based on the morphology of the polymer. The gas transport through amorphous polymers is further divided into gas transport study through rubbery and glassy polymers. Because glassy polymers are the subject of interest in this research, only solubility and diffusion of gases in these polymers will be reviewed, here.

2.2.1 Solubility of Gases in Glassy Polymers

The dual-mode sorption model

While the solubility of gases in rubbery polymers follows Henry's law, in glassy polymers Henry's law is generally not applicable. According to Henry's law, the concentration of a gas in polymer (C) is proportional to the gas partial pressure (p),

$$C = Sp \tag{2.5}$$

where S is the Henry's solubility constant for the polymer-gas pair. The deviation from the Henry's law in case of gas sorption in glassy polymers provides the basis for the dual mode sorption theory.

The dual mode sorption theory postulates the existence of two types of sorption sites in glassy polymers. One accommodates mobile gas molecules following Henry's law. The other sorption sites, Langmuir sites, which are unique to the glassy polymers, arise from the presence of the excess free volume. Consequently, sorption of gases in glassy polymers is given by the following equation:

$$C = C_D + C_H = Sp + \frac{C_H' bp}{1 + bp} \tag{2.6}$$

where C_D is the concentration in the Henry type-sites, C_H is the concentration in the Langmuir sites, b is the hole affinity constant, and C_H' is the hole saturation constant. At low pressures when bp is much less than 1, Eq. (2.6) reduces to the linear expression consistent with modified Henry-like behavior

$$C = (S + C_H' b)p. \tag{2.7}$$

At sufficiently high pressures, when bp is much greater than 1, additional penetrate can no longer be accommodated in the Langmuir sorption sites. The Langmuir sorption sites reach the saturation limit and the Eq. (2.6) further reduces to the linear form

$$C = Sp + C_H' \tag{2.8}$$

Total solubility of gases in glassy polymers is higher than that in rubbers, which is consistent with the existence of additional sorption sites in these polymers (Kesting and Fritzsche, 1993). In the absence of groups that specifically attract a given penetrate, the solubility in a polymer is largely determined by condensability of that penetrate. The

critical temperature of a gas is a good indicator of its condensability (Koros and Fleming, 1993).

2.2.2 Diffusion of Gases in Glassy Polymers

Molecular models

DiBenedetto and Paul (1965) described the transport of gas molecules to be parallel to the polymer chains. Here the gas molecule is assumed to be trapped in the bundle under equilibrium. During a thermal fluctuation the expansion of the chains near the molecule leads to a creation of cylindrical passage, thereby allowing the gas molecule to make a diffusional jump to the other end of this passage. With the closing of the passage, the gas molecule is at a new position under thermal equilibrium. On the macroscopic scale, this movement coincides with a small displacement of the gas molecule along the chain length. These random displacements then result in the diffusion of the gas molecule through the membrane.

The diffusion coefficient shows an Arrhenius dependence on temperature,

$$D = D_o \exp\left(\frac{-E_d}{RT}\right) \tag{2.9}$$

where D_o is a pre-exponential factor and E_d is the activation energy. The activation energy can be interpreted as the energy required to open a path between the pockets of free volume. Meares (1965) proposed that

$$E_d = \frac{\pi \lambda_d D_k^2 CED}{4} \tag{2.10}$$

where CED is the cohesive energy density of the polymer, D_k is the kinetic diameter of penetrate, and λ_d is the jump length.

Vieth and Sladek (1965) developed a model for kinetic diffusion of gases in glassy polymers on the basis of the dual sorption theory. They assumed that penetrates sorbed in Langmuir sites do not contribute to the diffusive flux and; therefore, the diffusive flux is determined by the diffusion of penetrates sorbed in Henry's sorption sites. There is a local equilibrium between mobile and immobilized species throughout the polymer. They also assumed that the diffusive flux is driven by the concentration gradient, and the diffusion coefficient is constant and independent of concentration or position in the membrane.

Petropoulos (1970) modified the model of Vieth and Sladek by allowing for a partial immobilization of penetrate in Langmuir sorption sites. The partial immobilization model also referred to as the dual mobility model, accounts for two distinct molecular environments with different inherent mobilities D_D and D_H, where D_D and D_H are the diffusivity coefficients in Henry and Langmuir environments, respectively. Both coefficients were assumed to be independent of pressure (Petropoulos, 1970).

Paul and Koros (1976) modified the partial immobilization model of Petropoulos. They assumed that the total gas concentration could be divided into a mobile part with a diffusion coefficient D and concentration C_m and the remainder, C - C_m, which is totally immobilized. The mobile part of the gas comprises all penetrate molecules sorbed in the Henry's sorption sites and a fraction (PI) of penetrate molecules sorbed in the Langmuir sorption sites. The model developed by Paul and Koros reduces in one limit to the total immobilization model ($PI = 0$) and in the other limit ($PI = 1$) to a situation with a linear isotherm with no distinction between sorption mechanism and transport behavior for any of the sorbed gases (Paul and Koros, 1976).

2.3 Influence of the Polymer Structure and Segmental Flexibility on Gas Transport

Even if the polymer chemical structure does not have a straight forward relation to the permeability, replacing different chemical groups with each other changes the gas transport properties of a membrane. Gas permeation is not only affected by the free volume, which is related to chain packing, but also is affected by segmental flexibility, interchain space, and segments attraction. For instance, the introduction of methyl or phenyl groups to poly (phenylene sulfide) PPS results in opening up the polymer matrix and in a greater permeability coefficient. On the other hand, the presence of methyl groups instead of the bulky phenyl groups resulted in lower density and higher d-spacing and T_g (Aguelar-Vega and Paul, 1993; Alentiev et al., 1998; and Illinich et al., 1999). However, sometimes increasing the side-chain length leads to a better packing and thus to a lower permeability. The substitution of $-C(CH_3)_2-$ groups by $-C(CF_3)_2-$ groups in the backbone of poly(aryl ether ketone) (PEK) resulted in a higher T_g and thus in a decreased chain mobility due to the hindered molecular rotations brought up by the large fluorine atoms (Vieth et al. 1976). The increase in free volume resulted in increased permeability, diffusion, and solubility coefficients. A more attractive interaction of the gas molecules with the $-C(CF_3)_2-$ groups was also believed to be responsible for the enhanced solubility coefficient. In addition, the interactions between the gas and the polymer play also a major role in gas transport. Hydrogen bonding for instance, results in a denser material with restricted segmental motion. Hence lower gas permeability and diffusion coefficients are obtained when a particular group is replaced by another one that can form hydrogen bonds (Felder and Huvard, 1980). The same holds true when the interchain

interaction is enhanced due to the substitution of one group by another capable of inducing ionic bonds. Sulfonation of PPO increases density and T_g. This is ascribed to – the formation of hydrogen bond via SO_3H, leading to an increase in the interaction between chains. Nevertheless, the permselectivity is increased (Polotskaya et al., 1997). On the other hand, polarity was considered to reduce the CH_4 pemeation in the presence of $-SO_2(OH)$ group (Percec and Li, 1988).

Ideally, gas separation membranes should have both high permeability and high permselectvity. In reality, however, an increase in permeability results in a decrease in permselectivity, and vice-versa. This "trade-off" relationship is shown in the literature (Robeson, 1991). In order to achieve good membrane performance the polymer should ideally possess two particular characteristics: a high fractional free volume and a narrow free volume distribution. Some exceptions have however been noticed and increases in both permeability and permselectivity have been reported. This is the case for instance for a polymer with bulky substituents and with groups capable of strong intermolecular interactions (Felder and Huvar, 1980). Polynorbornenes with aliphatic pendant groups, hence a stiff backbone with flexible side chains, for example, showed a reversed trade-off (Kamiyu et al., 1988). In conclusion, gas transport properties are affected by main chain rigidity, bulkiness and flexibility of side chains, attraction between segments and the polarity of side groups.

2.4 Relationship between Permeability and Free volume of Polymer

Free volume model

The free volume theory postulates that the movement of gas molecules is dependent upon the available free volume in the polymer matrix, as well as, sufficient energy of the gas molecules to overcome attractive forces between chains (Vrentas and Duda, 1976). The simplicity of the free volume theory, as being a single parameter model, has been the important reason for its wide application in gas transport studies through polymer membranes (Fang et al, 1975).

The permeability, as indicated by Eq. (2.3), is comprised of both kinetic and thermodynamic factors, which in principle depend on different aspects of the gas/polymer combination. In general, for a given gas, the diffusion coefficient (D) varies much more than the solubility coefficient (S). Among the many parameters on which D might depend, the free volume of polymer is among the most important. Free volume has also a strong influence on S. As a result, permeability has been successfully correlated to the free volume of polymer (Lee, 1980; Stern, 1994; Park and Paul, 1997) by the following general expression,

$$P(Barrer) = A\exp(-B/FVP) \tag{2.11}$$

where A and B are constants for a particular gas, and FVP is a free volume parameter. The numerical values of constants A and B depend not only on the type of a gas but also on the type of free volume parameter used, that is, whether the FVP is represented by a specific free volume [Lee, 1980], or fractional free volume (Park and Paul, 1997). Out of these FVP parameters, the fractional free volume (f), which is defined as,

$$f = (v - v_o)/v \tag{2.12}$$

where v is the specific volume of polymer and v_o is the volume occupied by polymer chains, is most commonly used for the prediction of permeability. The values of constants A and B associated with f as a FVP for different gases are presented in Table 2.1. In addition, for each gas the table provides the number of polymers used for the evaluation of A and B.

Table 2.1 The values of constants A and B recommended to be used with the fractional free volume (f) as a free volume parameter (FVP) in Eq. (2.11) [Park and Paul, 1997].

Gas	CH_4	N_2	O_2	CO_2	H_2	He
Number of Polymers	105	104	104	105	65	81
A	114	112	397	1750	1070	1800
B	0.967	0.914	0.839	0.860	0.643	0.701

2.5 Gas Permeation of PPO

Poly-2,6-dimethyl-1,4-phenylene oxide, commonly called poly (phenylene oxide) or PPO is an aromatic polymer from the family of polyphenylene ethers. With the exception of PTMSP, this polymer has one of the highest permeabilities among glassy polymers. Also, it was the subjected of very intensive studies for gas separation (Illinich et al, 1999). The polymer has a high average T_g of 212 °C and average molecular weight M_w of 400,000. PPO is mechanically strong, but thermally the polymer is known to decompose if it is heated to its T_g in the air (Kim et al., 2002).

Toi et al. (1982) compared PPO to other glassy polymers and found that it has higher free volume, which results in higher gas permeability. The higher free volume

enhances the permeability by increasing the solubility and diffusivity of gases in and through this polymer. Aguilar and Paul (1993) found that PPO has higher permeability than some polymers which have higher free volume, like PPPO (poly phenyl phenylene oxide). This was attributed to the higher flexibility of the PPO backbone chain due to smaller methyl constituent.

A scatter of data is reported on the permeability of gases through PPO. For example O_2 permeability range between 12 and 19 Barrer, and CO_2 permeability ranged between 42 and 200 Barrer (Kruczek and Matsuura, 2000). The scatter of the permeability data of any polymer is mainly a result of three factors. (i) The physical properties of this polymer are known to be widely distributed. (ii) The testing protocol and the system applied for the measurements. (iii) The history of the used films, which includes the membrane making process, the starting time of facilitating, the pressure it is subjected to, etc.

2.6 Feed Gas Pressure Effect on Membranes Permeation permeance?

Ideally, the gas pressure should not affect the membrane permeation, as both diffusion and solubility are independent of the gas pressure. However, marked deviations are observed between the theoretical predictions and the experimental gas transport parameter values, particularly at elevated pressures. The effect of pressure is a major challenge in predicting the gas transport process. Typical effects of gas pressure on permeability are shown in Fig. 2.1 (Koros and Chern, 1987). The first response (response A) is for the ideal case as both diffusion and solubility are assumed independent of gas pressure. This type of behaviour is observed for the case of supercritical gas permeation

in amorphous polymers. The response B is characteristic of a gas plasticization effect or gases with high affinity to the polymer material. Response C corresponds to the case of highly soluble gases in glassy polymer. The last response is a combination of responses (B) and (C).

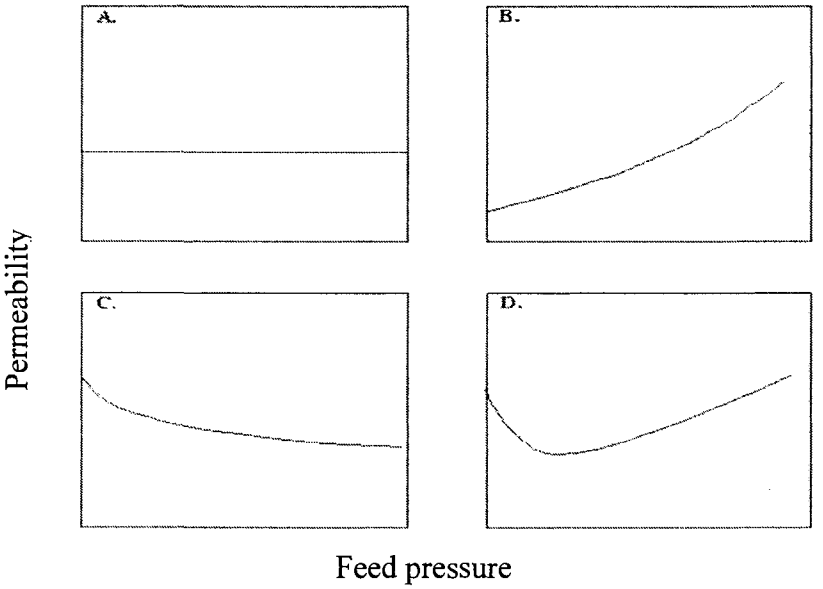

Figure 2.1 Typical forms of permeability dependence on gas concentration during gas transport through polymer membranes. (Koros and Chern, 1987).

The deviations from the ideal behaviour are caused by the effect of pressure on either the solubility or the diffusivity. The above interpretations for these deviations are not taking the thermodynamic changes that accompany gas sorption and the changes that occur to the polymer matrix into consideration. Also, they consider the membrane as a solid material that does not change to accommodate gas molecules. Therefore, these are not the possible explanations to pressure induced changes and more models are used to describe gas sorption through glassy polymers.

2.7 Experimental Methods

The experimental techniques employed in the field of gas permeation and separation are based on measurement of either changing pressure at constant volume or changing volume at constant pressure. These techniques are basically the same as those adopted in the very first design. The availability of more accurate and sensitive tools improved the data acquisition techniques.

The first experiment to prove gas diffusion through membranes was done by Mitchell in 1831. This was based on the shrinking rates of pig skin filled with ten different gases. Gas permeation through non-porous homogeneous polymeric membranes was suggested by Sir Thomas Graham in 1866 to occur by the well-known solution-diffusion model (Vieth et al, 1976). He also designed the first systematic experimental work. The simple design consists of a tube connected to a mercury column from one side and a membrane stretched on the other end of the tube. The permeation rate was calculated from the displacement of the mercury in the column. In 1918, Dewar used an evacuated chamber and monitored the pressure rise in the chamber due to gas permeation through a membrane. The rate of increase in pressure was then used as a measure of the gas permeability. Based on the different experimental methods employed to estimate gas transport properties through polymers, the methods can be broadly divided into four categories (Felder and Huvard, 1980).

i) Volume Loss Method

The permeation rate through a membrane is calculated from the loss of a known volume of gas under constant pressure. The pressure is kept constant by the weight plug in the column, it moves down the column with the gas permeate through the membrane.

ii) Sweep gas-Constant Pressure method

This method includes the sweep of the permeate by an inert gas and the mixture is then analyzed for gas concentration. The gas concentration analysis is conducted using either thermal conductivity or flame ionization detector in gas chromatography. The permeation rate is then calculated from the concentration of the permeating gas and the flow rate of the sweep gas. The introduction of gas chromatography and mass spectrometer, gave more importance to this method, as experiments could be carried out employing feed gas mixtures (Koros and Chern, 1987).

iii) Constant Volume Method

This technique is based on the accumulation of gas in a closed permeate chamber as it permeates through the membrane. The system is initially degassed by use of a high vacuum pump. The feed gas is supplied to the feed chamber under a certain pressure and kept at the same pressure for the entire period of the experiment. Because of the pressure difference, the gas will permeate through the membrane. The pressure increase in the permeate chamber, due to gas accumulation, permits the gas permeability calculation. The design is limited by its strict requirement for a perfect leak proof volume chamber. High pressure setup requires stainless steel tubing with special tube connectors for constructing a leak proof system.

iv) Gravimetric Method

Wroblewski in 1879 used gravimetric method to calculate gas solubility in vulcanized rubber. This method requires the penetrant to be adsorbed by some adsorbent material after it permeates through a polymer membrane. The weight gained due to adsorption with respect to time then gives a measure of the permeation rate. A variation to this technique consists of measuring sorption of a membrane by suspending it from a calibrated quartz spring in a closed chamber. After the penetrant is introduced into the chamber at constant pressure, the extension rate of the spring is then related to the rate of mass uptake and the total mass adsorbed by the material.

All the methods described can be used to measure two out of the three transport parameters required to characterize the transport properties of the membrane, namely: diffusivity, solubility and permeability. The limitations of the techniques sometime restrict the measurement to just one parameter value. For example, employing the volume loss method, it would be difficult to quantify the unsteady state of the permeation process.

2.8 Mixed Gas Permeation

The first permeation experiment using gas mixtures was carried out in 1900. It studied the permeation of air through a rubbery polymer membrane. The oxygen content was first measured before it was liquefied to measure the argon gas content. The results were then used to gauge the separation property of a polymer.

With pure gas permeation studies having provided the foundation for the membrane based gas separation, the focus then shifted to studying real time mixed gas

permeation. This was deemed necessary, not only to validate the observed pure gas permeation but also to derive theoretical correlations for estimating the selectivity and permeability of a mixture of gases through the same materials. In order to detect the gas composition of the feed and the permeate streams, various analytical devices, commonly employed for simple gas concentration analysis, were used with proper interface with the pure permeation experimental setup. Two analytical tools have shown their compatibility with the membrane separation techniques for measuring gas composition in a mixture, a mass spectrometer and a gas chromatograph.

CHAPTER 3

Literature Review on Physical Aging and Its Effect on the Gas Transport Properties

3.1 Introduction

This section summarizes the basic concepts in polymer physics, which are necessary to understand the phenomenon of physical aging in glassy polymers. The topics discussed below include different polymer morphologies, glass transition, specific properties of glassy state, segmental mobility, and the excess free volume. Finally, the phenomenon of physical aging is introduced in general terms.

3.2 Physical Aging Origin and Aspects:

3.2.1 Polymer Morphology

There are two distinct morphologies in which polymer chains can be arranged below the melting temperature (T_m). These are the amorphous and crystalline

morphologies. The amorphous morphology is characterized by a lack of any orderly arrangement, while in the crystalline morphology polymer chains are aligned in some orderly fashion (Callester Jr., 1997). Based on the arrangement of polymer chains, the polymers are classified as amorphous or crystalline. Many amorphous polymers, however, at some specific conditions can form crystalline regions. For example, polyphenylene oxide isolated by precipitation in methanol could be up to 15% crystalline (Hay, 1986). Such polymers are often referred to as semi-crystalline polymers.

Different polymer morphologies result in different behavior at the melting temperature (T_m). This different behavior is illustrated in Fig. 3.1. An amorphous polymer at T_m transforms from melt to rubbery state. This transition however, is not associated with any change in specific volume. Moreover, the rate at which the specific volume changes with temperature is the same in both states. Consequently, the behavior of amorphous polymers below the T_m is often compared to the behavior of a very viscous liquid. Eventually, however, a further decrease in temperature results in another transition, glass transition, at which the rubbery polymer transforms into a brittle solid (Hodge, 1995; Hutchinson, 1995; and Kauzmann, 1994). The temperature at which this transition occurs is called the glass transition temperature (T_g). Unlike the transition at T_m, the transition at T_g is associated with a change in the rate of heat capacity and specific volume change with temperature.

On the other hand, when crystalline polymers reach T_m, the removal of heat from the polymer does not result in any changes in temperature until the polymer solidifies completely. Consequently, at T_m crystalline polymers experience a step change in specific volume. Moreover, unlike the amorphous polymers, the rate at which the specific

volume changes with temperature below T_m is different from that above T_m. In addition crystalline polymers do not undergo glass transition.

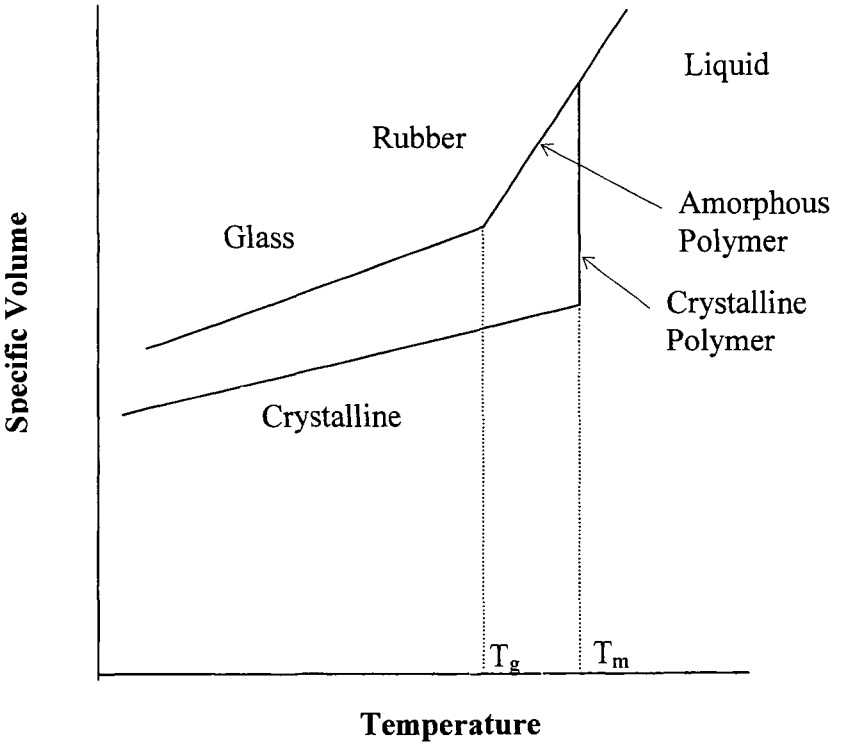

Figure 3.1 Specific volume of amorphous and crystalline polymers as a function of temperature.

3.2.2 Glass Transition and Glassy State

Glassy state occurs only in amorphous and semi-crystalline materials. It is a non-equilibrium thermodynamic state at which the material maintains the structure, energy, and volume of liquid, but the changes in energy and volume with temperature are similar in magnitude to those of crystalline material (Kauzmann, 1948).

The glass transition temperature has many definitions due to a large variety of properties used to observe it, but most often it is defined as the temperature at which the thermal coefficient of expansion changes (Kesting and Fritzsche, 1993). The thermal coefficient of expansion is simply the rate at which the specific volume changes with temperature. For a given amorphous polymer, the glass transition temperature and the specific volume at given temperature are not constant. For example, it was reported that the faster the annealing of polyvinylacetate the bigger the specific volume and the higher the T_g of this polymer (Kesting and Fritzsche, 1993).

The term glass transition is an analogy to softening of an ordinary glass at high temperatures. However, glass transition can occur not only by a thermal excursion through the T_g of a polymer. For example, upon an isothermal pressurization of a rubbery polymer, it transforms into a glass at glass transition pressure (p_g), that is, at the pressure at which molecular motions of polymer chains become "frozen" (Hutchinson, 1995). In formation of polymeric membranes by the phase inversion process, there are three distinct states known as sol (polymer solution), gel and solid. Increasing the concentration of polymer in polymer solution by solvent evaporation or solvent extraction, will lead to transitions similar to those observed in case of quenching amorphous polymers, and the sol, gel and solid will correspond to the melt, rubber and

glass. Similar to glass transition in thermal processes, specific volume in the latter process depends on the kinetics of solvent removal (Kesting and Fritzsche, 1993).

3.2.3 Segmental Mobility, Glass Transition and Excess Free Volume

Unlike crystalline materials in which molecular movements are restricted to vibrations of individual bonds and atoms, molecular movements in amorphous materials also involve rotations of units of consecutive chain atoms. It is estimated that at T_g, the rotating units consist of 20-50 atoms (Sperling, 2001). Segmental mobility strongly depends on temperature. In rubbery state the unoccupied space existing between polymer chains is sufficiently high to accommodate the segmental mobility to access it. The above mentioned rotational movement is characteristic of the segmental activity. By closing the distance between these segments, they cease to rotate. Therefore, the segments accommodate to the new space by moving in vibration style. The unoccupied space, often referred to as the free volume of the polymer (v_f), is simply the difference between the specific volume of polymer (v) and the volume occupied by polymer chains (v_o).

Eventually, as temperature decreases, a point is reached at which segmental mobility becomes insufficient for the segments to access all the available free volume and polymer is said to undergo a glass transition. Segmental mobility continues to decrease below T_g, and the free volume not accessible for segmental movement increases, even though the specific volume decreases. The free volume not accessible for segmental movement is called the excess free volume. The changes in the excess free volume and the total free volume with temperature for a typical amorphous polymer are schematically shown in Fig. 3.2.

3.3 Physical Aging

Because of the presence of the excess free volume, glassy state is a non-equilibrium thermodynamic state. Consequently, in thermodynamic equilibrium, a glass would not have any excess free volume, and the equilibrium specific volume would be determined by extrapolating the line describing the changes in specific volume with temperature in the rubbery state, into the glassy state (Fig. 3.2).

Although the term physical aging was introduced for the first time only in 1978, this phenomenon was known before under different names such as structural relaxation, annealing, or stabilization (Hodge, 1995). Physical aging occurs in all amorphous materials below their T_g including polymers, inorganic glasses, composites, and amorphous metals. It is known that physical aging is more evident in polymers than in inorganic glasses, because the latter have generally significantly higher T_gs than polymers and the rate of physical aging accelerates close to T_g (Dorkenoo and Pfromm,1999). Also, the physical aging rate increases with the increase in the initial free volume. The accelerated physical aging close to T_g is attributed to increased segmental mobility of polymer chains (M). At the same time, the segmental mobility of polymer chains, at given temperature, is restricted by the free volume of the polymer (v_f). Considering that the rate of physical aging can be expressed by the rate of change in the free volume (dv_f/dt), Struik (1978) proposed the following qualitative relationship between M, v_f, and dv_f/dt, which is schematically presented below.

The prefix physical, before the word aging, is included to distinguish this phenomenon from other types of aging, for example chemical or biological. In the latter cases, the change in the properties of the material is a result of irreversible changes in its

structure, for example involving permanent chemical modification or a rupture of primary atomic bonds. In contrast, physical aging is a reversible phenomenon with no permanent changes in the chemical and physical structure of the material. The effects of physical aging can be erased by heating the aged sample above its T_g, or by decreasing the pressure under p_g, if the glass transition occurred through pressurization of the sample. Re-dissolving the aged polymer sample can also erase the effects of physical aging.

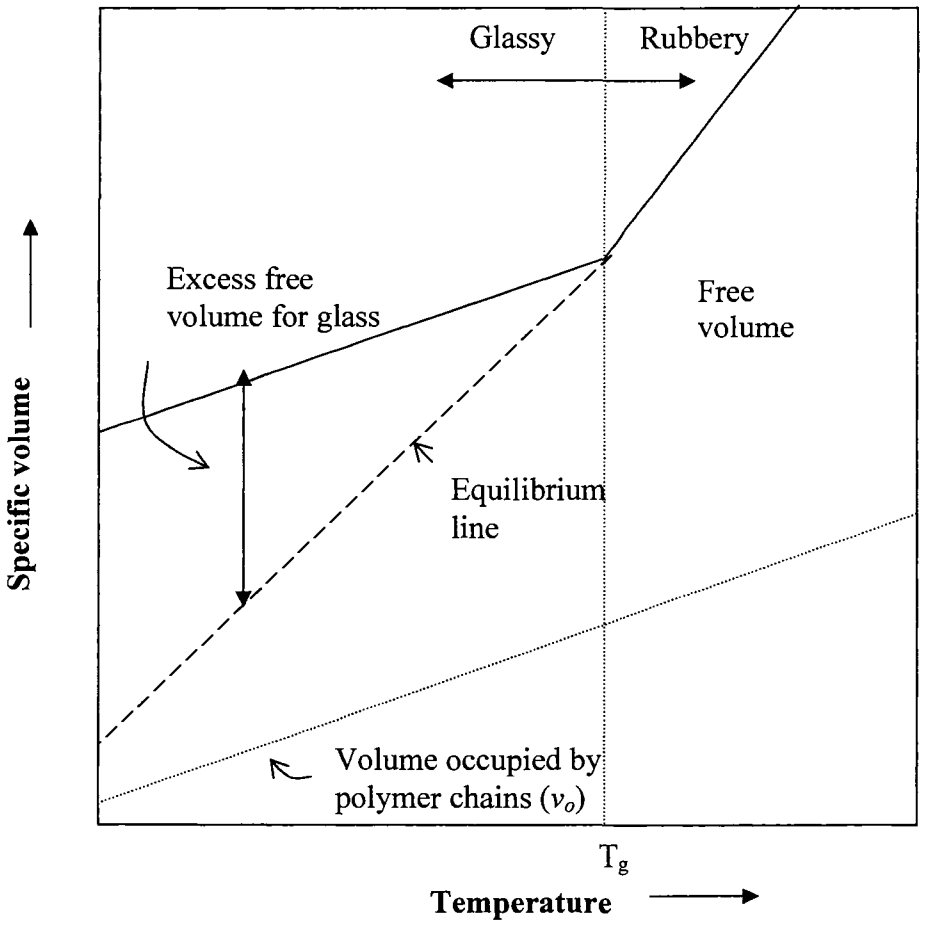

Figure 3.2 The change in specific volume as a function of temperature for a typical amorphous polymer.

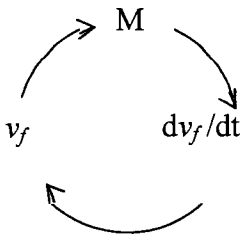

According to the above scheme, the rate of change in the free volume is controlled by the segmental mobility of polymer chains, which in turn is controlled by the free volume. In other words, since as a result of physical aging the free volume of polymer decreases, this decrease in the free volume leads to a decrease in segmental mobility, which in turn decreases the rate of physical aging. The above model implies that physical aging is self-retarding process.

A decrease of the excess free volume of glasses in time is a natural process. A gradual approach of glasses towards their equilibrium was named physical aging by Struik (1978), who also recognized that this process leads to gradual changes in properties related to the free volume of polymer. These properties include macrostructural and bulk properties such as specific volume, enthalpy, density, mechanical and electrical response, as well as, microstructural (molecular scale) properties, which may be probed by spectroscopic and scattering techniques [Hutchinson, 1995].

3.4 Macrostructural and Microstructural Aspects

Due to their versatility and adaptability, polymers are used in a wide range of applications. Versatility of polymers is a result of a wide range of properties that arise from their flexible bulk morphology and diverse molecular composition. Physical aging

affects each application in a different way and a different technique is usually needed to probe physical aging. Investigating thermodynamic and structural changes also added to the vast techniques used in the field of physical aging research. In general, the techniques used could be divided to two categories: techniques probe the bulk (macrostructural) properties, and techniques probe the molecular (microstructural) properties.

3.4.1 Macrostructural Relaxation

Changes in bulk properties have been investigated by several techniques, such as dilatometry, differential scanning calorimetry (DSC), creep, stress relaxation, dynamic mechanical analysis (DMA), tensile testing, and gas permeability.

3.4.1.1 Volume relaxation

As a polymer is isothermally annealed, its volume decreases as well as the value of its glass transition temperature T_g. The specific volume is observed to decrease linearly with the logarithm of annealing time.

The relative departure from equilibrium is given by:

$$\delta = \frac{v - v_\infty}{v_\infty} \tag{3.1}$$

Where is v the volume and v_∞ is the equilibrium volume at a constant temperature. δ is usually plotted as a function of $\log(t\text{-}t_i)$ where t_i is the initial time.

The volume relaxation rate β_V is expressed as:

$$\beta_v = \frac{d\delta}{d\log(t - t_i)} \approx -\frac{1}{v}\frac{dv}{d\log(t - t_i)} \tag{3.2}$$

The changing rate in specific volume should start after reaching the inflection of the contraction isotherm. The essential features of the structural relaxation, i.e. the distribution of relaxation times and the non-linearity of the response are clearly observed by dilatometry. The non-linearity of the relaxation is observed while studying the kinetics of isothermal recovery for a sample that is heated or cooled from a particular temperature (Hutchinson, 1995).

3.4.1.2 Enthalpy relaxation

In a DSC experiment, when an aged sample is heated to a temperature above its T_g, the absorption of heat will appear as an endothermic peak. The height of the peak increases in magnitude with the aging time (t_e), and its position shifts to higher temperatures with higher aging temperature (T_e). Furthermore, the higher the aging temperature, the higher is the value of T_{max} at the same annealing time. It has been demonstrated that T_{max} increases linearly with T_e and with log t_e (Struik, 1976 and Hutchinsom, 1995). As expected from free volume concepts, the glass transition temperature increases with annealing time. The distribution of relaxation times can be observed by the presence of an overshoot peak in the DSC scan, however enthalpy relaxation studies do not show the non-linearity aspect of the behaviour, as do volume relaxation studies (Hutchinson, 1995).

The excess enthalpy δ_H is given by:

$$\delta_H = H_t - H_\infty \qquad (3.3)$$

where H_t is the enthalpy at some time t and H_∞ is the equilibrium enthalpy. δ_H has been shown to be linearly dependent on log t_e. In order to get the value of H_∞, samples have to

be scanned until no further change can be noticed in DSC traces. Obviously, the higher the annealing temperature, the faster the equilibrium achieved.

The enthalpy relaxation rate β_H is expressed as:

$$\beta_H = d\delta_H / d \log t \tag{3.4}$$

The sample is rapidly cooled and scanned again. The two scans are superimposed and the difference in the areas under the two curves can be evaluated.

3.4.1.3 Viscoelastic response and mechanical properties

It is believed that the approach to equilibrium is affecting all properties related to segmental mobility. It has been explained as a lengthening of the time scale of molecular motion as the segmental mobility is reduced. Therefore, the viscoelastic response is shifted to longer time. Creep and stress relaxation tests are commonly carried out to study physical aging through the viscoelastic response (Hutchison, 1997). Shift factors can easily be obtained from those two types of tests. The shifting of the curve along the time axis with aging is due to longer relaxation times τ, and is related to aging time t_e by:

$$\tau = \tau_0 t_e^{\mu} \tag{3.5}$$

Where μ is the Struik shift factor (Struik, 1978). Viscoelasticity in glassy polymers is an evidence of a significant segmental mobility controlled by the free volume and the entropy (Hudge, 1995).

Tensile testing also shows that the modulus and the yield point are increased with annealing. The yield stress and the drawing stress have been reported to increase linearly with log aging time (Hutchinson, 1997).

3.4.1.4. Conclusions

Physical aging can be measured by volume or enthalpy relaxation; or increase in relaxation times. There is no relation that accounts for the differences between any two of the above techniques. The rate of the volume relaxation is generally considered to be greater than the one for enthalpy relaxation (Struik, 1978 and Hutchinson 1995). Furthermore, the time scale for volume relaxation is shorter than that for enthalpy relaxation. Mechanical measurements may be more correlated to one type of relaxation than another. Mechanical response tends to reach equilibrium before the volume (McKenna et al, 1995).

3.4.2. Microstructural Aspects

Changes in the bulk properties of the polymer are the result of changes taking place on the molecular level. Therefore, to interpret the macroscopic changes an understanding of the microscopic structure is needed. Some of the techniques used to probe these changes are, Electron spin resonance, fluorescence spectroscopy, positron annihilation life time spectroscopy, NMR and small angle X-ray scattering (SAXS). These techniques are already known and used for material characterization.

The observations from these techniques are rather different from the ones taking place at the macrostructural level. The changes in the macroscopic scale are universal, on the other hand the changes on the microscopic level seem to depend on the chemical structure of the examined sample. No techniques are developed to measure the physical

movement of the polymer segments. This is definitely due to lack of understanding of the nature of this movement.

3.5 Parameters Influencing Physical Aging in Glassy Polymeric Films

Despite the fact that intensive research on gas separation membranes has begun more than three decades ago, the importance of physical aging on the performance of membranes made of glassy polymers has been recognized only in mid 1990s. In this section the research involving physical aging in films made of glassy polymers will be reviewed. However, before reviewing the works in this area, it is important to discuss how the progress of physical aging is monitored in case of gas separation membranes.

3.5.1 Measurement of Gas Permeation Rate through Polymeric Membranes

According to Eq. (2.11) and Eq. (2.12), a time-dependent reduction in free volume of a glassy polymer will lead to the corresponding decrease in permeability coefficient. In turn, as indicated by Eq. (2.1), the changes in permeability coefficient of the polymer can be detected by the changes in gas permeation rate through the film. Therefore, the measurements of gas permeation rate represent a very convenient tool for the monitoring physical aging in glassy polymeric membranes.

In general gas permeation rates are measured in constant-pressure or constant-volume testing systems. In constant-pressure systems, permeate-side is at atmospheric pressure and the gas permeation rate is measured directly using some kind of a flow-measuring device. In constant-volume systems, permeate-side is initially at vacuum and

as the gas permeates through the membrane, the pressure increases. The permeation rate is determined from the rate of pressure increase in a known volume on the permeate side.

Nagai et al. (1995), studied physical aging of poly[1(trimethylsilyl)-1-propyne] (PTMSP) films by monitoring the changes in gas permeability using a constant-volume testing system. The permeate-side in the testing system was brought to vacuum either by a regular oil-lubricated pump or an oil-free pump. While in both cases permeability of PTMSP films decreased with time, the permeability reduction, when the regular-oil lubricated pump was used, was significantly greater than when the oil-free vacuum pump was used. The authors suggested that the vacuum conditions initially existing in the permeate side could have allowed for partial evaporation of an oil present in the oil-lubricated pump. At the same time, some of the oil vapors could be adsorbed on the tested films, reducing their free volume. Therefore, the reduction in permeability coefficient observed when the oil-free pump was used was probably due to physical aging of PTMSP, while the permeability reduction when the regular oil-lubricated pump was used was probably due to both physical aging and contamination of PTMSP by the oil vapors.

The effect of testing system on the reduction of gas permeability was also studied by Morisato et al. (1999), who considered poly(4-methyl-2-pentyne) (PMP). The authors reported that in case of films tested in a constant-pressure system, the N_2 permeability decreased 25% from its initial value during a 29 day-test, while in case of identical films tested in a constant-volume system, over the same period of time, the N_2 permeability decreased 90% from its initial value. Since the constant-volume system utilized a regular oil-lubricated vacuum pump, the different extent of permeability reduction in the two

testing systems could be explained considering the free volume reduction by the oil vapors.

It is evident from the above two examples that contamination of a sample by the oil vapors in constant-volume systems with oil-lubricated vacuum pumps, might lead to very significant overestimation of extent of physical aging. To overcome the problem of sample contamination by the oil vapors, liquid nitrogen traps can be installed on all permeation equipment and vacuum ovens (McCaig and Paul, 2000).

3.5.2 Time Zero – Film History

The time an amorphous polymer undergoes the glass transition can be considered as time zero, which is the time when the physical aging begins. Because physical aging is a nonlinear process with respect to time, it is very important to define the time zero and the history of the film being considered as accurately as possible (Dorkenoo and Pfromm, 2000). Most commonly, the glassy films to be investigated are thermally treated to erase previous film history before the beginning of any actual physical aging experiments (for example, Pfromm and Koros, 1995; Dorkenoo and Pfromm, 1999; McCaig and Paul, 2000). Such thermal treatment involves annealing the film above its T_g followed by quenching to the temperature at which physical aging is to be investigated. Because the latter temperature is generally significantly lower than the respective T_g, it might take several hours before the first gas permeation measurements through the film are performed.

Some researchers do not use thermal treatment at all. Nagai et al. (2000), for example, soaked PTMST films in methanol prior to any physical aging experiments.

Methanol acts as a swelling agent for PTMSP. As a result, the free volume of swollen PTMST is twice that of a dry film. The time zero is considered to be the time when the methanol is completely removed from the films, that is, when the weight of the methanol treated films becomes constant. Nagai et al. (2000) justified their method by showing that the original properties of PTMSP films could be restored by treatment with methanol. Tiemblo et al. (2001), who studied PVC and PVC modified films, utilized a similar method. As a part of the film preparation protocol, they extracted residual solvent with ether and considered the end of the extraction process as time zero.

3.5.3 Effect of Film Thickness

Several research groups have studied the effect of film thickness on the rate of physical aging. Pfromm and Koros (1995) studied physical aging of thin (0.5 μm), intermediate (2.5 μm) and thick (25 μm) films prepared from polysulfone and polyimide, respectively, by occasionally monitoring their gas permeation properties. In between the gas permeation measurements, the films were exposed to a dry air at ambient pressure to avoid mechanical stress to which the films would be exposed in a pressurized gas permeation cell. The authors counted the aging time from the moment the films were quenched through the glass transition temperature. The results for the thin film showed a significant decrease in the N_2 permeability coupled with an increase in the permeability ratio of He/N_2 in thin polyimide films over a period of 7000h. Over the same period of time, in case of the thick and intermediate films the changes in N_2 permeability and He/N_2 permeability ratio were relatively small. In case of polysulfone, the thick films showed virtually constant gas permeation properties over a period of 1500h, while the

intermediate films experienced some decrease in permeability and a slight increase in permeability ratio. Similarly to polyimide, thin polysulfone films exhibited accelerated aging.

The effect of film thickness on physical aging was also studied by Dorkenoo and Pfromm (1999), who considered polynorbornene films of different thicknesses. The authors reported accelerated physical aging in films of thickness of 0.8 μm. In addition, they developed a theoretical model relating physical aging to the thickness of polymer sample, which was based on the dependence of gas diffusion in polymers on free volume and the dependence of glass transition temperature on film thickness. In their other work, Dorkenoo and Pfromm (2000) observed significant reduction in permeability of poly[1(trimethylsilyl)-1-propyne] (PTMSP) only in films of thickness 1 and 3 μm, but not in an 85 μm-thick film. The studies of the effect of film thickness on physical aging were continued by McCaig and Paul (2000), who considered polyarylate films of thickness ranging from 0.254 μm to 33 μm. This work lead McCaig et al. (2000) to develop a quantitative model for the prediction of changes in permeability coefficient with time.

3.5.4 Effect of Initial Free Volume of Polymer

Nagai et al. (2000) studied the effect of initial free volume of PTMSP on physical aging. The initial free volume of PTMSP was varied by the selection of different catalysts used in polymerization. The authors considered only thick films (70-130(μm)) and observed significant reduction in film thickness associated with some reduction in permeation rate of methane through the films. Since permeability coefficient is a product

of pressure normalized flux and film's thickness, the permeability coefficient for methane decreased significantly for all films. The magnitude of this decrease was greater for the films having larger initial free volume. These films also showed a faster reduction in permeability coefficient.

The effect of the initial free volume on the progress of physical aging was also studied by Tiemblo et al. (2001). The authors used films made from polyvinyl chloride (PVC) and modified PVC of thickness ranging from 35 μm to 65 μm. The PVC was modified by introduction of pyridine groups. As the degree of substitution with pyridine groups increased, the initial permeability and the initial free volume decreased. Similarly to Nagai et al. (2000), the films having the larger initial free volume and permeability coefficient showed more significant reduction in these parameters with time. However, unlike PTMSP the PVC and PVC modified films exhibiting larger initial free volume and permeability coefficient required longer times for these parameters to stabilize.

3.5.5 Effect of Pressure on the Glass Transition and Physical Aging

Glass transition is, by tradition, described as a reduction in segmental mobility due to temperature reduction. In general, however, the glass transition will be observed, during which a gradual reduction in the rate of molecular motions take place, even if the material is at a temperature above its T_g. This includes an increase in pressure or concentration of the system in addition to cooling. Upon increasing of pressure, a glass transition pressure (p_g) would be defined by the freezing of the molecular motion, and the relaxation in free volume would take place isobarically if a pressure higher than (p_g) is held (Hutchinson, 1995). Since pressure is more difficult variable to change and control

than temperature and also because most of polymers are used at atmospheric pressure, there is scarcity of information concerning the pressure dependence of dynamic quantities in the glass transition regime, especially where relaxation times depend strongly on the instantaneous state of the system (Ramos et al, 1988). This is not the case in polymeric membranes for gas separation, where the process is driven by pressure difference across the membrane, which makes those membranes under pressure throughout the time of application.

Qualitative observations due to rapid changes of pressure were found to be similar to those obtained at atmospheric pressure by rapid changes in temperature (Tribone et al, 1989). Quantitative studies by Deng and Jean (1993) on the effect of pressure using positron annihilation lifetime spectroscopy found that the free volume and free volume distribution decreased by increasing the pressure. Other researchers criticized those studies due to extraordinary decrease in the free volume caused by small changes in pressure (Hutchinson, 1995).

In glassy polymeric membranes for gas separation, there are little studies on the effect of pressure on the physical aging of glassy polymers. McCaig and Paul (2000) carried out one experiment to study the effect of gas pressure. They compared the aging time for a 0.74μm membrane aged under vacuum with the aging time that for a 0.58μm film aged under operating gas pressure in a constant pressure system, and they concluded that changing the operating conditions does not influence the aging response i.e. gas pressure or the used system has no effect on physical aging. This is opposite to what was concluded earlier by Pinnau et al. (1997) that, the details of how permeation rates were measured could influence the observed aging.

3.6 Physical Aging Models Development

Alfrey et al. (1943) proposed a qualitative model for the excess free volume relaxation in glassy polymers. According to the proposed mechanism, the excess free volume in glassy polymers exists in form of mobile free volume holes, which can divide or combine, that is their individual identity is not necessarily preserved. As long as the holes remain within the sample, the free volume of polymer is unchanged. However, once the holes reach the surface of the sample, they disappear and the free volume of polymer decreases. This mechanism for the free volume relaxation has been referred to as free volume diffusion in glassy polymers.

Kauzmann (1948) objected to the general notion of diffusion of free volume, and Hiary and Earing (1958) proposed an alternative model in which they explained relaxation of the excess free volume in glassy polymers by a lattice contraction mechanism.

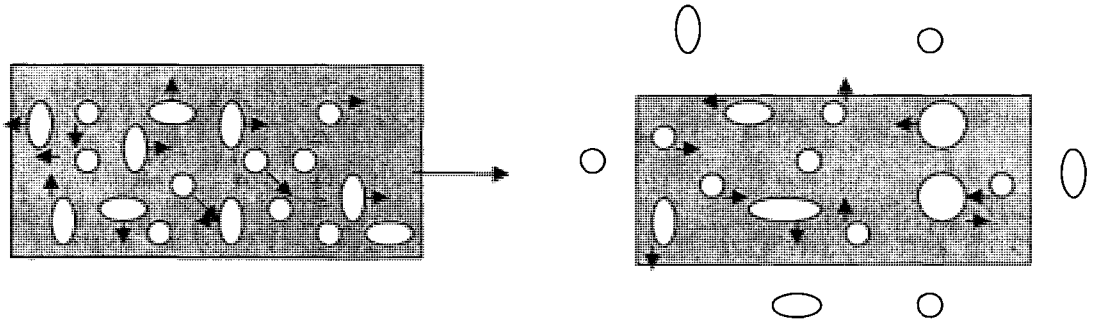

Figure 3.3 Schematic representation of free volume existence in polymeric film and its reduction by diffusion from the surfaces.

The authors suggested the following equation,

$$v_f = v_{f2} + (v_{f1} - v_{f2}) \exp\left(-t/\tau B\right) \tag{3.13}$$

where v_f is the free volume, t is the aging time, τ is a material relaxation time, and B is a dimensionless correction factor.

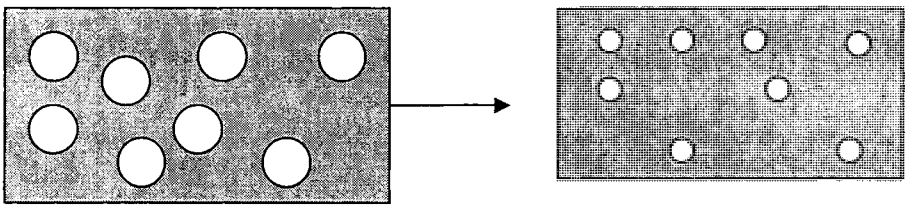

Figure 3.4 Schematic representation of the reduction of free volume by lattice contraction mechanism.

Curro et al. (1982) argued that lattice contraction could be coupled with free volume diffusion to describe the overall volume reduction upon aging. They proposed a quantitative analysis for the diffusion of free volume holes limited by chain segmental motion, in which they described the change in fractional free volume using the Fick's second law of diffusion. They also proposed that the diffusion coefficient for the free volume holes should be correlated with the fractional free volume via a Dolittle-type equation.

3.6.1 Model of McCaig et al.

The model proposed by Curro et al. (1982) was recently further developed by McCaig et al. (2000), who studied physical aging of thick and thin films made from a glassy polyarylate. According to this model, the fractional free volume (f) at any time and any position is given by the following equation,

$$f = f_i - (f_i - f_{LC}) - (f_i - f_D) \tag{3.14}$$

where f_i is the initial fractional free volume, (f_i - f_{LC}) represents the reduction in fractional free volume due to lattice contraction, and (f_i - f_D) represents the reduction in fractional free volume due to diffusion of free volume holes to the film surface. To describe the changes in f_{LC} with time the authors proposed expression similar to Eq. (2.13),

$$f_{LC} = f_g + (f_i - f_g)\exp\left(-t/\tau\right) \tag{3.15}$$

where f_g is a bulk fractional free volume, that is, a pseudo-equilibrium fractional free volume which is observed in thick films, and τ is the material relaxation time, which is a material property.

To describe the changes in fractional free volume due to diffusion of free volume holes to the film surface the authors utilized one-dimensional form of Fick's second law of diffusion,

$$\frac{\partial f_D}{\partial t} = \frac{\partial}{\partial x}\left(D\frac{\partial f_D}{\partial x}\right) \tag{3.16}$$

Similarly to Curro (1982), McCaig et al. (2000) considered the diffusion of free volume holes as a self-retarding process, and used a Dolittle-type equation (1951) to correlate the diffusion coefficient of the free volume holes (D) with the fractional free volume (f),

$$D = D_g \exp\left[-Z\left(\frac{1}{f} - \frac{1}{f_g}\right)\right] \tag{3.17}$$

where D_g is the diffusion coefficient for free volume holes at $f = f_g$ and Z is another material constant.

To solve Eq. (3.16), and hence to find f_D as a function of time and position, one initial and two boundary conditions are required, and McCaig et al. (2000) proposed the following conditions,

$$f_D = f_i \quad \text{at} \quad t = 0 \quad \text{for} \quad -\frac{l}{2} < x < \frac{l}{2} \tag{3.18a}$$

$$f_D = f_e + (f_i - f_g) \quad \text{for} \quad t > 0 \quad \text{at} \quad x = \pm\frac{l}{2} \tag{3.18b}$$

$$\frac{\partial f_D}{\partial x} = 0 \quad \text{for} \quad t \geq 0 \quad \text{at} \quad x = 0 \tag{3.18c}$$

The first boundary condition arises from the notion that after infinitely long time the fractional free volume at the outer surface of the film must be equal to an equilibrium fractional free volume (f_e). The second boundary condition, Eq. (3.18c), arises from the assumption that the diffusion of free volume holes in homogeneous polymeric films is a symmetrical process occurring from the mid-plane to both surfaces of the film simultaneously, and thus at any time the fractional free volume is maximum in the mid-plane, that is, at the position $x = 0$.

Since permeability is correlated with fractional free volume by Eq. (2.11), McCaig et al. (2000) verified their model by monitoring the changes in gas permeability with time. However, since the model provides a distribution of f across the film, Eq. (3.16) is assumed to apply point by point so that the permeability is a function of x and t, $P(t,x)$, and then it is necessary to integrate the calculated permeability coefficient over the

thickness of the film to compare with the experimentally observed values of permeability coefficient, $P(t)$. The appropriate integration is given by the following expression,

$$\frac{1}{P(t)} = \frac{1}{l}\int_{-l/2}^{+l/2} \frac{dx}{P(x,t)} \tag{3.19}$$

The model of McCaig et al (2000) requires several parameters. Some of these parameters such as the fractional free volumes, f_i, f_g, f_e were obtained from the PVT data for polyarylate, that is, from the experimentally determined relationship between the specific free volume of polyarylate and the temperature and pressure. On the other hand, D_g and Z, which appear in Eq. (3.17) were obtained by fitting the experimental data, while for τ the value reported in previous works for the structurally similar polymer was utilized.

3.6.2 Modifications of the Lattice Contraction Model Proposed by Tiemblo et al.

Tiemblo et al. (2001), studying thick films made from PVC and modified PVC, suggested that material relaxation time (τ), which determines the kinetics of the reduction of free volume in the lattice contraction model, is not constant. Rather, it changes with the free volume of the aged material, that is, is a function of time. To incorporate the dependence of τ on free volume, they proposed to introduce a "stretched exponential" in Eq. (3.15),

$$f_{LC} = f_g + (f_i - f_g)\exp\left(-t/\tau\right)^{\beta} \tag{3.20}$$

The new parameter β adopts values lower than or equal to unity. Interestingly, out of 12 aging experiments performed by Tiemblo et al., (three different polymers times four

different gases) only in one case, physical aging of a PVC film in CH_4, it was necessary to use $\beta < 1$. In all other cases, good fit of experimental data was obtained using $\beta = 1$.

CHAPTER 4

Experimental Details

4.1 Preparation of Dry Membranes

4.1.1 Polymeric Material

Poly-2,6-dimethyl-1,4-phenylene oxide, commonly called poly (phenylene oxide) or PPO, was kindly supplied by General Electric Company, Selkirk, NY. It is an aromatic polymer from the family of polyphenylene ethers (Ilinich et al., 1999). The repeat unit of the polymer is shown in Fig. 4.1. With the exception of PTMSP, this polymer has one of the highest permeabilities among glassy polymers. Also, it has been subjected to very intensive studies for gas separation, but despite severe deterioration in permeability, the first study in which the physical aging was dealt by Huang and Paul, 2005.

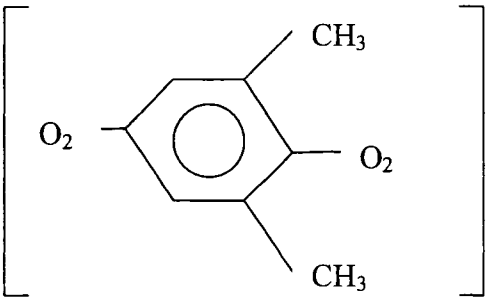

Figure 4.1 Repeat unit for Poly-2,6-dimethyl-1,4-phenylene oxide.

The polymer has a high average T_g of 212 °C and average molecular weight M_w of 400,000. PPO is mechanically strong, but thermally the polymer is known to decompose if it is heated to its T_g in the air (Kim et al., 2002). Its free volume is estimated to be 0.2. It has a broad *d*-spacing, according to x-ray diffraction scans, with a maximum at 6.1 A and a shoulder at 3.7 A (Aguilar-Vega and Paul, 1993). The measured density for the cast film was equal to 1.06 g/cm^3.

4.1.2 Preparation of Membranes

The polymer was put in glass flask covered by Teflon and dried in fume hood for at least 24 hrs before solution preparation. A 1 wt% solution of aromatic PPO is prepared by dissolving the polymer in 98% pure trichloroethylene (TCE) from Aldrich, in a glass bottle. A magnetic stirrer stirred the solution for 24 hours to dissolve the polymer completely. The solution then was filtered using a 1.2 μm Millipore filter and left for at least 24 hrs for the air bubbles to leave the solution.

The membranes are prepared by the solvent evaporation method. A certain amount of the filtered solution is poured to a stainless steel ring that is fixed on a very precisely leveled glass plate. The amount of the solution is changed for the purpose of

thickness change. The solution in the ring is then let, in a fume hood at room temperature (~ 22°C), approximately 6 hours, to evaporate the solvent. After that, the glass plate is immersed in a water bath until the membrane can be easily peeled off the glass plate. The membranes are visually examined for defects such as dirt and pinholes and numbered. Then the membranes are let to dry for more than six hours, and then put in the permeation cells for permeation testing.

4.2 Constant Pressure System

In the current research two experimental set-ups will be used for observing mixed gas permeation through non-porous membranes with real time resolution. A development of a sweep gas constant pressure-variable volume (C-P) system for gas permeation and separation measurements will be included in this work. An available and proven constant volume-variable pressure (C-V) system will also be used. The next section contains a detailed description of the C-P system and its development, data acquisition, handling and analysis.

4.2.1 Automated Multi-Cell Sweep-Gas Constant Pressure System

This method is known as the continuous flow or the constant pressure-variable volume method. It is also known as the carrier gas method (Koros and Chern, 1987). It involves sweeping the permeated gas and routing it to GC to be analysed for the fluxes of each permeant. The technique employs a gas chromatograph (GC) as the selective detector for monitoring the variation in gas concentration, as the gases permeate through the membrane. A GC enables quantitative analysis of gas mixtures by calculating areas

underneath peaks that correspond to all components in a mixture. The amount of each component is proportional to the area underneath the peak.

The schematic of the experimental technique is shown in Figure 4.2. The set-up is best described by categorizing it into five broad sections. Every section is interconnected and performs different functions at various stages of an experimental run. Besides allowing mixed gas permeation experiments, the same set-up can be used for carrying out single gas permeation experiments, with minor modifications during data collection. For mixed gas permeation experiments, besides monitoring the gas flow rate, the concentration of the permeate gas mixture is also measured at regular time intervals. The present set-up employs in-line sampling technique for gas sample by subsequent injection into a gas chromatograph for concentration analysis. The set-up is constructed with 316 stainless steel tubing and fittings for high pressure feed studies (0 to 500 psia). The entire set-up is automated for unsupervised operation by employing controller cards for the solenoid valve operation and data acquisition cards for pressure transducer and mass flow meter readings.

Feed Gas Supply and Regulatory system

The feed section supplies the test gases to the feed side of the membrane. The feed pressure is regulated by a two-stage pressure regulator and measured by a variable reluctance pressure transducer, from MKS, having a range 0 - 500 psia. The feed section is connected to the membrane cell through a 3-way valve. The feed side is connected to air-actuated pneumatic valves operated by solenoid valves to stop the feed to the cell in case of pressure increase, due to membrane rapture, in the permeate side.

A sweep gas (methane) is fed to the permeate side of the cell to push the permeate gas out of the cell to a 9-position multi-port valve to be injected to the GC. A mass flow controller, from MKS, with range of 0-10 cc/min, controls the sweep gas flow.

Permeate and Retentate Sections

The gas permeation rate is monitored by mass flow meter (MFM) from MKS Instruments, having a range of 0-10 $\pm$ 0.1 cm^3/min. The pressure in the permeate side is monitored by a pressure transducer, from MKS Instruments, having a range of 0-50 psia. The transducer is connected to the permeate side, which is a safeguard against over pressurization in the section due to membrane breakdown. A feedback closed loop control system monitors the opening and closing of the feed gas valve during an experimental run.

The retentate pressure is, also controlled by a pressure transducer, from MKS Instruments, having a range of 0-500 psia. The retentate flow rate is controlled by a needle valve (NV) and its flow rate is measured by a MFM similar to the one installed on the permeate side. This valve helps in maintaining proper stage cut flow rates to avoid concentration polarization. The stage-cut for such systems is defined as the relative gas flow rate through the membrane with respect to the gas flow rate of the feed. The sweep-permeate and retentate streams are connected to the multi position valve (MSV) through 3-way valve. The 3-way valve is put to make it possible to check these streams flow rate using other device, such as a bubble flow meter or a volumeter.

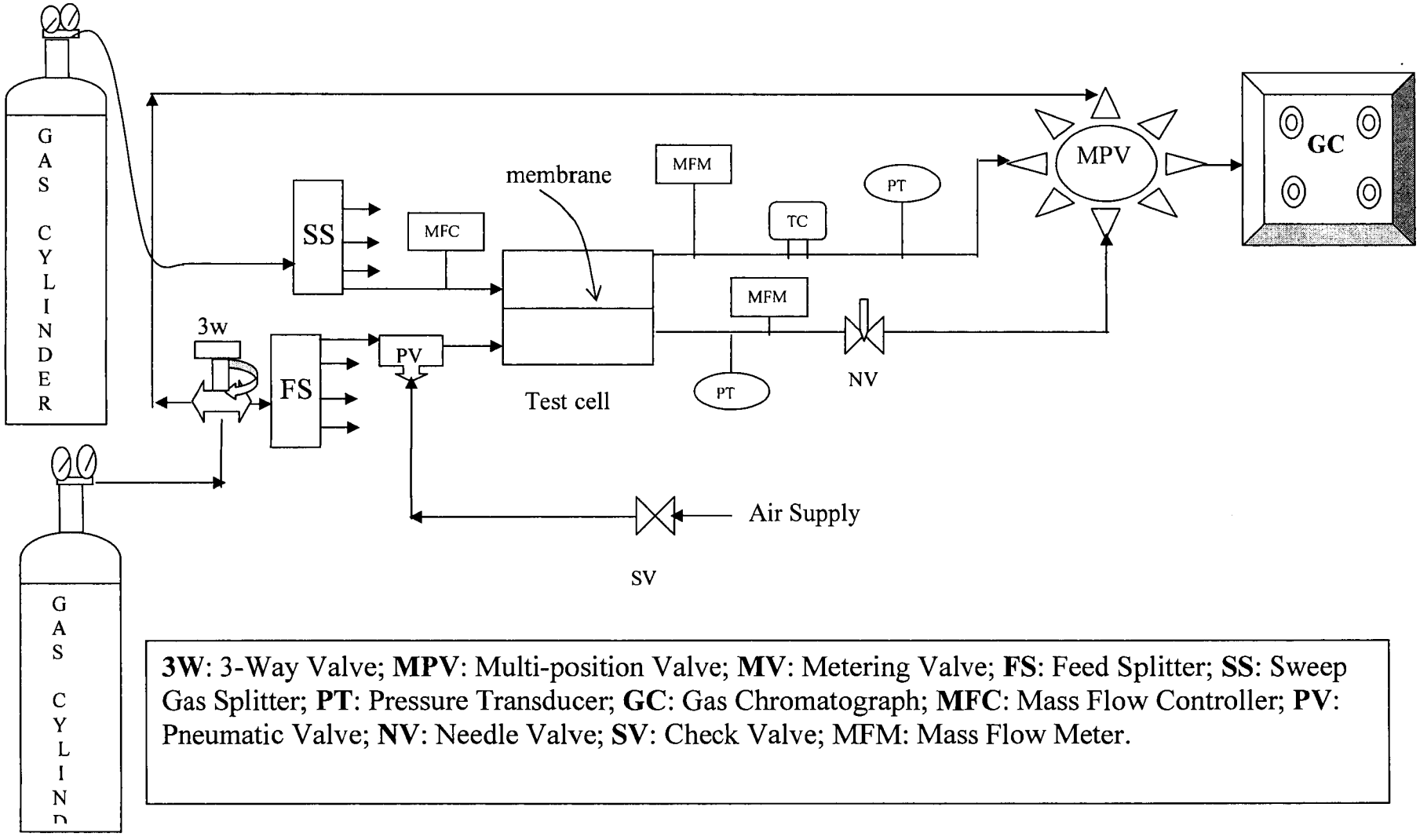

Figure 4.2 Schematic diagram of the sweep gas constant pressure (CP) system.

Series 580 TCD gas chromatograph, from GOW-MAC instrument Co., is used for analyzing the gas streams coming from the gas permeation system. It is two columns isothermal gas chromatograph with thermal conductivity detector (TCD). One of the columns contains porous polymer and the other contains molecular sieve 5A, as separation media. All the outlet streams from the cells, permeate and retentate, are connected to the GC through the nine-port multi-position valve.

Data Acquisition and Control System:

A switching controller module and a data acquisition controller board control the entire experimental system, including the gas chromatograph. The hardware is programmed using a graphical, user friendly, programmable software, LabVIEW 6.0, by National Instruments Inc. The program is capable of, continuously, recording and storing pressures, upstream and down stream, flow rates of permeate, sweep and retentate, and the temperature in every cell. The process control includes operation of the valves and mass flow controllers according to preset parameters such as up-stream and down-stream pressures, temperature, sweep flow rate and status of the valves.

The system controls the GC operation such as the switching between injecting and purging, and between series and by-pass positions. It also records data from the GC, and calculates peak areas representing the analyzed gases.

4.3 Analysis of the Experimental Data

Figure 4.3 presents one of four membrane cells. All streams come in and go out from the cell. The figure also shows the devices that are used to control and monitor the gas separation process.

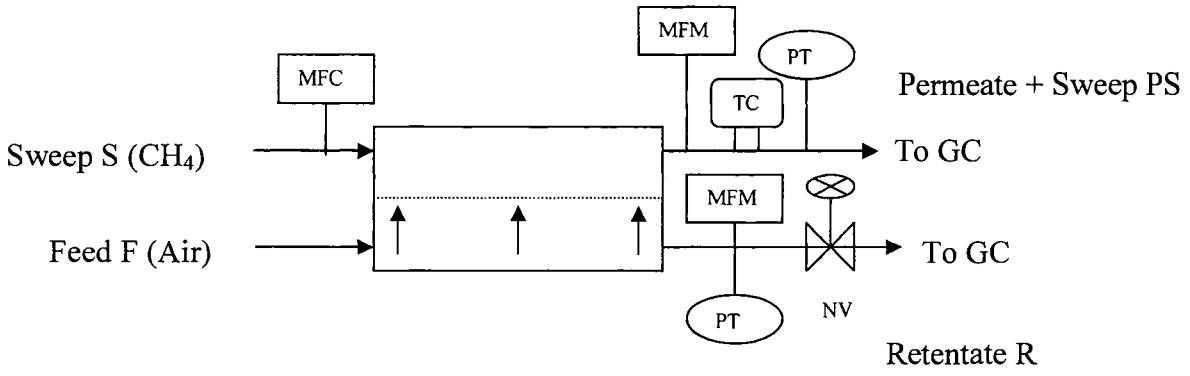

Fig. 4.3 The streams coming in and out from a membrane cell during an air separation test and the instrumentation for monitoring the process.

The flow rate of sweep stream, S, is controlled and measured using a mass flow controller (MFC); the flow rate of permeate + sweep stream, PS, is measured using a mass flow meter (MFM). Unlike stream S, the flow rate of feed stream, F, is not controlled using the MFC. This is because installing the MFC in the feed line would limit the range of pressures at which gas separation / permeation tests could be carried out, to the outlet pressure of the MFC, which is 150 psig. Instead, the flow rate of retentate stream, R, and hence stream F is controlled using a high precision needle valve (NV) installed right after the MFM, which measures the flow rate of stream R. Since the maximum inlet pressure of the MFM is 400 psig, the gas separation / permeation tests can be carried out at pressures up to 400 psig. The gauge pressures of streams PS and R are

measured using respective pressure transducers (PT). These pressures represent the values at the permeate (low pressure) side and the feed (high pressure) side of the membrane, respectively. The temperature at which the gas separation / permeation tests are carried out is measured by a thermocouple (TC) installed in the PS line. The compositions of streams PS, R and F are determined using a gas chromatograph (GC). Table 4.1 shows a sample of raw data obtained during an air separation experiment using a PPO membrane and CH_4 as sweep gas.

Table 4.1. Sample of raw data from one membrane cell recorded during an air separation test with methane as a sweep gas.

Raw Data		Stream			
		Feed (F)	Retentate (R)	Sweep (S)	Permeate + Sweep (PS)
Peak area from GC analysis	O_2	4145.85	4432.48	-	1886.27
	N_2	19150.72	20922.72	-	2362.40
	CH_4	_	0	-	12915.59
Apparent flow rate[1] ($\dot{Q}_i$) [cm^3(STP)/min]		_	2.2908	0.4096	0.4756
Pressure [psig]		_	25.65	_	0
Temperature [°C]		_	_	_	21.6

[1] Apparent flow rate is the flow rate recorded by MFM or MFC.

4.3.1 Determination of Composition of Gas Streams

The composition of gas streams that are mixtures of at least two gases is evaluated using the data from the gas chromatograph. Each gas is eluted from the GC column at a specific time known as the retention time. Knowing the retention times at given GC conditions, it is possible to assign each peak to the appropriate gas in the gas mixture. In general, the concentration on a molar (volumetric) basis of a gas in the mixture is

proportional to the peak area. According to Deitz (1967), however, there are some small deviations from the proportionality between the concentration and the peak area, and it is necessary to use correction factors. A thermal response factor (TRF), which is a ratio of the signal to the sample size, is used as a correction factor for each gas in the mixture. Therefore, the mole fraction of component i (x_i) is calculated using the following equation,

$$x_i = \left(\frac{A_i / \mathrm{TRF}_i}{\sum_i A_i / \mathrm{TRF}_i} \right) \tag{4.1}$$

where A_i and TRF_i, are the peak area and the thermal response factor of the component i, respectively. Tables 4.2 – 4.4 show the compositions of streams PS, F and R, respectively, calculated using Eq. (4.1) and the raw data listed in Table 4.1. These tables also show the TRFs values for each gas in the mixture [Dietz, 1967].

Table 4.2 Composition of stream F based on the raw data listed in Table 4.1.

Gas	Area (A_i)	TRF_i	Mole fraction $x_{i,F}$
O_2	4145.85	40	0.1852
N_2	19150.72	42	0.8148

Table 4.3. Composition of stream PS based on the raw data listed in Table 4.1.

Gas	Area (A_i)	TRF_i	Mole fraction $x_{i,PS}$
O_2	1886.27	40	0.1014
N_2	2362.40	42	0.1209
CH_4	12915.59	35.7	0.7777

Table 4.4. Composition of stream R based on the raw data listed in Table 4.1.

Gas	Area (A_i)	TRF_i	Mole fraction $x_{i,R}$
O_2	4432.48	40	0.1820
N_2	20922.72	42	0.8180
CH_4	0	35.7	0

4.3.2 Determination of Permeability Coefficient

The permeability coefficient of component i (P_i) in a gas mixture is calculated using Eq. (4.2),

$$P_i = \frac{Q_i l}{\Delta p_i A} \tag{4.2}$$

where, Q_i and Δp_i are the permeation rate and the pressure driving force of component i, respectively, l is the membrane thickness, and A is the effective area for permeation of the membrane.

4.3.2.1 Q_i from the composition and the apparent flow rate of PS stream

In this approach, the apparent flow rate and the composition of stream PS are used to determine the permeation rates of individual gases (Q_i) of O_2 and N_2 through the membrane.

The mole fraction of component i in a stream consisting of at least two components is related to the flow rates of individual components by the following equation,

$$x_i = \frac{Q_i}{\sum_{i=1} Q_i} \tag{4.3}$$

Since stream PS consists of three components, one can write the following three equations

$$Q_{N_2} / \left(Q_{O_2} + Q_{N_2} + \dot{Q}'_{CH_4} \right) = x_{N_2,PS} \tag{4.4}$$

$$Q_{O_2} / \left(Q_{O_2} + Q_{N_2} + \dot{Q}'_{CH_4} \right) = x_{O_2,PS} \tag{4.5}$$

$$\dot{Q}'_{CH_4} / \left(Q_{O_2} + Q_{N_2} + \dot{Q}'_{CH_4} \right) = x_{CH_4,PS} \tag{4.6}$$

In Eqs. (4.4) to (4.6), Q_{O_2}, Q_{N_2}, and $\dot{Q}'_{CH_4}$ are the three unknown flow rates. Since $\Sigma x_i = 1$, the above equations are not independent and one additional equation is required. This additional equation is obtained by relating the above three knowns.

$$(Q_{O_2}/GCF_{O_2}) + (Q_{N_2}/GCF_{N_2}) + (\dot{Q}^*_{CH_4}/GCF_{CH_4}) = \dot{Q}'_{PS} \tag{4.7}$$

where GCF_i is a gas correction factor of component *i*. Since all MFMs and MFCs were calibrated using N_2 at the STP conditions, the measured flow rates (the apparent flow rates) are equivalent to the flow rate of N_2 at 0°C and 1 atm. The values for the GCFs were provided by the manufacturer of the MFCs and MFMs and are listed in Table 4.5. The unknown flow rates are determined by solving Eqs. (4.4), (4.5) and (4.7) simultaneously, and the results are shown in Table 4.5.

Table 4.5 The flow rates of individual gases in stream PS.

Gas	GCF_i	$Q_{i,PS}$ (cm^3(STP)/min)	$Q_{i,PS}$ (cm^3(STP)/s)
O_2	0.993	0.0370	0.000616
N_2	1.00	0.0441	0.000735
CH_4	0.72	0.2838	0.004731
PS	-	$\Sigma Q_{i,PS} = 0.3650$	$\Sigma Q_{i,PS} = 0.006082$

4.3.2.2 Driving force for gas permeation

The driving force for the permeation of component i (Δp_i) through a membrane is the difference between the partial pressures of component i on the high-pressure side and the low-pressure side of the membrane. In case of gas mixtures, the compositions of feed and permeate change as they flow along the membrane. In the absence of significant resistance to gas flow on either side of the membrane and when membrane area is very small, as in this work, the separation process can be described by the complete mixing model (Stern in Meares, 1976). According to this model, the driving force for permeation of component i through a membrane is given by,

$$\Delta p_i = p_R x_{i,R} - p_{PS} x_{i,PS} \tag{4.8}$$

4.3.2.3 Membrane area and thickness

The effective area of membrane for gas permeation (A) is determined by the diameter of a seal, which when the upper and lower part of the membrane cell are put together, is in contact with the membrane surface, preventing leaks from the high-pressure side of the membrane to the atmosphere. In each membrane cell, the diameter of seal is 4.1 cm and therefore, the effective area of membrane for gas permeation is 13.2 cm^2.

All films were prepared by pouring a polymer solution inside a stainless steel ring of 3 inches diameter fixed on glass plate. The solution concentration was adjusted to obtain the desired film thickness. The films were removed from the glass plate by floating them off the glass surface. The polymer density used for calculating the thickness was 1.06 g/cm^3.

The average thickness of a membrane is calculated from the mass (m) and density (ρ) of membrane, and A, using the following equation,

$$l = \frac{m/\rho}{A} \tag{4.9}$$

Since membranes investigated in this project were prepared by complete evaporation of solvent, they had a dense homogeneous structure. Consequently, the density of membrane was considered to be equal to the density of polymer, which for PPO is $\rho = 1.06$ g/cm^3. The mass of the membrane was measured using an AG204 balance, purchased from Mettler Toledo, which had a resolution of 0.1 mg. The samples for the determination of the average thickness were cut along the mark imprinted by the seal on the membrane surface. Therefore, the sample area was the same as the effective area of membrane for gas permeation ($A_m = 13.2$ cm^2).

In Figure 4.4, the thickness is plotted vs to the volume of the solution used to prepare the membranes. The thickness does not increase proportionally with the solution volume, e.g. increasing the solution from 1 ml to 2 mL does not necessarily double the thickness. This happens because some of the polymer solution sticks to the metal ring forming a thick edge of the polymer around the membrane.

4.3.2.4 Error estimation

The error in the calculation of permeation is inherited from random errors in the measuring instruments and the reading thereof. If permeance is calculated by equation (4.2):

$$P_i/l = \frac{Q_i}{\Delta p_i A} \tag{4.2}$$

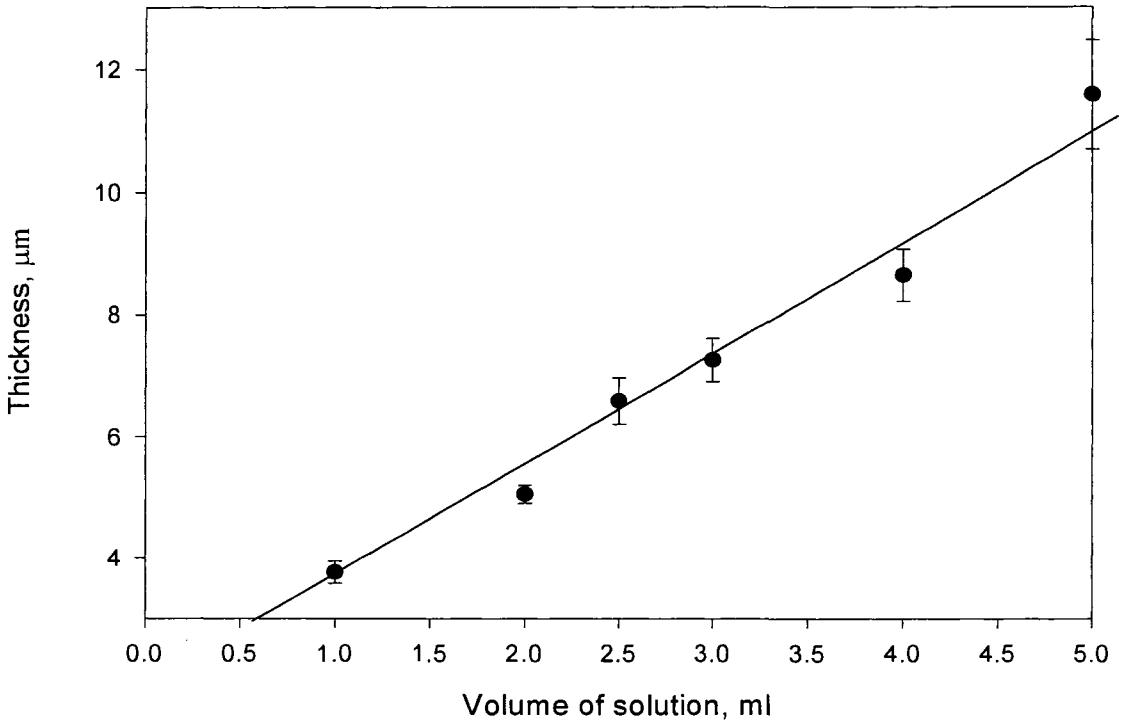

Figure 4.4 Thickness change with the cast solution volume for PPO membranes cast in 3 inches ring.

The probable collective error in the permeance is approximately the sum of the products of the errors in each term times the effect that term has on the value of the permeation rate. If the error of the mass flow controller (MFM) is 0.1 cm^3/min, and the error of the pressure transducer is 0.1 bar, the calculated probable error is calculated to be around 0.0438 for the sample data used in this section, which is 4.38 %. This could become larger if the apparent reading by MFM is lower. Therefore, keeping the flow of the sweep gas high will not only improve the GC sensitivity, but also decreases the probable error.

CHAPTER 5

The Effect of Gas Pressure and the End Effect of Physical Aging on Gas Transport Properties of Poly (Phenylene Oxide) (PPO) Membranes

5.1 Introduction

Membrane gas separation emerged as an alternative gas separation technology almost three decades ago. Since then the research on gas separation membranes has concentrated in two major areas, development of new polymeric materials with very high intrinsic selectivities for gases, and fabrication of defect-free, high productivity membranes. This research has lead to some commercial applications of gas separation membranes including the production of high purity nitrogen from air, recovery of hydrogen from mixtures with larger components such as nitrogen, methane, and carbon monoxide, and purification of natural gas by removal of carbon dioxide (Prasada and Shaner, 1994).

Capitani et al. (1993) attributed the higher permeability of O_2 over N_2 to the presence of chemical affinity between O_2 molecules and the PPO material. They found that O_2 molecules were preferably adsorbed to the benzene ring in the PPO repeat unit, which was thought to be the reason for the higher permeability of O_2 over N_2 in this polymer. On the other hand, Alntiev et al. (1998) ascribed the higher permeability of O_2 in PPO to physical construction of PPO membranes. They pointed out similarity between the PPO membrane structure and that of zeolites. They called it the cavity and throat construction, where the throat has an average size between the kinetic diameters of O_2 and N_2, 3.46 and 3.64 A, respectively. They attributed the higher permeability of O_2 to the presence of this mesopores-like construction, which allows more O_2 molecules to be adsorbed to the membrane and diffuse through its matrix. Singh and Koros (1996) rationalized for the higher O_2 permeation to the entropic selectivity of the diffusion process in the membrane.

5.2 Theoretical Background

Permeability, P, of gas through a polymeric membrane is often related to the thermodynamic properties by the following equation,

$$P = DS = D_0 \exp[-\frac{E_D}{RT}] S_0 \exp[-\frac{\Delta H_s}{RT}] \tag{5.1}$$

where D and S are diffusion and solubility coefficient, respectively, E_D and H_s are the activation energy of diffusion (energy required to create a gap between polymer segments through which the gas molecules diffuse) and enthalpy of solution, respectively, and D_0 and S_0 are pre-exponential factors (Vieth, 1994).

Looking into the diffusion coefficient more in detail, Singh and Koros further derived the equation for diffusion selectivity between gases A and B.

$$\frac{D_A}{D_B} = \exp[\frac{\Delta S^{\pm}_{A,B}}{R}]\exp[\frac{-\Delta E^{\pm}_{A,B}}{R}] \tag{5.2}$$

where $\Delta S^{\pm}_{A,B}$ and $\Delta E^{\pm}_{A,B}$ are differences of activation entropy and enthalpy, respectively, for the gases A and B. They have emphasized the importance of the entropic factor in the selectivity of the membranes made of zeolite and carbon molecular sieve (Singh and Koros, 1996). Using a similar relationship, Acharya and Foley evaluated activation energies experimentally for nanoporous carbon membranes. The activation energies were further correlated to the molecular sizes of gases, assuming that the entropy term is dominant (Acharya and Foley, 2000).

As for the membrane structure-performance relationship, it was reported that the selectivity of the top skin layer of the asymmetric membrane was higher than the dense membrane of the same polymeric material (Pfromm et al, 1993). Kawakami et al. further reported that the gas selectivity of asymmetric polyimide membranes with an ultrathin and defect-free surface thin layer increased with a decrease in the skin layer thickness. They attributed this phenomenon to the formation of a better packed structure in a thinner skin layer, increasing density and order in the molecular arrangement (Kawakami et al., 1998). Thus, the higher selectivity in the thinner polyimide membranes may have been caused by the decrease in entropy of gas molecules in the highly ordered macromolecular structure. Khulbe et al., on the other hand, studied the morphology of dense polyphenylene oxide (PPO) membranes by the combination of atomic force microscopy (AFM) and plasma etching technique and showed that the packing of nodules was the

most compact at the top surface, the surface faced to air when the polymer dope was cast into a film, and the compactness diminished gradually as the distance from the top surface increased (Khulbe et al., 1998).

In this work, the membranes were prepared by the standard method described in Chapter 2. Here, the definition of the membrane surface is in order. The surface which was exposed to air, when the polymer solution was cast, is called "top side", while the surface that was in contact with the glass plate is called "bottom side". Unless otherwise stated, the air top surface faced the feed gas stream in the permeation experiments, unless otherwise stated. The membranes were subjected to stabilization to complete, almost, membrane aging before they were mounted to the permeation cell. Since there are several membranes of different thicknesses involved in this section and they were stabilized under different conditions and subjected to different permeation tests, the membrane thickness, the stabilization method and the permeation experiments to which the membranes were subjected are summarized in Table 5.1.

The automated multi-cell sweep-gas constant pressure system was used for the permeation experiments.

The permeability, P_i, for oxygen and nitrogen was calculated by

$$P_i = Q_i l / \Delta p_i A \tag{5.3}$$

from the permeation rate, Q_i, data obtained from the permeation experiments.

The permeability ratio, α, is obtained by

$$\alpha = (P_{oxygen})/(P_{nitrogen}) \tag{5.4}$$

It should be noted that the above equations are applicable for both single gas (either oxygen or nitrogen) and mixed gas (air in the feed) experiments.

Table 5.1 Summary of membrane thickness, stabilization method and permeation experiment

Membrane		Treatment	Permeation experiment
Thickness	**Membrane surface faced to pressurized feed**		
6.7	Top	Continuous air permeation experiments for two weeks	Air and single gas permeation test at pressures from 20 to 100 psig
10.6	Top	Continuous air permeation experiments for two weeks	Air and single gas permeation test at pressures from 20 to 100 psig
12.4	Top	Dried at 100°C in a vacuum oven for 3 days and dried at ambient temperature	Air and single gas permeation test at pressures from 20 to 100 psig
8.6	Top and bottom	Continuous air permeation experiments for two weeks	Air permeation test at pressures from 20 to 100 psig
3.9A	Top	Dried at 100°C in vacuum for a week	Air permeation test at 50 psig for 160 hours, pressure relaxation test, and then air permeation test at 100 psig
3.9B	Top	Dried at 100°C in vacuum for a week	Air permeation test at 50 psig for 160 hours
20.0	Top	Dried at 100°C for a week	Air permeation test at 50 psig for 120 hours and then air permeation test at 100 psig
15.5	Bottom	Dried at 100°C for a week	Air permeation test at 50 psig for 120 hours, pressure relaxation test, and then air permeation test at 100 psig

5.3 Results

5.3.1 Effect of Gas Pressure on Membrane Properties

The first three membranes with thicknesses of 6.7, 10.6 and 12.4 μm were subjected to air and pure O_2 and N_2 gas permeation tests under different gas pressures. Figure 5.1 shows the results of air permeation experiments. The permeability of O_2 and N_2 is shown for membranes of different thicknesses at different feed air pressures. O_2 permeability increases with an increase in pressure continuously from 25 to 100 psig. On the other hand, O_2 permeability decreases with an increase in membrane thickness. N_2 permeability decreases from 25 to 50 psig, and then levels off for a further increase in pressure. N_2 permeability increases with an increase in membrane thickness from 6.7 to 10.6 μm and then levels off with a further increase in the thickness.

Figure 5.2 shows that the permeability ratio increases with the feed pressure with an exception of the 12.4 μm membrane, for which the permeability ratio decreases from 50 to 100 psig. It is also observed that the permeability ratio decreases with an increase in membrane thickness. Nearly the same trends observed for the three different membranes ensure that the membranes were equally stabilized regardless of the adopted stabilizing procedures.

Figure 5.3 shows experimental results for the permeation of single gases, when the membrane thickness was 12.4 μm. Generally, higher permeability values were obtained from the air experiments than the single gas experiments for both oxygen and nitrogen, although the trend observed for the effect of the pressure on the oxygen and nitrogen permeability was the same for both air and single gas experiments. Differences

in the permeability values between the air experiments and the single gas experiments suggest that the presence of one gas affects the permeability of the other.

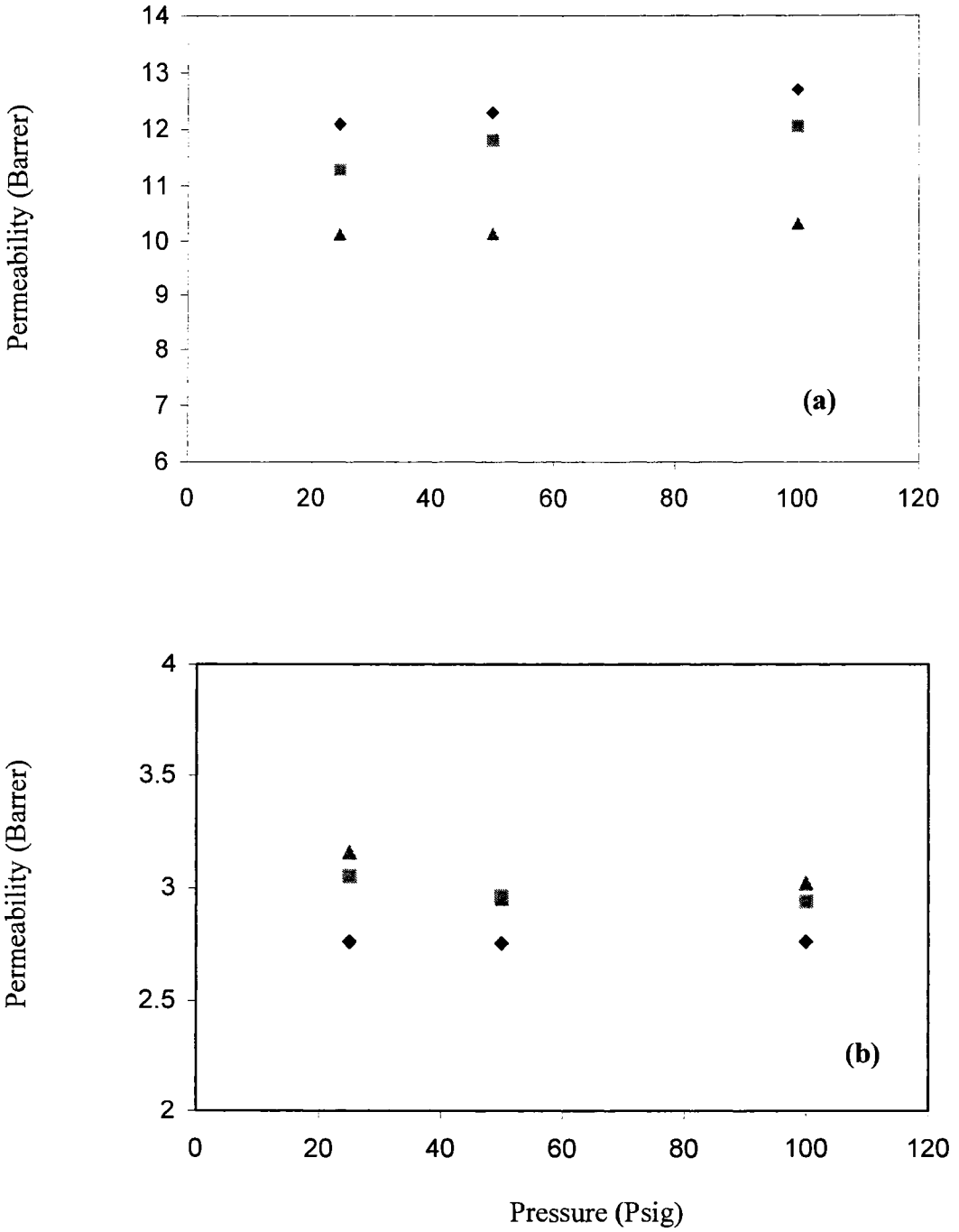

Figure 5.1 Permeability change with air pressure (a) O_2 (b) N_2 of membranes with different thicknesses ♦ 6.7 μm, ▪10.6 μ m and ▲12.4 μm.

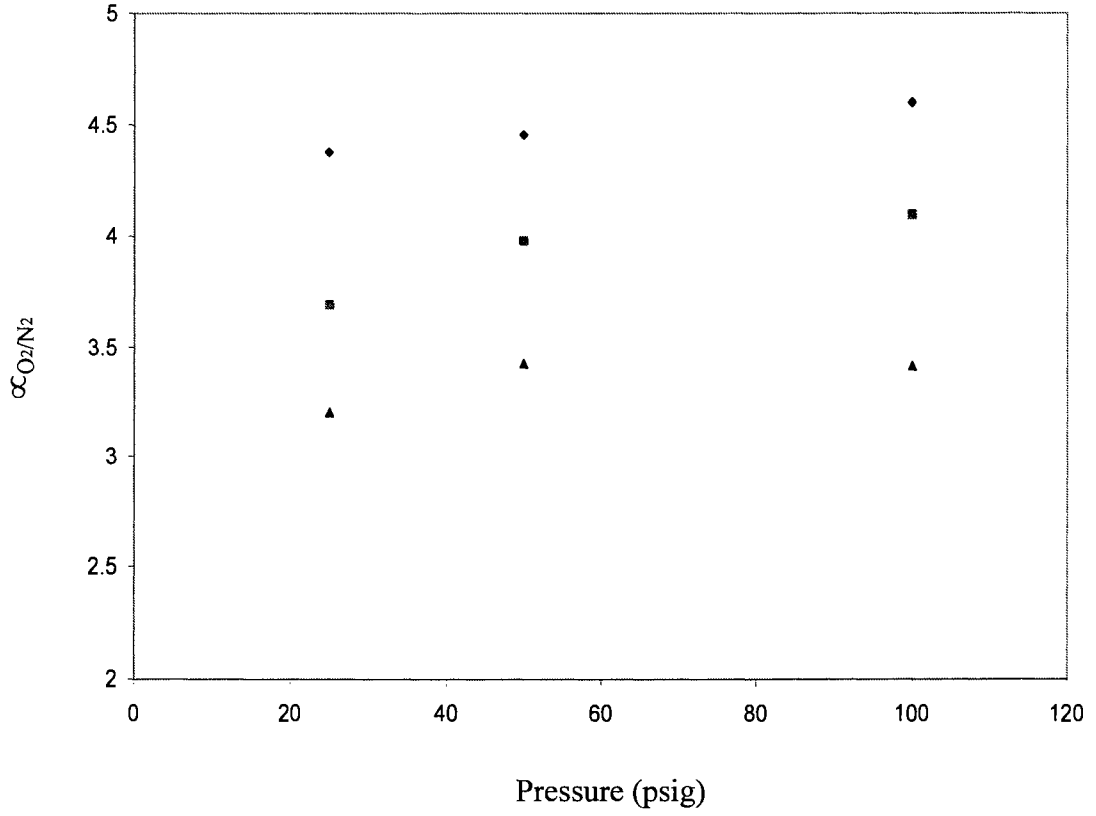

Figure 5.2 Permeability ratio $\alpha_{O2/N2}$ change with air feed pressure for membranes with different thicknesses ♦ 6.7 μm, ▪10.6 μm and ▲12.4 μm.

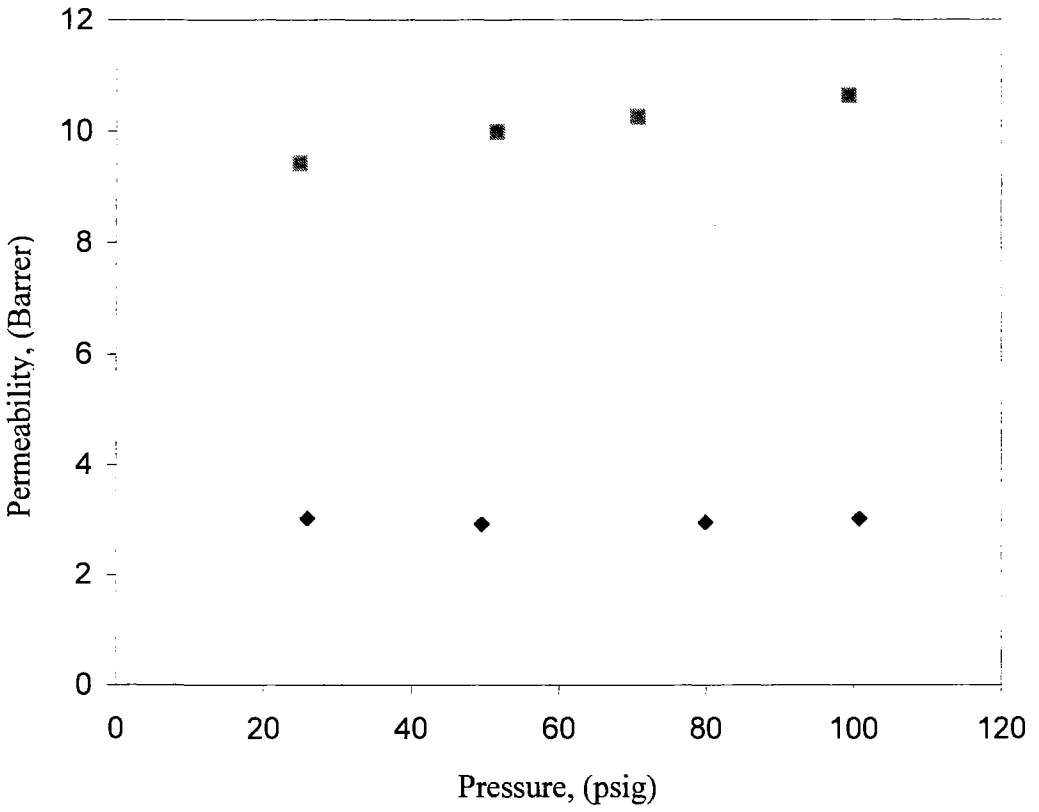

Figure 5.3 Change in permeability of single gases permeation ■ O_2 and ♦N_2 for 12.4 μm.

A symmetry test was conducted by a set of experiments using the fourth membrane in Table 5.1 with a thickness of 8.6 μm. The membrane was subjected to a stabilization procedure similar to the membranes with thicknesses 6.7 and 10.6 μm. Here, the definition of the membrane surface is given once more. The surface which was exposed to air, when the polymer solution was cast, is called "top side", while the surface that was in contact with the glass plate is called "bottom side". The top side was always in contact with the air stream during the permeation and separation experiments, unless otherwise stated. In the symmetry test, pressure was changed progressively from 100 (689 kPa) to 50 (344 kPa) and then to 25 (172 kPa) psig within the first 15 hours, maintained at 25 psig for 13 hours and then brought back to 100 psig during the last 17 hours. This pressure change is illustrated in Fig. 5.4.

Then, the membrane was flipped upside down; i.e. the bottom side was brought into contact with the feed air stream. The same program for the pressure change was applied. The permeability data are also shown in Fig. 5.4. The following trends are observed from the figure.

1) The permeability of both oxygen and nitrogen decreased when the direction of the air permeation was changed.

2) For nitrogen gas, permeability decreased as the pressure increased regardless of the air permeation direction. This trend is the same as those shown in Figs. 5.1 and 5.3.

3) For oxygen gas, permeability increased as the pressure increased when the direction of air permeation was from the top to the bottom side. This trend is the same as those given in 5.1 and 5.3.

4) The oxygen permeability, however, decreased as the pressure increased when the direction of air permeation was reversed.

In other words, the performance of the membrane was not symmetric across the cross-section.

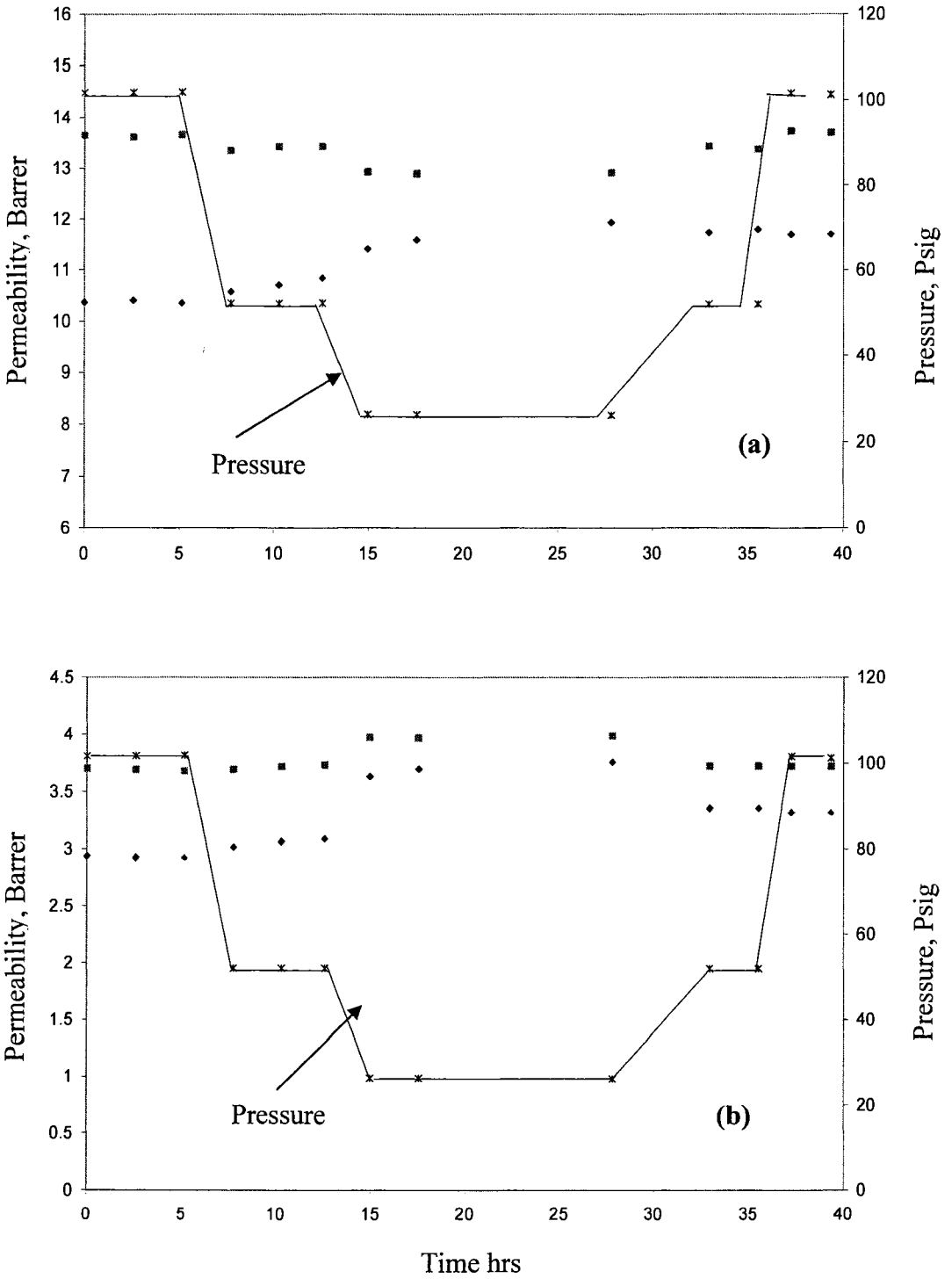

Figure 5.4 Permeability change with air pressure (a) O_2 (b) N_2 for membranes fed from different surfaces ▪ top surface,♦bottom surface.

The experimental data presented in Figs. 5.1-5.4 can be explained within the framework of the following assumptions.

1) As the pressure increases, the macromolecular segments are displaced close to each other. As a result of this segmental motion, inter-segmental void space decreases and the density of the polymer increases. Unlike aging that requires a long period to take place, the segmental motion under the pressure is sudden and reversible.

2) The energy barrier to be overcome for the transport of gas molecules through the membrane is directly related to the molar Gibbs free energy of gas molecules in the void space. In the presence of affinity forces between the gas molecule and the macromolecular segment, enthalpy of the gas decreases with a decrease in the void volume since more gas molecules will be under the influence of the affinity forces. The Gibbs free energy, as well as the energy barrier for the transport, decreases ($\Delta G = \Delta H - T\Delta S$), leading to higher permeability. With a further decrease in the void volume, entropy of the gas molecules starts to decrease, since the gas molecules are packed in more ordered form in the smaller void space. Then, the Gibbs free energy increases leading to lower permeability. In the absence of affinity forces between the gas molecule and the macromolecular segment, on the other hand, the enthalpy effect can be ignored. In this case, gas permeability decreases monotonically as the void space decreases. The effect of void space decrease on the permeability is schematically presented in Fig. 5.5a (in the presence of affinity forces) and b (in the absence of the affinity forces).

Oxygen molecules are more attracted to macromolecular segment of PPO than nitrogen molecules. This is evidenced by the higher solubility of oxygen in PPO (Capitani et

al., 1993 and Alntiev et al., 1998). Therefore permeability pattern given in 5.5a is applicable for oxygen, while pattern 5.5b for nitrogen.

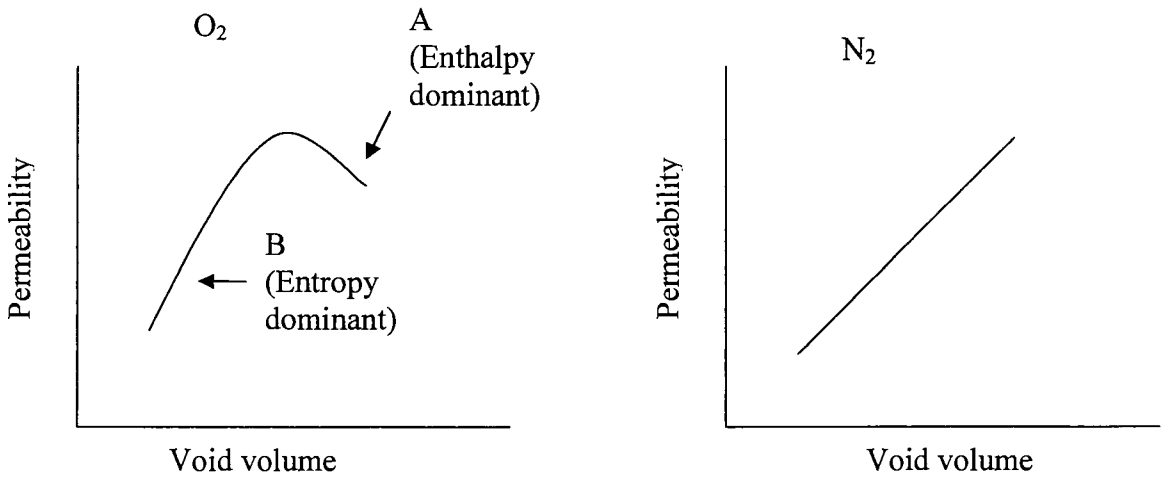

Figure 5.5 Permeability change with void volume: schematic illustration (a) oxygen, (b) nitrogen.

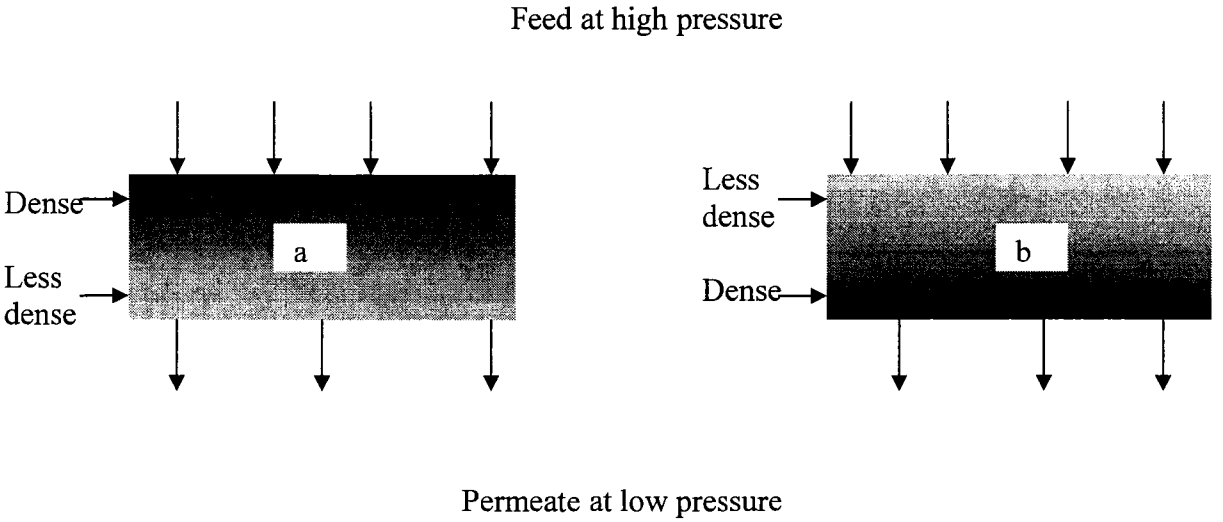

Figure 5.6 Membrane surfaces facing feed air (a) top surface is in contact with feed air, (b) bottom surface is in contact with air.

3) Even though dense PPO membranes were prepared in this work, they have morphological asymmetry. The polymer density is a function of the distance from the top surface. As the distance increases the density decreases while the inter-segmental void space increases.

With the three assumptions stated above, the experimental results given in Fig. 5.1a and 5.1b can be explained. In the case of oxygen, the inter-segmental void space decreases and gas permeability increases with an increase in the total gas pressure, particularly when gas molecules are in the region governed by enthalpy. (region A in Fig. 5.5a). As the membrane thickness increases, the overall density of the membrane decreases, therefore gas permeability decreases. In the case of nitrogen, on the other hand, the enthalpy dominant region does not exist (Fig. 5.5b). As a result, nitrogen permeability decreases with an increase in pressure and increases with an increase in membrane thickness. Fig. 5.2 is simply a result of the combination of Figs. 5.1a and b. Fig. 5.3 confirms the trend observed in air experiments by the experiments with individual gases.

The results shown in Fig. 5.4 can be explained considering the pressure distribution across the membrane changes from high to low as you go down from the feed side to the permeate side. When the membrane is flipped upside down, the lower density side of the membrane is near the feed gas and compacted more under higher pressure (Fig. 5.6b). Before flipping the membrane, the high density side of the membrane was near the feed gas (Fig. 5.6a) and compaction was not as strong as after membrane flipping. Therefore, the overall density of the membrane is higher with membrane flipping than without membrane flipping. This increase in density brings the membrane to the entropy governing region (region B in

Fig. 5.4a) of oxygen permeation. The membrane with a small thickness, 8.6 μm was used in this experiment. Since this membrane had already a quite high density due to its thinness, a further increase in density may bring the permeability into the entropy dominate region. Hence, the oxygen permeability decreases as the pressure increases. The oxygen permeability is also lower after membrane flipping than before flipping. Nitrogen permeability on the other hand, always decreases as the pressure increases according to Fig. 5.5a. It also decreases when the membrane is flipped.

5.3.2 Final Effect of Aging on PPO Membranes with Different Morphology

The permselective properties of glassy membranes could be affected by irregularity in their structure. Asymmetry, which affects thick membranes, and the presence of defects, which affects thin membranes, cause an increase in permeability and a decrease in selectivity. Because the physical aging of gas separation membranes is observed by the changes in the permselective properties, structural irregularity might affect these observations, too. To investigate the possible effect of these irregularities, thick and thin membranes were aged for a week in vacuum at 100 ^{0}C. Then, these membranes were subjected to gas pressure to compare the changes in their permselective properties. The purpose of the thermal aging step is not to stabilize the membrane, but to eliminate as much free volume as possible from these membranes. By eliminating most of the excess free volume, it is easier to interpret the effect of structure irregularities on the time dependent changes in such membranes.

5.3.2.1 Effect of defects on the aging of thin membranes

Even though it was attempted to make each membrane dense and homogeneous, sometimes invisible defects were formed. These defects and pinholes, when exist, affected the permeability, and hence selectivity, of the membranes considerably. Some interesting observations were made when the permeability was monitored as a function of the operating period.

Air permeation experiments were conducted with 5th and 6th membranes listed in Table 5.1, designated as 3.9A and 3.9B, respectively, prepared under the same conditions; i.e. the thickness was 3.9 μm and the membranes were isothermally aged in vacuum for one week at 100°C. Other details of the membrane preparation are given in Chapter 2. Membranes were placed in the permeation cell and air permeation experiments were conducted at 50 psig for more than 160 hours. Fig. 5.7 shows the results of the air permeation experiments. The permeability for the gas components, O_2 and N_2, is plotted individually versus the operating period. Fig. 5.8 shows the permeability ratio.

From Fig. 5.7, the following observations were made.

1) The permeability of 3.9A is much smaller than that of 3.9B.
2) The permeability of both O_2 and N_2 showed continuous decrease throughout the experimental period for 3.9A, while O_2 permeability showed slightly a maximum at 70 hours and N_2 permeability kept increasing for 3.9B.
3) As for the permeability ratio, it was almost constant for 3.9A throughout the experiment, while for 3.9B it kept decreasing.

These above observations can be interpreted by the following assumptions.

1) Membrane 3.9A is defect free, while 3.9B has defects.
2) In the membrane matrix, the macromolecular segments keep moving toward each other during the operational period, leading to the decrease in free volume.
3) When defects are present, the sizes of the defects keep increasing with an increase in the operating period. This assumption can be justified since the gas pressure works from inside the defect to its wall.

Since membrane 3.9A is defect free, only the second effect (decrease in free volume) works, which leads to the steady decrease in the permeability of both O_2 and N_2. Since membrane 3.9B has defect, the sizes of which will increase with the operating period, the permeability ratio will gradually decrease (Fig. 5.8). Consider that the theoretical permeability ratio for O_2/N_2 pair is only 1.07 for the Knudsen flow that is supposed to be dominant in the pinholes.

The steady increase in the nitrogen permeability through 3.9B (Fig. 5.7) is due to the increase in the defect size and the resulting increase in the Knudsen flow contribution. This increase, however, should level off since the defects can not grow infinitely. The initial increase in the oxygen permeability through 3.9B is also due to the defect growth. However, in the latter stage of experiment, the free volume effect (the 2^{nd} effect) will manifest itself, in the case of oxygen, since the permeation rate through the polymer matrix contributes to the total permeation rate much more for oxygen than for nitrogen. The oxygen permeability then starts to decrease. It was also found later the permeability of 3.9B increased more than two fold, while for 3.9A the permeability was practically

unchanged as the operating pressure was increased, which is another evidence of the presence of pinholes in membrane 3.9B.

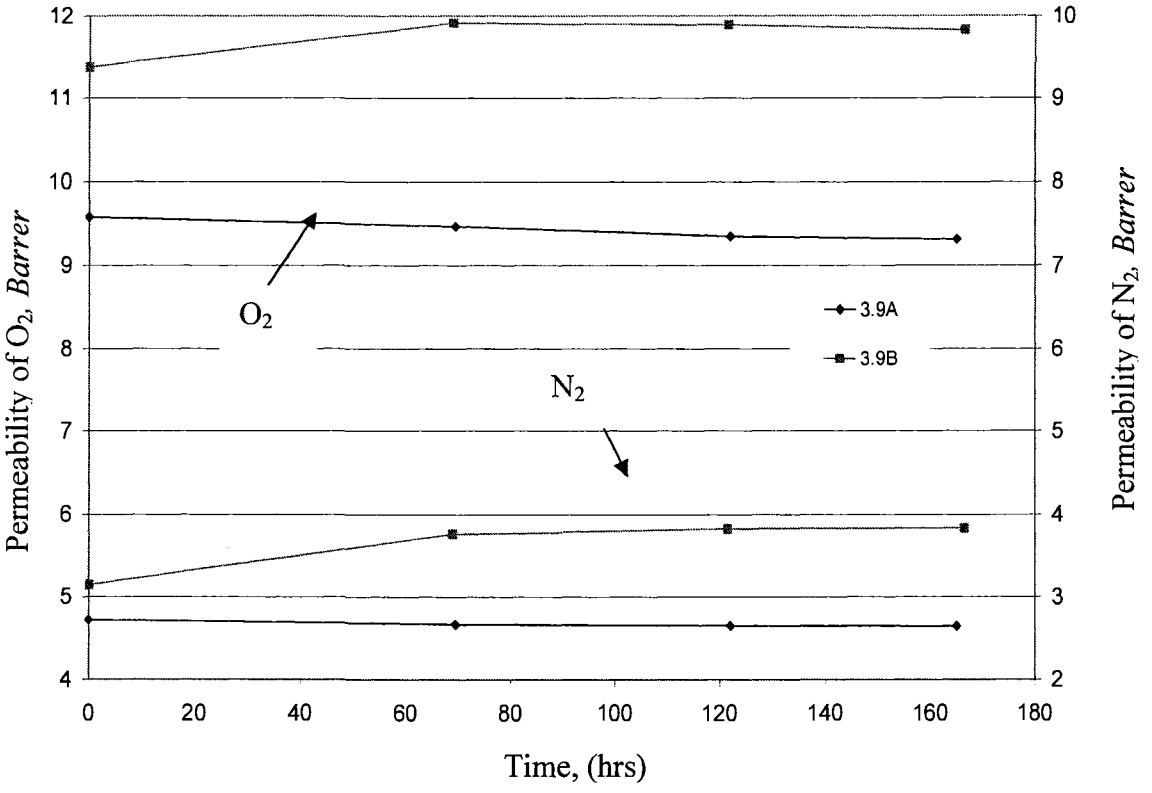

Figure 5.7 The changes in the permeability of O_2 and N_2 with time for pre-aged membranes with 3.9 μm; feed gas pressure is 50 psig.

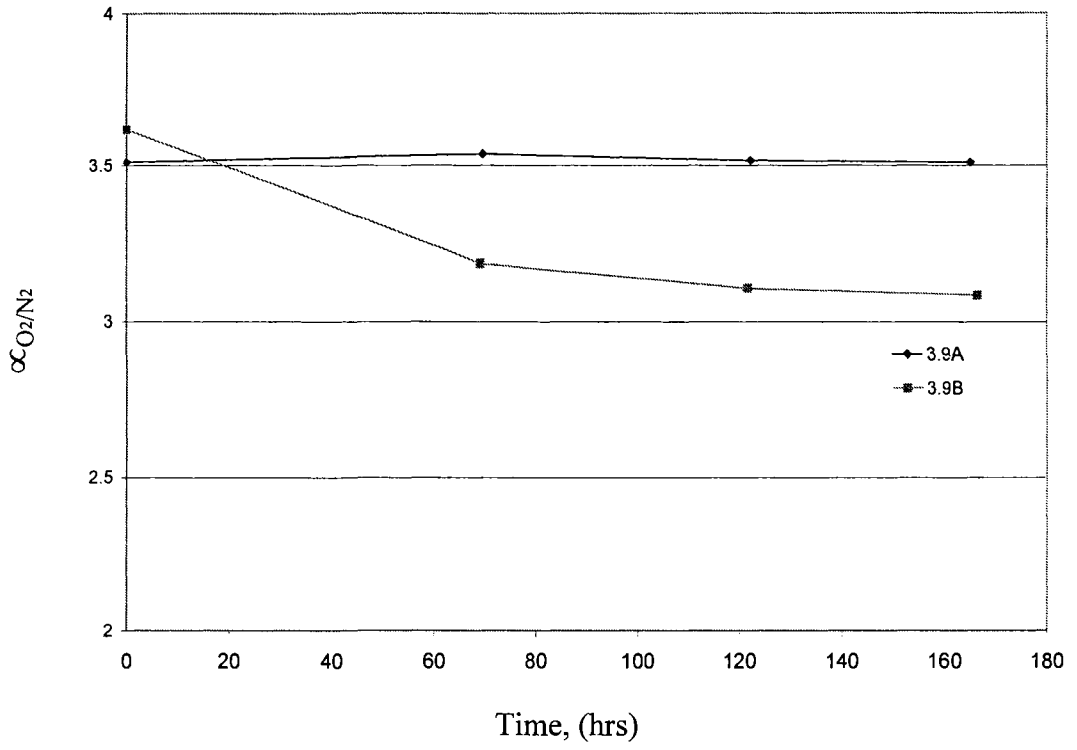

Figure 5.8 The changes in permeability ratio $\alpha_{O2/N2}$ with time for thermally aged membranes with 3.9 μm thickness; feed gas pressure is 50 psig.

5.3.2.2 Effect of asymmetry on the aging of thick membranes

The next set of air permeation experiments were carried out using the last two membranes listed in Table 5.1, i.e. with thicknesses of 20.0 and 15.5 μm, respectively. The membrane preparation followed the standard procedure. Then, they were treated under vacuum at 100°C for one week. After the membranes were cooled to the room temperature, they were mounted to the permeation cell and the air permeation experiments were conducted at the feed air pressure of 50 psig for 120 hours. Therefore, the membranes are considered to be aged when the following experiments are started. Both membranes are considered to be thick membranes with a density profile illustrated in Fig. 5.6 (a); i.e. the top surface has the highest density and as the distance from the top surface increases the density decreases.

Membrane 3.9A was also used in this set of experiments after it was proved defect-free by the experiments described in section 5.3.2.1. This membrane is much thinner than the other two thick membranes. Since the distance from the top layer is limited to below 3.9 μm, the density of this membrane is considered high from the top to the bottom.

When the two thick membranes were mounted to the permeation cell, one of the membranes (with 20 μm thickness) was mounted as shown in Fig. 5.6 (a), i.e. the top dense surface faced the feed stream under pressure. On the other hand, when the other membrane (with 15.5 μm thickness) was mounted, the membrane was flipped, i.e. the least dense surface faced the feed stream under pressure.

The air permeation experiments were conducted with these two membranes under the feed pressure of 50 psig for about 120 hrs. The results are shown in Fig. 5.9 (a), where

the individual permeabilities of O_2 and N_2 are given versus the operating time, and in Fig. 5.9 (b), where the relative permeability ratio, defined as (the permeability at time t/ the initial permeability) is given. Figs. 5.9 (a) and (b) show clearly,

1) The permeability becomes lower when the membrane is flipped, i.e. the bottom side of the membrane is brought to contact with the feed under pressure.
2) The relative permeability is lower when the membrane is flipped. The decrease in relative permeability is most remarkable for the nitrogen permeability of the flipped membrane.

The first observation is in accordance with the observations given in Fig. 5.4 (a) and (b), which have already been explained. The second observation is also reasonable, since membrane compaction takes place faster when the bottom (the less dense) side of the membrane is in contact with the feed stream under high pressure.

Another set of experiments was conducted using the thin membrane with a thickness of 3.9 μm (3.9A) and a thick membrane with a thickness of 15.5 μm. Remember that these membranes have been subjected to air permeation experiments at 50 psig for a long time, i.e. 160 hours for 3.9 μm and 120 hours for 15.5 μm. It should also be reminded that the latter membrane was flipped upside down when mounted in the permeation cell.

After the air permeation experiments under the feed pressure of 50 psig, the pressure on the feed side of these two membranes was released and maintained at atmospheric pressure for 20 hours. Then, the feed pressure was increased again to 50 psig and the air permeation experiments were repeated. The individual permeability data of O_2

and N_2 for both membranes are shown in Table 5.2. It is clear that the permeability decreased both for O_2 and N_2 significantly with respect to the membrane of 3.9A, while the change was insignificant with respect to the membrane of 15.5 μm. The decrease in the permeability of the membrane 3.9A is due to the aging that has been proceeding even during the period of pressure release. The aging must be likewise proceeding with the membrane of 15.5 μm. It should be remembered however that the less dense side of this membrane was in contact with the feed gas of high pressure and the membrane was subject to a strong compaction effect during the air permeation experiment before the pressure release. Since the compaction is reversible, the membrane was temporarily relaxed while the pressure was released. These two opposing effects, one the aging and the other the membrane relaxation during the pressure release, compensate with each other, resulting in the insignificant change in the permeability.

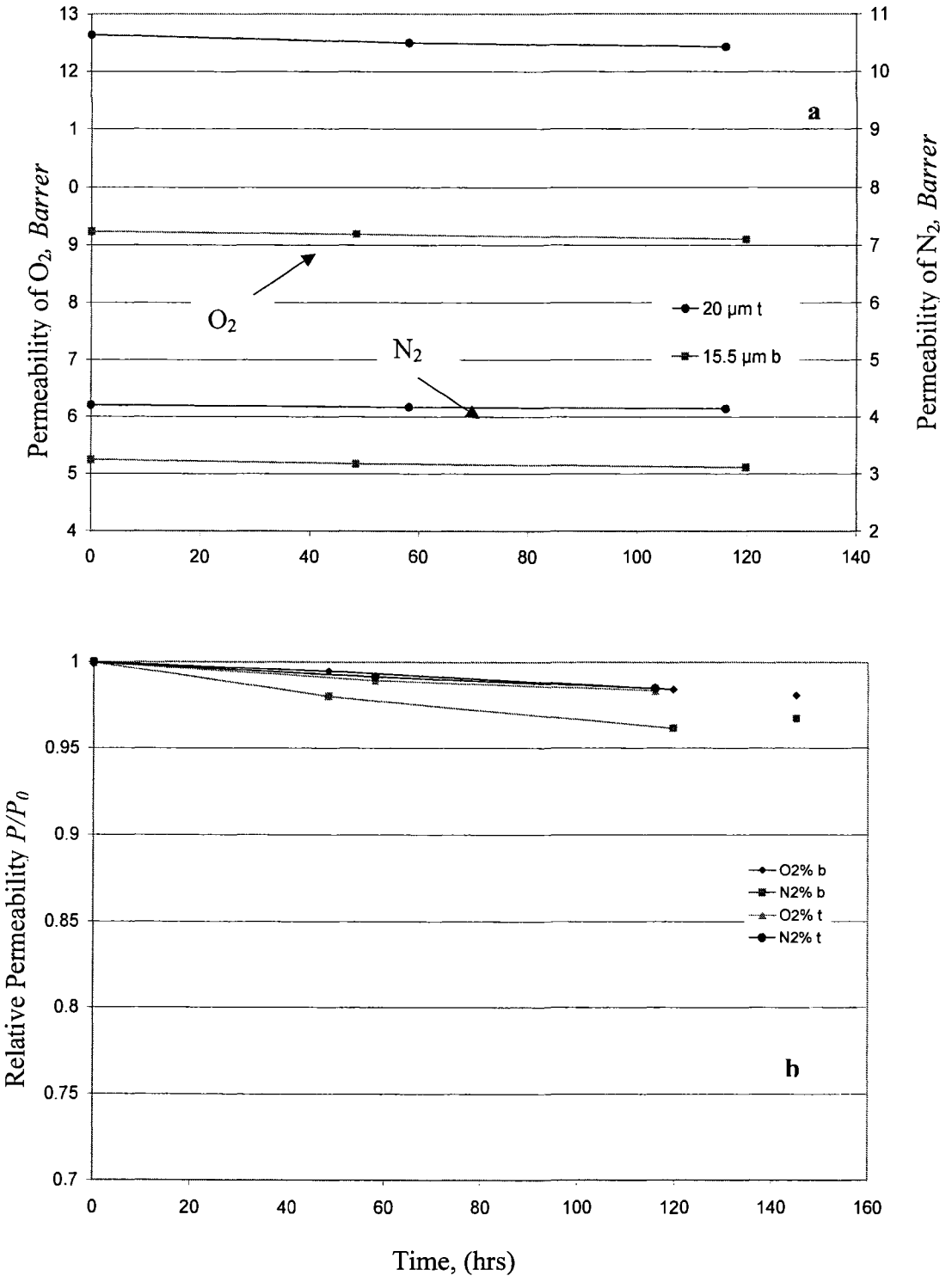

Figure 5.9 The changes in the permeability and the relative permeability of O_2 and N_2 with time for membranes with 20 µm (top side in contact with feed gas) and 15.5 µm thickness (bottom side in contact with feed gas); feed gas pressure is 50 psig.

Table 5.2 Changes in permeability through thin membrane and thick membrane fed from the bottom.

Membrane		**Permeability, Barrer**			
Thickness	**Surface in contact with feed air**	**Before pressure release**		**After pressure release**	
		O_2	N_2	O_2	N_2
3.9 μm	Top	9.31	2.65	9.07	2.53
15.5 μm	Bottom	9.09	3.11	9.08	3.13

5.3.3.3 Effect of asymmetry on the properties of thick membranes

The last two membranes in Table 5.1 with thicknesses of 20 μm and 15.5 μm, respectively, and one thin membrane with a thickness of 3.9 μm (3.9A) were subjected to air permeation experiments at 100 psig after all the earlier experiments under 50 psig were completed. This is to confirm the effect already observed in the section 5.3.1. It should be recalled that the top side of the membrane with a thickness of 20μm was in contact with the pressurized feed air stream. The thin membrane 3.9A would also behave like the membrane with a thickness of 20 μm, since both of them are supposed to be less susceptible to the compaction effect. On the other hand, the membrane with a thickness of 15.5 μm was flipped and should be more susceptible to the compaction effect. Looking into the results of the symmetry test (Fig. 5.4a), the O_2 permeability increased with an increase in pressure from 50 to 100 psig when the top surface was in contact with pressurized air, which was the case for the membranes with 20 μm thickness and 3.9 μm thickness. On the other hand, O_2 permeability decreased with an increase in pressure for the flipped membrane.

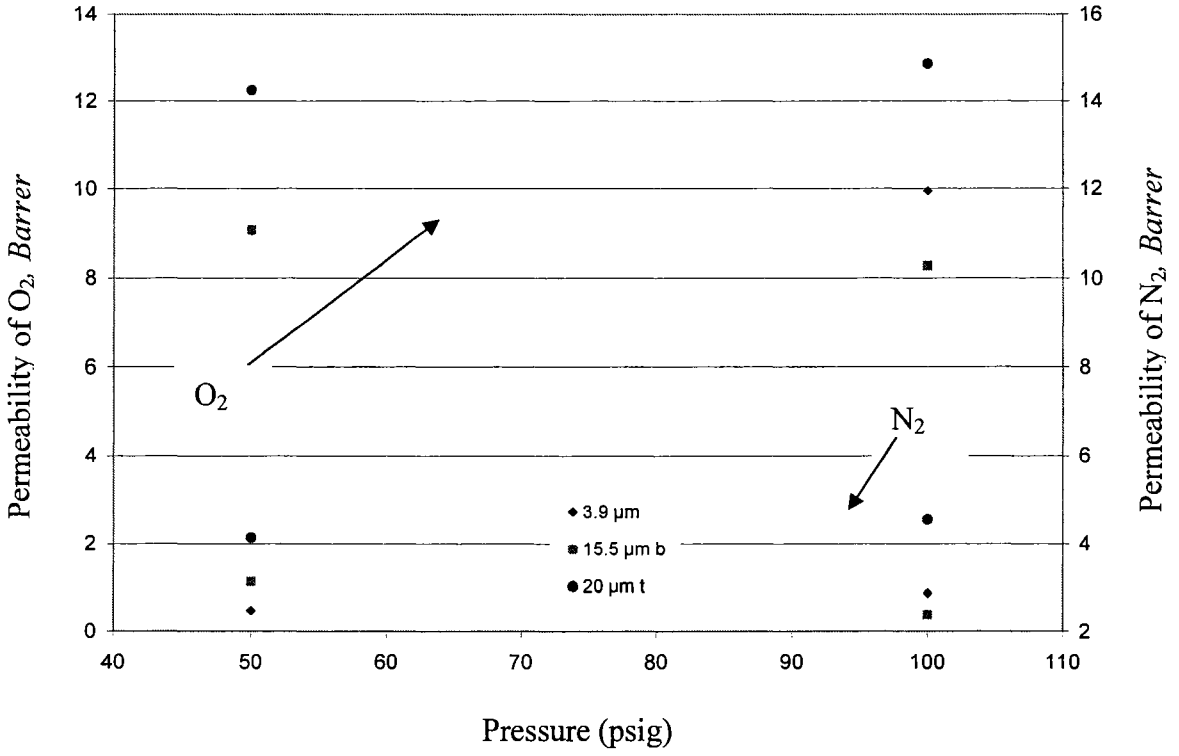

Figure 5.10 The changes in the permeability of O_2 and N_2 with air pressure for membranes with 3.9 µm, 20 µm and 15.5 µm thickness; t (top side) b (bottom side) indicates the side of the membrane facing the feed pressure.

The membrane with a thickness of 15.5 μm should follow the latter tendency. Fig. 5.10 clearly shows the expected trends, confirming the results depicted in Fig. 5.4 (a). Regarding the N_2 permeability, Fig. 5.4 (b) shows that it should either decrease or remain constant as the pressure is increased from 50 to 100 psig, regardless of whether the membrane is flipped or not. Fig. 10 shows that N_2 permeability decreases indeed for the flipped 15.5 μm membrane but for 20 μm membrane N_2 permeability increases with an increase in pressure. This is rather contradictory to the results shown in Fig. 5.4 (b). This may be due to more error in N_2 permeability since their values are much smaller than those of O_2 permeability.

5.5 Conclusions:

The effect of feed gas pressure and membrane thickness on the permeability of oxygen and nitrogen gas has been evaluated. They are characterized by the decrease in the volume of the void space where the gas permeation takes place, the change in the entropy and enthalpy of gas molecules with the change in the void volume as well as asymmetric structure of the dense PPO membranes. The dependence of the feed gas pressure effect on the direction of gas permeation can also be explained.

PPO membrane morphology and aging could be characterized as follows:

1. PPO membranes could be described as thin and thick membranes. Thin membranes are symmetric and dense and their free volume decreases as aging progresses.

2. There is asymmetricity in distribution of free volume of the thick PPO membrane. The free volume increases from the top to the bottom. The larger free volume at the bottom of the membrane is more susceptible to compaction effect.
3. The dense layer is more permeable to O_2. Increase in O_2 permeability with pressure is only the characteristics of thin membranes or the dense top layer of thick membranes.
4. As aging proceeds the contribution of the top dense layer to gas permeation property of the membrane decreases and that of the less dense bottom layer increases.

CHAPTER 6

Effect of Pressure on the Aging of Dense (PPO) Membranes

6.1 Introduction

While glass transition is a change in the thermodynamic status of the polymer,aging is a time dependent process of a glassy polymer. During this process, the excess free volume gradually disappears and the specific volume approaches the equilibrium line (see Figure 3.2) due to macromolecular relaxation. It has been mentioned earlier that the gas permeability is related to free volume. Hence, the change in free volume can be monitored by gas permeability measurements. One of the characteristics of the aging process is its non-linearity. It is featured by the fast reduction of the free volume in the beginning, which is followed by a slower reduction at the later stage.

Physical aging of glassy polymer membranes has been mathematically represented by three models. Zhou et al. (2005) suggested a log-log empirical equation that linearly relates the permeability change to the aging time:

$$\ln P = A + B\ln(t) \tag{6.1}$$

P is gas permeability, t is aging time, and A and B are constants.

The log-log relation has also been applied to physical aging by other researchers (Hutchinson, 1995). This linear relation neglects the fast reduction in free volume in earlier stage of the membrane life.

Teimblo et al. (2001) used the lattice contraction to model the physical aging of PVC membranes. It is in an exponential form that relates the free volume to the aging time.

$$f_{LC} = f_g + (f_i - f_g)\exp\left(-t/\tau\right) \tag{6.2}$$

where f_i is the initial fractional free volume, f_g is a bulk fractional free volume, that is, a pseudo-equilibrium fractional free volume, t is the aging time and τ is the relaxation time. The relaxation time value was adjusted to fit the calculated free volume data to the experimental ones. It was further considered that the relaxation time was not necessarily a single value but had a broad spectrum, depending on the temperature and available free volume.

McCaig et al. (2000) adopted the idea of Curro et al. (1982) to fit their data to a combined model of the lattice contraction and the hole diffusion mechanisms, after they failed to apply the above mechanisms individually. This model is still phenomenological and needs some adjusting parameters for data fitting.

Despite all these attempts, an exact relationship between the gas transport properties and other time dependent changes of the glassy polymer is lacking, which is the result of the absence of definite description of the relaxation process of the glassy polymer.

Moreover, all the presently available models have originated from the earlier studies on liquid viscosities. For example, the relation between gas permeability and polymer free volume (Eq. (2.11)) was originally proposed by Dolittle (1951) based on the dependence of liquid viscosity to the free volume,

$$\ln \eta = a + b/f \tag{6.3}$$

where a and b are constants, and f is the fractional free volume. It should be noted that Eq. (2.11) was applicable to polymeric membranes after they were aged under an isothermal condition for a long time, during which period their semi-stable state is approached. Therefore, it does not contain any time factor. Thus, the utilization of these relations and models to express the aging of the glassy polymer falls short of a success, primarily because of the difference in the molecule structures between the polymer and the liquid.

In glassy polymeric membranes used for gas separation, there are not enough studies on the effect of pressure on the physical aging of glassy polymers. Some examples are the results of Pfromm and Koros (1995) that show acceleration of aging, when the gas pressure is reduced. McCaig and Paul (1999) carried out one experiment to study the effect of gas pressure. They compared the aging time for a 0.74 μm membrane aged under vacuum with that for a 0.58 μm film aged under operating gas pressure in a constant pressure system, and concluded that changing the operating conditions did not influence the aging response; i.e. the gas pressure or the used system had no effect on physical aging. This is opposite to what was concluded earlier by Pinnau et al. (1997) that, the details of how permeation rates were measured could influence the observed aging. Nagai et al. (1995) and Morisato et al. (1999) have found out that aging was faster in constant volume system and suggested that contamination of a sample by the oil vapors

in constant-volume systems with oil-lubricated vacuum pumps might have lead to very significant overestimation of extent of physical aging.

As mentioned above, the physical aging is the time dependent reduction in free volume, which arises from the slowness of the segmental movement (Kauzmann, 1948). The reduction in free volume, in turn, slows down the segmental movement, resulting in reduction in the number of segment repeating units and a change in the movement style from rotational to vibration (Sperling, 2001). In other words, the degree of freedom is reduced (Kauzmann, 1948). The reduction of the degree of freedom affects their visco-elastic properties. In other words, there should be some relationship between the aging of membranes and the visco-elastic properties of the glassy polymer.

The objective of this paper is therefore to make a more thorough study of the aging of gas separation membranes, especially on the effect of the gas pressure on membrane aging. It is also attempted to interpret the gas permeation data based on the concept of mechanical stress-strain relationship such as visco-elasticity of the glassy polymer.

6. 2 Experimental

Although the general methods of membrane preparation and membrane permeation experiments have already described in chapter 4, the methods are briefly summarized below to facilitate the understanding of the contents of this chapter.

6.2.1 Membrane Preparation

The method of membrane preparation was described in chapter 4 with slight modifications. Briefly, a 1 wt% solution of polyphenylene oxide (PPO) (T_g of 212 °C and average molecular weight M_w of 400,000) in trichloroethylene (TCE from Aldrich) was poured into a stainless steel ring fixed on a precisely leveled glass plate. The solution was left for solvent evaporation either for 4 or 14 hours, before the glass plate together with the cast solution film was immersed into a water bath for a short period until the membrane peeled off the glass plate spontaneously. Since the surface of the membrane was wetted in the water bath, the membranes were further dried in ambient air for 2 hours in a free-standing position. The total drying times for all membranes used are either 6 or 16 hours, before being mounted to the permeation cells. The moment when the membrane was mounted to the permeation cell and the feed gas pressure was raised to a set value for the measurement of the permeation rate is defined as time t = 0, even though physical aging started before t = 0.

All membranes are specified in Table 6.1, together with the details of the experiments for which the membranes were used.

6.2.2 Gas Permeation Experiments

Since the permeability coefficient is directly proportional to the gas permeation rate, the changes in the permeability coefficient due to the physical aging of the investigated membranes will be expressed on the basis of the changes in gas permeation rates. Moreover, to facilitate the comparison of the extent of the physical aging in different membranes, a dimensionless permeation rates, Q/Q_0, will be used, where Q_0 is

the gas permeation rate immediately after installing a membrane inside the testing cell, i.e., at $t = 0$.

In this work two setups for gas permeation experiments were used. One is an automated multi-cell sweep-gas constant pressure system, abbreviated as C-P system hereafter. The other system is a constant volume system, abbreviated as C-V system hereafter. The C-P system was shown in details in the experimental part (chapter 4), and the C-V system is briefly outlined below.

6.2.2.1 Constant volume system (C-V system)

The schematic of the constant volume system is shown in Fig. 6.1. The details of the system are given elsewhere (Tabe et al. 1995). Briefly, the gas permeation rate is determined by monitoring the rate of pressure change on the permeate side, the total volume of which is maintained constant. Hence, it is called constant volume system. According to this technique, the total permeation rate, Q (cm^3 (STP)/s), is calculated by assuming the ideal gas behavior of the gas. Hence,

$$Q = (V/RT)(dp/dt) \tag{6.4}$$

where V is the total volume on the permeate side (cm^3), R is universal gas constant (62,356 cm^3 mmHg/mol K), T is absolute temperature (K) and dp/dt is the rate of the pressure increase on the permeate side (mmHg/s).

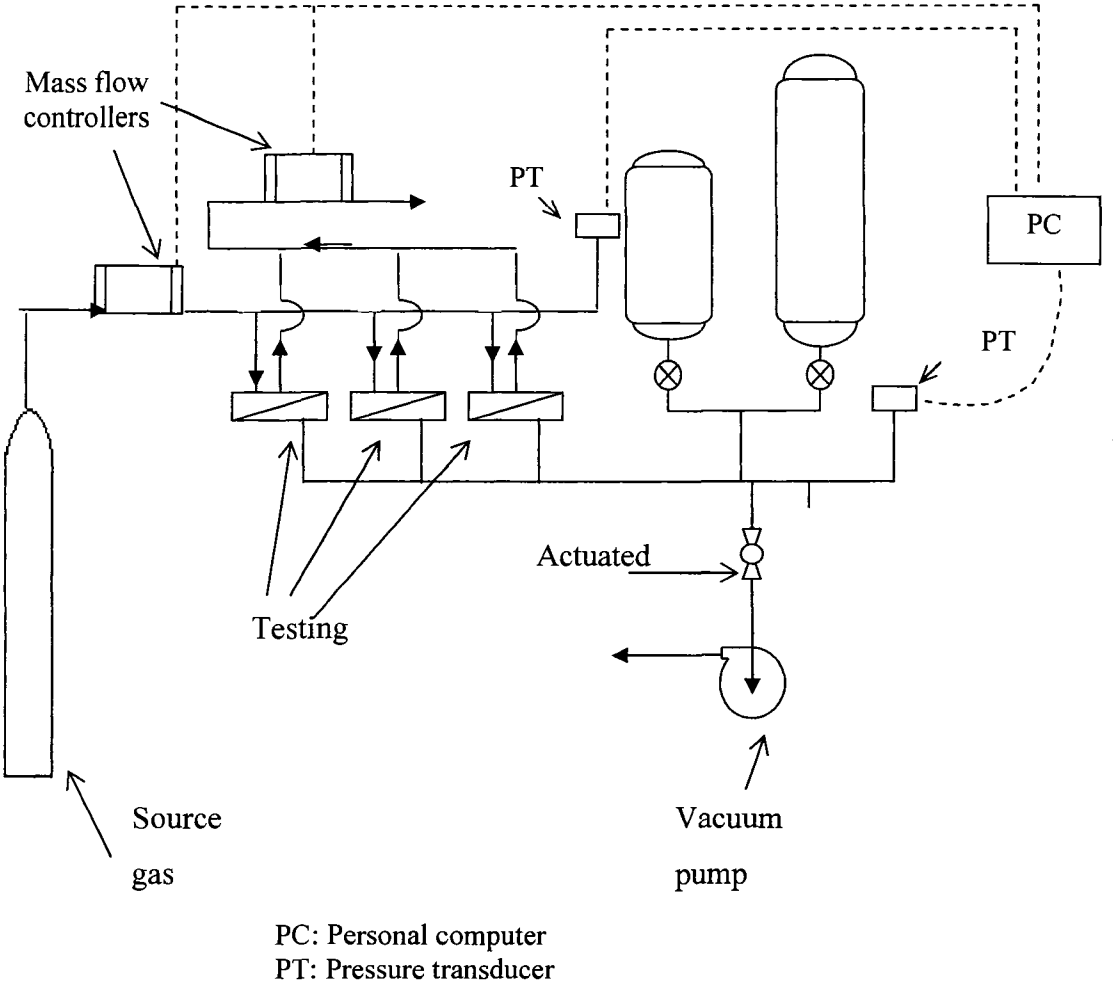

Figure 6.1 Schematic of the constant volume system used for membrane gas permeation testing.

6.2.2.2 Two operational routines

For both permeation systems two different operational routines, called respectively continuous routine and non-continuous routine, were applied. In the continuous routine, the membrane was under the normal operational conditions of gas permeation system throughout the experiment without any interruption; i.e. the membrane was always under the feed gas pressure on the feed side, while the permeate side was facing either sweep gas stream at atmospheric pressure (C-P system) or vacuum (C-V system).

In the non-continuous routine, the normal operational condition was interrupted from time to time by exposing both sides of the membrane either to an atmospheric environment (C-P system) or to vacuum (C-V system). Since the pressure on the feed side was decreased from the operating pressure to either atmospheric pressure or to vacuum, this period of interruption is called "period of pressure reduction". This period is indicated by blank spaces where the data points are unconnected in Figs. 6.2-6.8.

The systems used, feed gas pressures and the operational routines are given in Table 6.1 together with the membranes used for each experiment.

Table 6.1 Membranes and gas permeation experiment details.

Membranes				Experiments		
Used in Figure	Number	Thickness (μm)	Drying time (h)	System	Routine	Feed Pressure (psig)
Figure 6.2	1-A	3.9	16	CP	Continuous	25
	1-B	3.9	16	CP	Non-cont.	25
Figure 6.3	2-A	5.5	6	CP	Continuous	25
	2-B	5.5	6	CP	Non-cont.	25
Figure 6.4	3-A	7.25	6	CP	Continuous	25
	3-B	7.25	6	CP	Non-cont.	25
Figure 6.5	4-A	3.9	16	CP	Continuous	50
	4-B	3.9	16	CP	Continuous	25
Figure 6.6	5-A	5.5	16	CP	Continuous	50
	5-B	5.5	16	CP	Continuous	25
Figure 6.7	6-A	18	16	CP	Continuous	100
	6-B	18	16	CP	Non- cont.	100
Figure 6.8	7-A	15	16	CV	Continuous	100
	7-B	15	16	CV	Non-Cont.	100

6.3 Results

In Fig. 6.2, the relative permeation rate, Q/Q_0, is plotted versus operational period for two experiments (using membranes 1-A, 1-B) conducted with the C-P system. The two membranes used in these experiments had the same thickness, 3.9 μm, and the drying time in ambient air was 16 hours. In the figure, Q is the total, including oxygen and nitrogen, permeation rate at a time t $\left(\sum Q_i\right)$ while Q_0 is the total permeation rate at $t = 0$. Both membranes were under the feed gas pressure (25 psig) during the first 20 hours. In one experiment (1-A, continuous routine) the continuous routine was maintained throughout the experiment, while in the other experiment (1-B, non-continuous routine), there were several pressure reduction periods, that followed the first 20 hours of operation under pressure. Figure 6.2 shows that the aging rate is similar in both experiments during the first 20 hours. After this first stage of operation, the permeation rate decreases almost linearly in the continuous routine, but the slope of decline changes after 80 hours. In the non-continuous routine, on the other hand, the permeation rate decreases more steeply during the pressure reduction periods, particularly when the operational period is shorter than 50 hours. However, the slope of declining diminishes and the line becomes almost parallel to the continuous routine in the later stage of the permeation experiment.

Figure 6.3 shows the permeation rate data from another two sets of experiments. Two membranes of the same thickness (5.5 μm) were used. Both membranes were dried for 6 hours. One experiment (with membrane 2-A) was performed following the continuous routine for 160 hours, while in the other experiment (with membrane 2-B)

there was a pressure reduction period of 10 hours in the very beginning. Then, the feed pressure was applied.

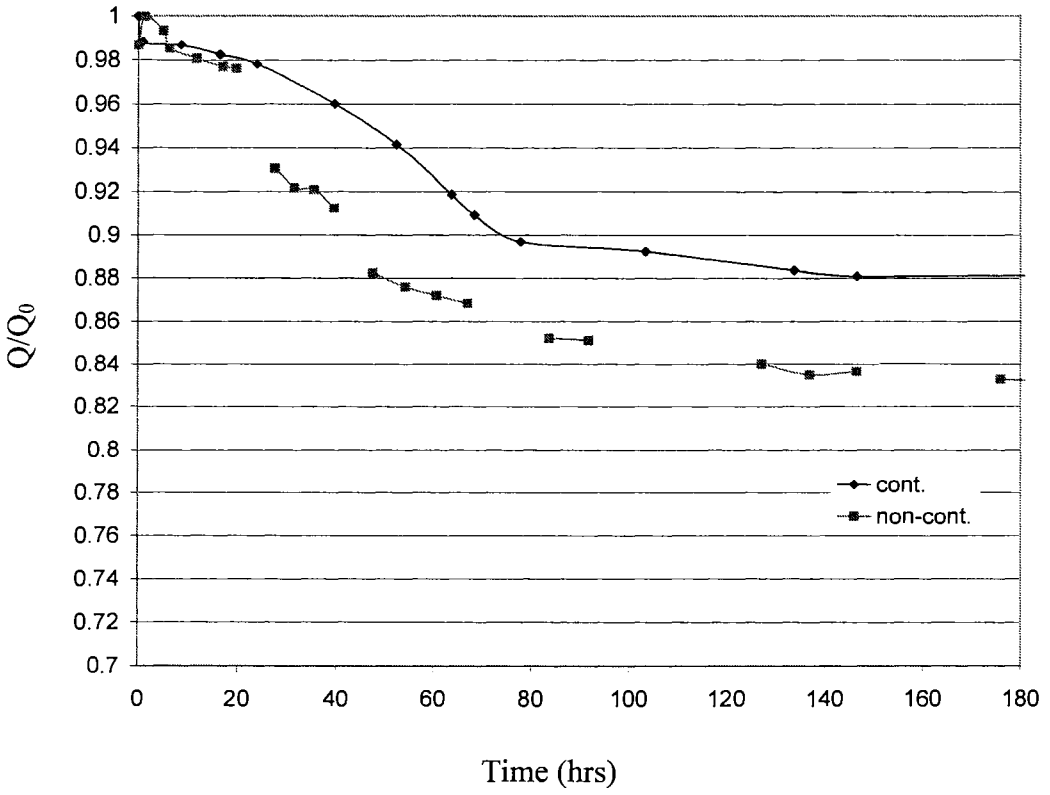

Figure 6.2 The change in the relative permeation rate with time. Membrane thickness, 3.9 μm; system, constant pressure system; feed pressure, 25 psig

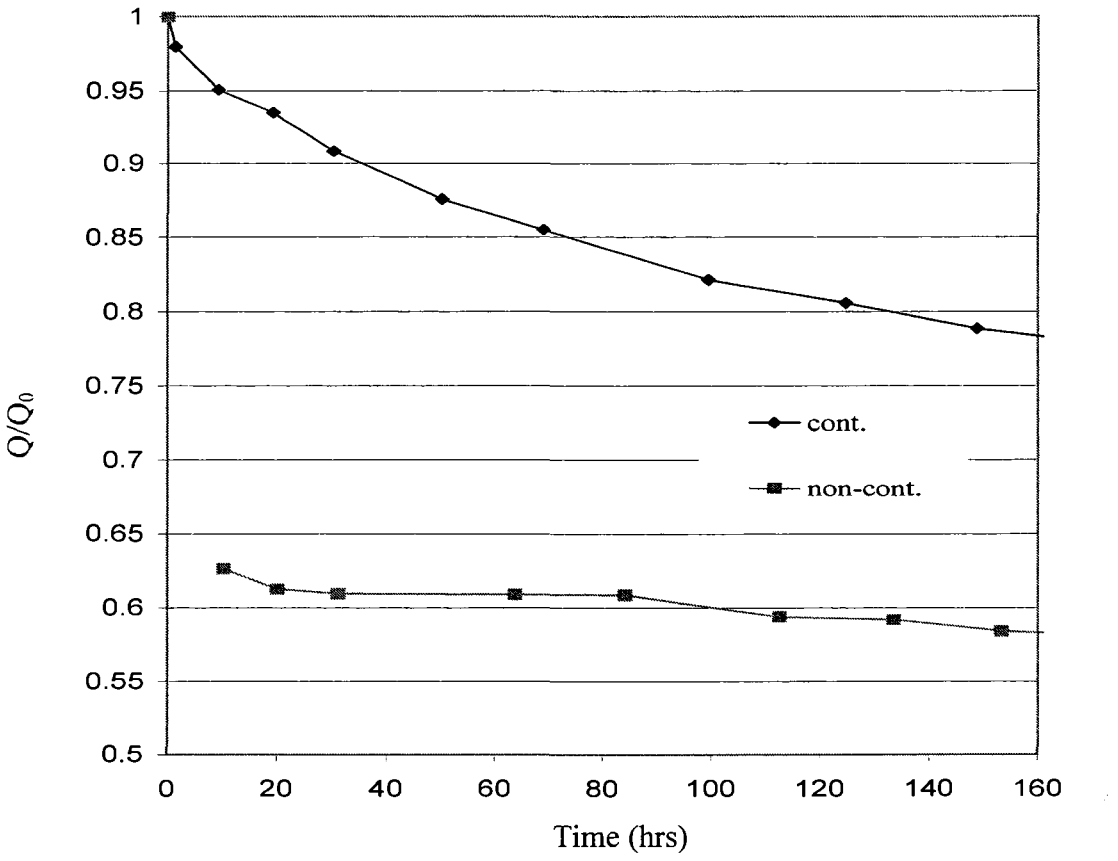

Figure 6.3 Effect of experimental scenario on the relative permeation rate. Membrane thickness, 5.5 μm ; system, constant pressure system; feed pressure, 25 psig

Figure 6.4 shows the results from the same experiments as Fig. 6.3 except for the membrane thickness that was 7.25 μm. In both figures, we can observe that the reduction in the permeation rate that occurred during the first 10 hours of non-continuous routine (with membranes 2-B and 3-B) is so severe that experiments with the continuous-routine (with membranes 2-A and 3-A) do not reach that level of flux reduction even after 160 hours. We can also observe that the thinner membrane (2-B) is subject to a higher degree of flux reduction than the thicker (3-B) membrane.

In Fig. 6.5, the relative permeation rate, Q/Q_0, is plotted versus operational period for two experiments (with membranes 4-A, 4-B) conducted with the C-P system under the air pressure of 50 and 25 psig, respectively. The two membranes used in these experiments had the same thickness, 3.9 μm, and the drying time in ambient air was 16 hours. The decrease in the relative permeation rate of about 12 % was reached for both membranes at the end of the operation. The curves representing both experiments (4-A and 4-B) can be divided to two parts, i.e. the earlier sharp drop in the permeation rate followed by a less steep decline.

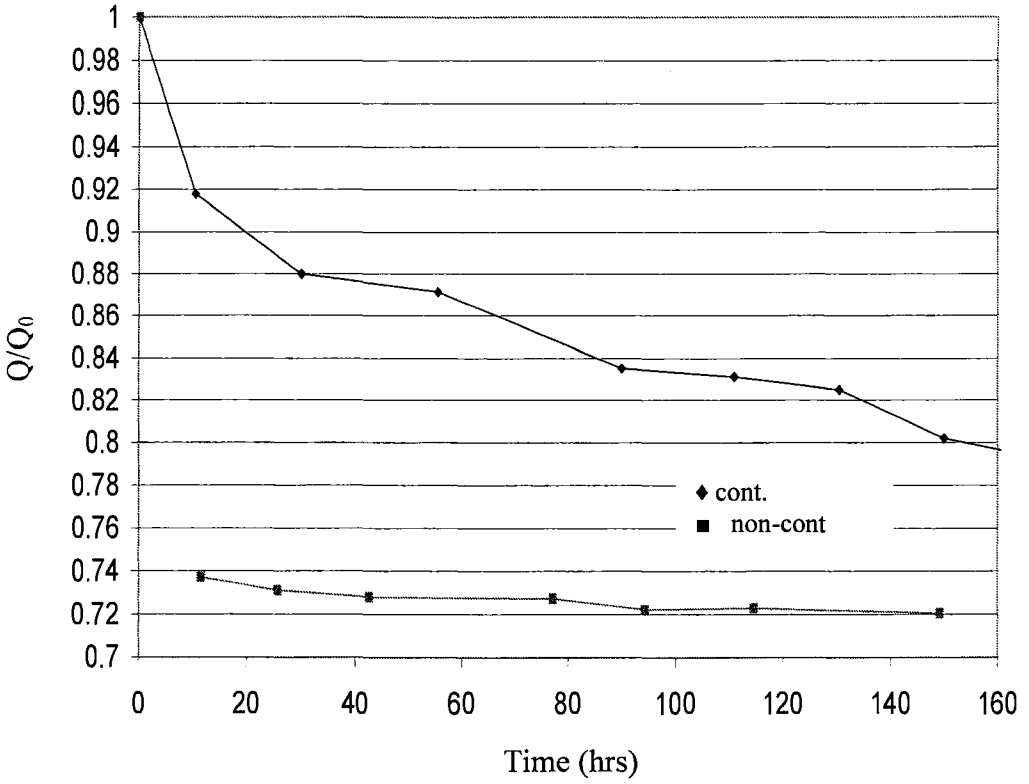

Figure 6.4 Effect of experimental scenario on the relative permeation rate. Membrane thickness, 7.25 μm; system, constant pressure system; feed pressure, 25 psig

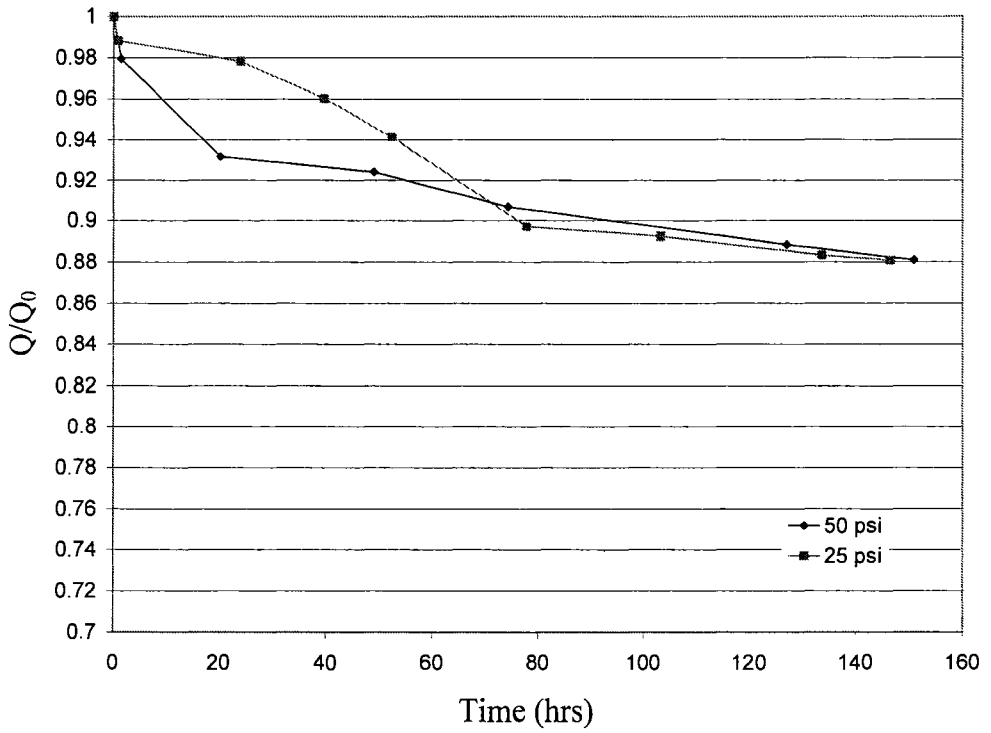

Figure 6.5 Effect of feed gas pressure on the relative permeation rate. Membrane thickness, 3.9 μm; system constant pressure system.

Figure 6.6 shows the results from the same experiments except for the membrane thickness that was 5.5 μm. The final decline in the relative permeation rates are around 13% and 15% for operating pressure of 25 and 50 psig, respectively.

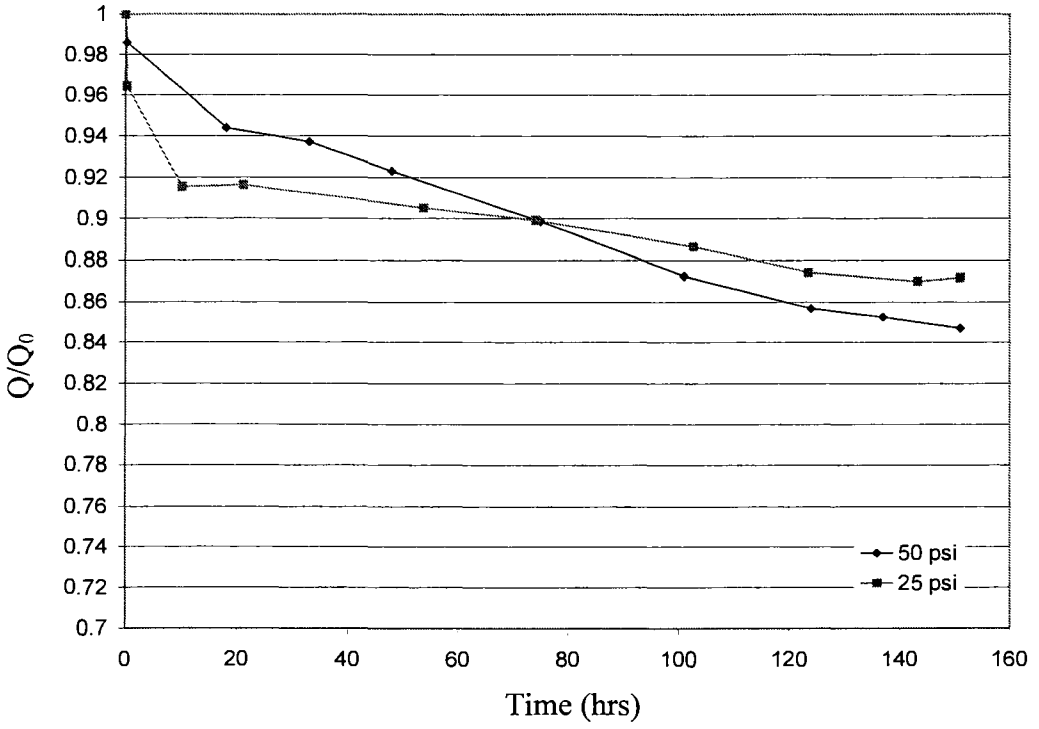

Figure 6.6 Effect of feed gas air pressure on the relative permeation rate. Membrane thickness, 5.5 μm; system, constant pressure system.

In Fig. 6.7, the relative permeation rate, Q/Q_0, is plotted versus the operational period for two experiments (with membranes 6-A, 6-B) conducted using the C-P system. The thickness of both membranes was 18 μm and the membranes were dried in ambient air for 16 hours before being mounted to the permeation cell. In both experiments, feed gas pressure (100 psig) was applied during the first hour and half of the permeation test. During this period of operation, the loss in permeation rate was about 4 % for both membranes. After this early stage of operation, the continuous routine was maintained throughout the experiment for the membrane 6-A (continuous routine). On the other hand, in the other experiment (6-B, non-continuous routine), the gas permeation experiment was interrupted by long periods of pressure reduction. It is evident that the permeation rate decline decreased significantly after the initial 1.5 hours of operation in both routines.

Figure 6.8 shows similar experimental results from the C-V system; i.e. one experiment was conducted following the continuous routine (7-A) throughout the experiment while another set of experiments followed the non-continuous routine (7-B) with several long pressure reduction periods. The relative permeation rates are reported in this figure. While, in the continuous routine, the loss in the relative permeation rate was a little more than 10.5 % after more than 100 hours of operation, in the non-continuous routine the loss in the relative permeation rate reached about 27 % after 98 hours of operation. Interestingly, 20 % of the loss occurred during the first 20 hours of operation.

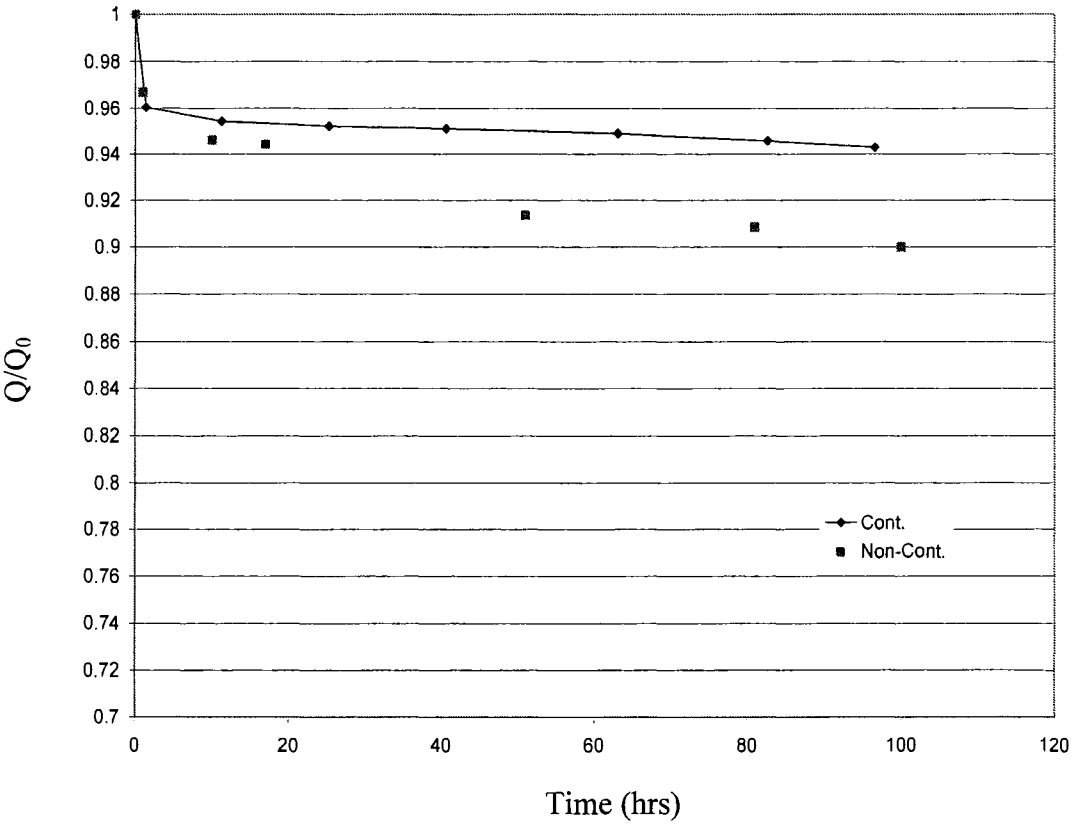

Figure 6.7 Effect of experimental scenario on the relative permeation rate. Membrane thickness, 18 μm,; system, constant pressure system; feed pressure, 100 psig.

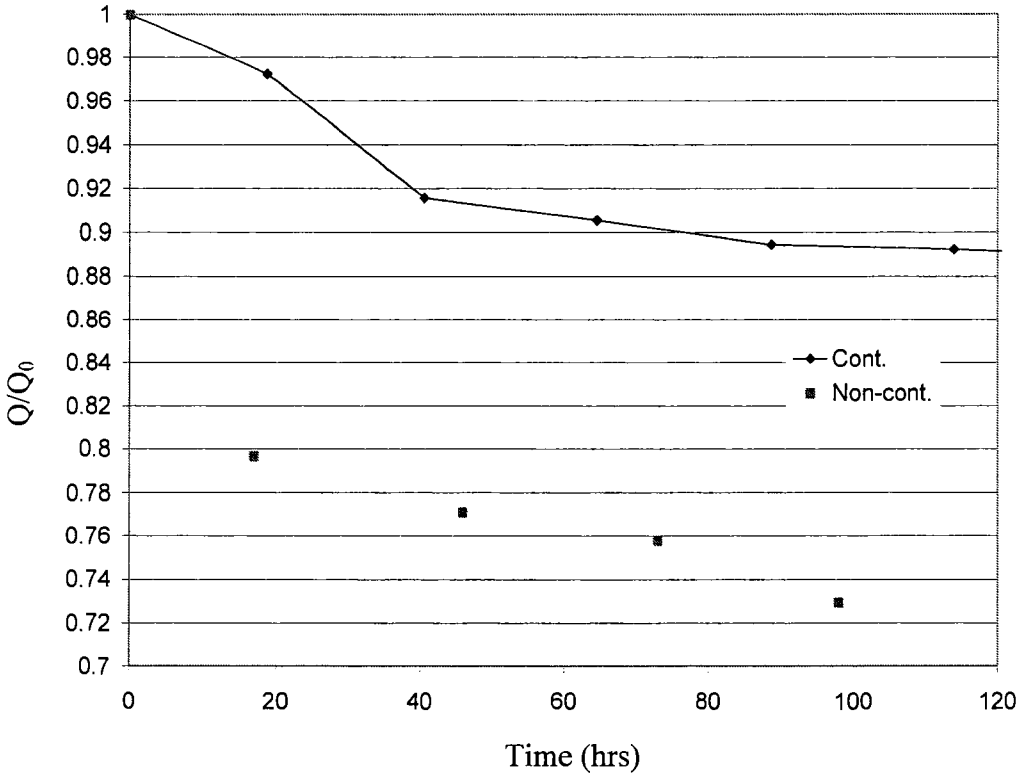

Figure 6.8 Effect of experimental scenario on the relative permeation rate. Membrane thickness, 15 μm; system, constant volume system; feed pressure, 100 psig

6.4 Discussion

Physical aging essentially affects the relaxation times. Relaxation time is not a single value, but a distribution of values that change with experimental time. Relaxation times calculated using mathematical relations, as in Eq. (6.2) are the effective relaxation time. The distribution of relaxation times and non-linearity are basic features of the relaxation process. It is best described by the visco-elastic theory. When a stress σ_o is applied during the time period t_1 to t_2 (creep, see Fig. 6.9), deformation of the material takes place. For an elastic material the deformation is shown by line a (broken line). There is a sudden increase in deformation at time t_1 and the deformation remains constant until time t_2. The viscous material follows the straight line b with gradual change in deformation with time. For the visco-elastic material, the response is represented by a solid line c, i.e. a sudden increase of deformation at time t_1 followed by a further gradual increase until time t_2. When the stress is released at t_2 the deformation decreases immediately to zero for the elastic material, while the deformation remains unchanged for the viscous material. The deformation of the visco-elastic material is featured by a sudden decrease of deformation at time t_2, which corresponds to the elastic component of the material, followed by a further gradual decrease, which corresponds to the viscous component of the material. As shown in Fig. 6.9d. The deformation versus time curve after time t_2 is called relaxation or recovery curve. Interestingly, similar relationship was observed between gas permeation rate and time [Pfromm and Koros (1995); and McCaig and Paul (2000)]. McCaig et al. (2000) ascribed the early steep stage to the dominance of lattice contraction and the later slow stage to the dominance of free volume diffusion

mechanism. In other words, lattice contraction corresponds to the elastic component and the free volume diffusion corresponds to the viscous component.

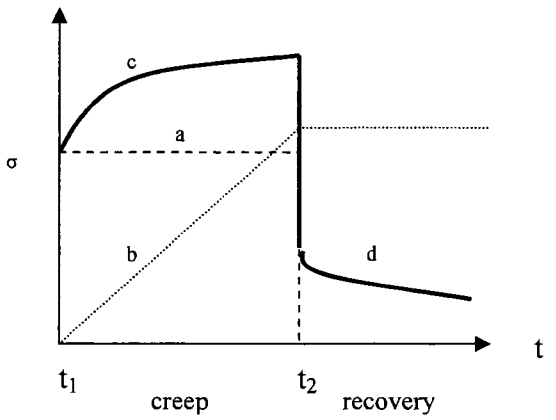

Figure 6.9 Creep and recovery. Strain vs. time.

Realizing resemblance between the gas permeation rate versus time curve and the visco-elastic response, the data from the gas permeation experiments will be interpreted based on the following assumptions.

1) The relaxation of the polymeric membrane starts from time zero. This assumption may seem unjustified since all membranes have their history of relaxation before being mounted to the permeation cell. The above assumption can, however be employed, when membranes with the same pre-gas permeation history are compared.

2) The gas permeation rate reflects the visco-elastic response of the glassy polymer; i.e. the initial steep decline in permeation rate corresponds to the elastic response of the

polymer. The following less steep and more linear drop in permeation rate corresponds to the viscous response of the polymer.

3) The behavior of the polymeric membrane is more elastic when the pressure of the gas that surrounds the membrane is lower, while the membrane's behavior is more viscous when the pressure is higher. Gas, when dissolved in polymer, acts like a solvent that makes the polymer "solution" more like viscous liquid. The higher the gas pressure, the more the polymer "solution" behaves like a viscous solution.

Looking into Fig. 6.2, Q/Q_0 keeps decreasing for the continuous routine from 20 to 80 hours, where the slope of the curve suddenly changes. The earlier part corresponds to the elastic response, turning later into a viscous response. The steep decrease in Q/Q_0 (elastic response) is more obvious in the non-continuous routine (1-B), when the pressure reduction was applied at the 20 and 40 hours of operation. After 80 hours, a transition in the permeation rate takes place and both response curves become more linear and parallel to each other. The transition occurs suddenly in the continuous routine, while it occurs more smoothly in the non-continuous routine.

In Figs. 6.3 and 6.4, we will first look at the curves 2-B and 3-B. Both are experiments of non-continuous routine. During the first 10 hours, no pressure was applied to the feed gas, so the effect is the same as the pressure reduction in the C-P system. The response contains a relatively large amount of elasticity, which is observed as steep decline in the permeation rate. This first stage is followed by a linear decrease where the viscous response dominates. It is worth noting that the flux reduction during the first 10 hours was more severe for a thinner (2-B) than thicker (3-B) membrane. Now looking into the response curves 2-A and 3-A (continuous routine), the transition from steep to

less steep reduction in permeation rate did not occur in the experiment 2-A with a membrane of 5.5 μm during the entire 150 hours of operation while the transition occurred at 30 hours in 3-A, which was with a membrane of 7.25 μm.

The fast appearance of transition for the thicker membrane is one of the important features of the experimental observation. By comparing the lines representing the operating pressure of 25 psig in Figures 6.5 and 6.6 (4-B and 5-B), the transition for 5-B (5.5 μm) occurred much earlier than in 4-B (3.9 μm).

Looking into Fig. 6.4, the relatively steep decrease in Q/Q_0 observed during the first 1.5 hours is considered to be an enhanced elastic response. Although this turns gradually into the viscous response of less steep decrease both in continuous and non-continuous routines, the decrease in permeation rate seems steeper for the latter operation due to the residual elasticity at the reduced pressure. Eventually, the viscous response of the membrane will dominate after 50 hours and the responses for both continuous and non-continuous routines become parallel.

The effect of the pressure on membrane aging was most clearly observed when the non-continuous routine was applied in the CV system (Fig. 6.5). It should be recalled that during the pressure reduction period in the CV system, the membrane was under vacuum. The fast decrease in Q/Q_0 has happened during the first 16 hours of the non-continuous routine due to the strong elastic behavior that occurred when the membrane was under vacuum. This is followed by a less steep and more linear response, indicating domination of the viscous component.

6.5 Conclusion

Resemblance of aging curves of gas separation membranes to the visco-elastic response curves is clearly observed for all the studied membranes. Thus, membrane aging curves consist of elastic and viscous components. It is further concluded that the elastic component of polymer relaxation is enhanced when membranes are aged at lower pressures while the viscous component is enhanced at higher gas pressures. It can also be concluded that the transition from the elasticity dominant to the viscosity dominant region occurs more quickly for thicker membranes.

CHAPTER 7

Effect of Physical Aging on the Permselective Properties of PPO Membranes

7.1 Introduction

Physical aging is a free volume relaxation that leads to decrease in permeability of glassy polymeric membranes. Even if different polymers age in a similar way, their aging rate is affected by several factors. Factors affecting the free volume and the segmental thermal fluctuation, such as chemical structure and aging temperature, should affect the aging and consequently the gas transport properties of tested polymers. But for membranes made from the same polymer and tested at the same temperature, their thickness and the gas pressure are the major factors that affect the aging and the gas transport properties.

7.2 Historical Background

It was first reported by Kapur and Rogers in 1972 that physical aging decreased the diffusion coefficient of glassy polymers. In 1982, Coady and Davis reported 20% reduction in the permeability of cellulose ester after two years of facilitation. In 1988 Kim reported decreases in permeability of different gases and more importantly, increases in He/CH_4, O_2/N_2, and CO_2/CH_4 selectivity in 6FDA-DAF and 6FDA-IPDA films as a function of time. An arrangement of polymer segments was thought to be the cause for the changes in the gas transport properties of glassy polymeric membranes.

With the progress made in the field of polymeric gas separation membranes, which included introducing new materials with high permeabilities, the problem of physical aging became more obvious and more attention has been paid to the problem. Polymers such as poly[1(trimethylsilyl)-1-propyne] (PTMSP) posses very large free volumes. The high free volume value makes the polymer very attractive as membrane material, but also makes it more susceptible to physical aging. Rezac et al. (1993) studied the aging of thin polyimide-ceramic and polycarbonate-ceramic membranes and reported decrease in permeability coupled with increase in selectivity of O_2/N_2 from single gas measurements. More detailed literature was provided in Chapter 3.

Even if aging was expected to affect smaller (thinner) samples more strongly, no experimental proof was found for such effect until membrane researchers started to be more seriously concerned about the phenomena of aging. In gas separation membranes, thin films are desirable because of their high productivity, but they also seem to show higher decrease in their productivity than thicker membranes. This is the second

important aspect of aging that received the attention of the gas separation membranes community to the aging phenomena.

It is generally accepted that the gas separation process follows indisputable trade-off relationship: the more permeable the membrane, the less selective it is. This understanding of gas separation process, as a sieving process, leads to selectivity increase because permeability decreases due to aging. One would expect that the greater the amount of free volume in a freshly processed polymer, the more permeable the material, the lower the activation energy for permeation, and the lower the selectivity. Nevertheless, although this trend has been observed for the transport of single gas molecules through various polymer structures (Robeson, 1991), the permselective properties of a particular gas mixture proved to be different when gas mixtures were used in the experiments. In some gas mixtures, gas transport is affected by competition between gases due to different degrees of affinity to the polymer. Similar to the field of gas separation, physical aging is often studied using single gases and conclusions are drawn for the effect on gas mixture separation on the basis of these measurements. It is believed, however, that the use of gas mixtures would offer a tool for the better understanding of the physical aging than single gas experiments.

Takada et al. (1985) investigated the gas transport properties in PTMSP for membranes dried in air after casting and reported a decrease in permeability coupled with a decrease in permselectivity. Chung and Teoh (1999) have reported a decrease in O_2/N_2 permselectivity coupled with the expected decrease in permeability because of aging of polyethersulphone and 6FDA-durene polyimide hollow fiber membranes. A decrease or no change in selectivity was ascribed by Lin and Chung (2000) to contribution of porous

mechanisms to the flux through defects in the skin layer of these membranes. Huang and Paul (2005) also reported faster aging of PPO membranes when the films were thinner and the temperature was higher.

Before the introduction of PTMSP as gas separation membrane material, PPO was considered the most permeable among the glassy polymers available for gas separation membranes. Although, research on the physical aging of poly (phenylene oxide) was not an exception in the sense that attention was mainly paid to its mechanical properties and applications, Chang et al. (1996) and Robertson and Wilkes (2000) studied the effect of aging on the changes in mechanical properties of PPO in blends. Yang et al. 1993 found that aging caused degradation of PPO films and caused the transition of their mechanical properties from ductile to brittle. The polymer ductility was related to segmental elasticity, which decreased by aging. Huang et Paul (2004) reported faster decrease of single gases permeabilities and increase in O_2/N_2 and N_2/CH_4 selectivity due to aging.

7.3 Experimental

The method of membrane preparation is the same as given in Chapter 6. The method of gas permeation experiment is also the same as the CP-system given in Chapter 6. The permeation experiment is described in Chapter 4 and 6 more in detail, as far as the permeability of the individual gases is concerned. Definitions of the overall permeability, individual permeability and permeability ratio should be, however, in order.

The definition of overall permeability, $P_{overall,}$ is

$$P_{overall} = \Sigma Q_i \, l/\Delta pA \qquad (7.1)$$

where ΣQ_i is the overall permeation rate including all the components in the gas mixture, l is the membrane thickness, Δp is the difference in total pressure between the feed and the permeate, and A is the effective area of the membrane.

The individual permeability, P_i, has already defined in the earlier chapter and they are:

$$P_i = Q_i l / \Delta p_i A \tag{7.2}$$

$$\alpha = (P_{oxygen})/(P_{nitrogen}) \tag{7.3}$$

The details of the membranes and gas permeation experiments involved in this chapter are summarized in Table 1.

7.4 Results

7.4.1. Effect of Gas Pressure

7.4.1.1 Aging in Continuous 25 psig and non-Continuous pressure

In Fig. 7.1, the overall permeability $P_{overall}$ and the permeability ratio $\alpha_{O2/N2}$, are plotted versus operational period for two experiments conducted using two membranes (1-A, 1-B) of the same thickness, 3.9 μm. The drying time, after casting, in ambient air was 16 hours. Both membranes started at practically the same permeability value and ended at different values. In contrast, the permeability ratios started at different values, and became closer to each other at the end of the experiment. Both membranes were under the feed gas pressure (25 psig) during the first 20 hours. In one experiment (1-A, continuous routine) the gas pressure was maintained throughout the experiment, while in the other experiment (1-B, non-continuous routine), there were several pressure reduction periods, that followed the first 20 hours of operation under pressure. The data points before and after these pressure reduction periods are unconnected.

Table 7.1 Membranes and gas permeation experiment details

Membranes				Experiments		
Used in Figure	Number	Thickness (μm)	Drying time (h)	System	Routine	Feed Pressure (psig)
7.1 and 7.2	1-A	3.9	16	CP	Continuous	25
	1-B	3.9	16	CP	Non-cont.	25
7.3 and 7.4	2-A	5.35	16	CP	Cont.-1	25
	2-B	5.35	16	CP	Cont-2	25
	2-C	5.35	16	CP	Non-cont.	25
7.5 and 7.6	3-A	3.7	16	CP	Continuous	50
	3-B	3.7	16	CP	Continuous	50
7.7 and 7.8	4-A	6.45	16	CP	Continuous	50
	4-B	6.45	16	CP	Continuous	50
7.9 and 7.10	5-A	5.5	6	CP	Continuous	25
	5-B	7.25	6	CP	Continuous	25
7.11 and 7.12	6-A	5.5	6	CP	Continuous	50
	6-B	7.5	6	CP	Continuous	50

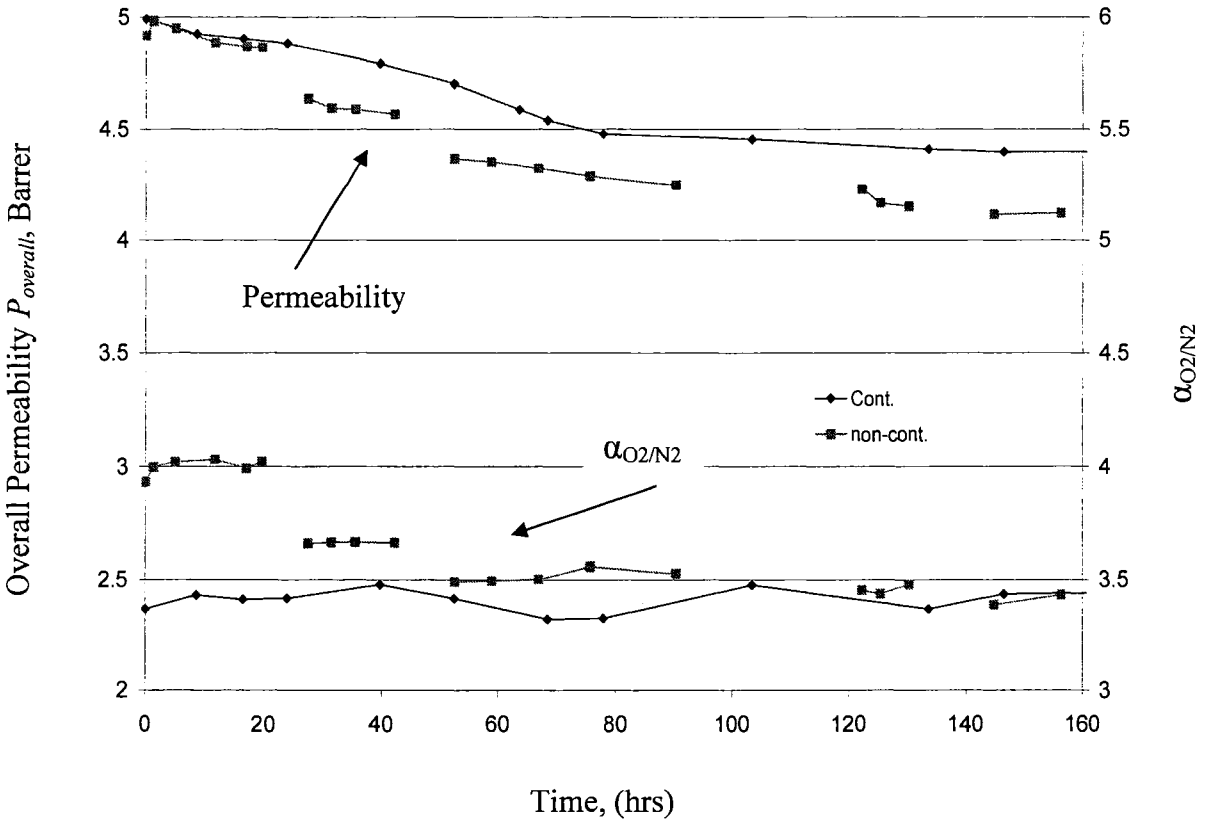

Figure 7.1 Changes in overall permeability and permeability ratio, $\alpha_{O2/N2}$, with time. Membrane thickness, 3.9 μm; operating pressure, 25 psig

Figure 7.1 shows that the reduction in the overall permeability is similar in both experiments during the first 20 hours. The permeability ratios of both membranes slightly increased after time zero and remained constant for the rest of this stage. After the first stage (20 hours) of operation, the permeability decreases almost linearly in the continuous routine, but the declining rate of permeability changes after 80 hours. In the non-continuous routine, on the other hand, the permeability decreases more steeply during the pressure reduction periods, particularly when the operational period is shorter than 50 hours. However, the slope of declining diminishes and the line becomes almost parallel to the continuous routine in the later stage of the permeation experiment. The permeability ratios were almost horizontal for the continuous routine and during the pressurized periods in the non-continuous routine. On the other hand, it decreased significantly during the pressure reduction periods.

Figure 7.2a shows the changes in the individual permeabilities of O_2 and N_2 through membranes 1-A and 1-B. The initial value of $\alpha_{O2/N2}$ for non-continuous routine is higher than continuous routine as shown in Fig. 7.1, which is a result of a higher O_2 and lower N_2 permeability of the non-continuous routine shown in Fig. 7.2. It is clear from this figure that the change in O_2 permeability of the non-continuous routine is the reason behind the dramatic reduction in overall permeability. The huge reduction in the overall permeability occurred at the same time as the reduction in O_2 permeability, while N_2 permeability did not suffer from such reduction and the data for both routines are parallel to each other. O_2 permeability of the non-continuous routine, on the other hand, decreased from above to below the values of the continuous routine, at about 20 hours of operational time.

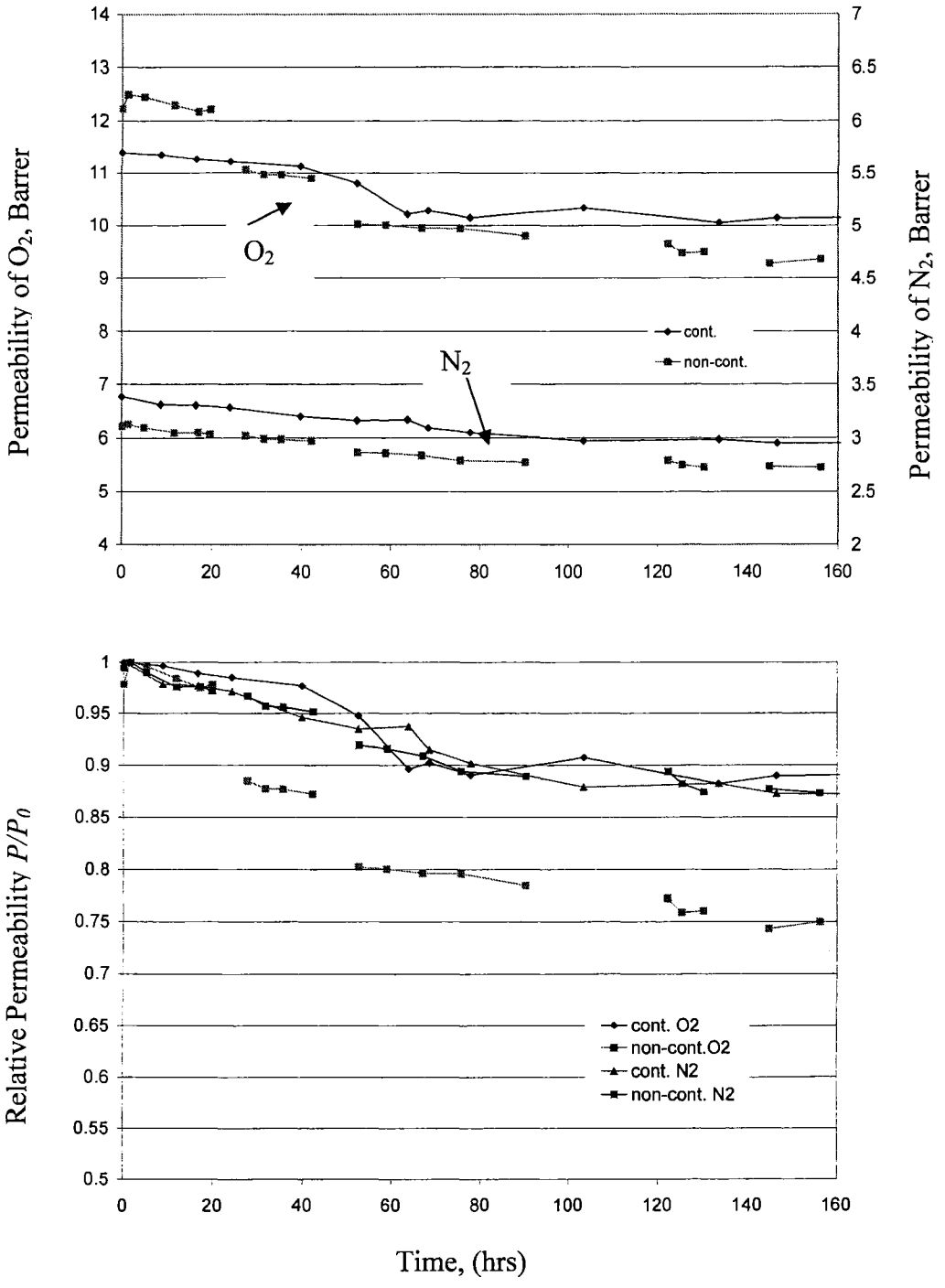

Figure 7.2 Time dependent change of (a) the individual permeability of O_2 and N_2 and (b) the relative permeability of O_2 and N_2. Membrane thickness, 3.9 μm; operating pressure, 25 psig.

The drastic reduction is the O_2 permeability is more clearly shown by Fig. 7.2b, where the permeability relative to the initial permeability is shown as the function of time. The relative permeabilities for N_2 are almost the same for both operational routines, while the reduction of O_2 permeability is far greater in the non-continuous routine than the continuous routine.

In Fig. 7.3, the overall permeability $P_{overall}$ and the permeability ratio $\alpha_{O2/N2}$, are plotted versus operational time for three experiments conducted using membranes (2-A, 2-B and 2-C) with an average thickness, $5.35\pm0.13\mu m$. The drying time in ambient air was 16 hours. All membranes were under the feed gas pressure (25 psig) during the first 20 hours. In two experiments with 2-A, and 2-B the continuous routine was maintained throughout the experiment, while in the other experiment with 2-C there were several pressure reduction periods after the first 20 hours of operation under pressure. The overall permeability of membrane 2-C started at a value higher than membranes 2-A and 2-B, while selectivity of 2-C started at a lower value. Their permeability decrease in the continuous routine was progressing at a constant rate, while it was greater when the pressure was interrupted in the non-continuous routine, particularly when the operational period was shorter than 50 hours. However, the slope of declining diminishes and the line becomes parallel to the continuous routine in the later stage of the permeation experiment. The permeability ratio decreased significantly during the pressure reduction periods. On the other hand, it did not change significantly for the two membranes used in the continuous routine. After a slight increase in the initial stage the permeability ratio went up and down, maintaining almost the same value.

Figure 7.4a shows the change in individual permeabilities with time. Again, the reduction in O_2 permeability, during pressure relief periods of the non-continuous routine, is very noticeable. In the beginning the O_2 permeability of 2-C (non-continuous routine) was higher than those of 2-A and 2-B membranes (continuous routine) but became lower than 2-A and 2-B after 20 hours of operation. In contrast, N_2 permeability decreased only slightly for all the tested membranes and the lines were parallel to each other.

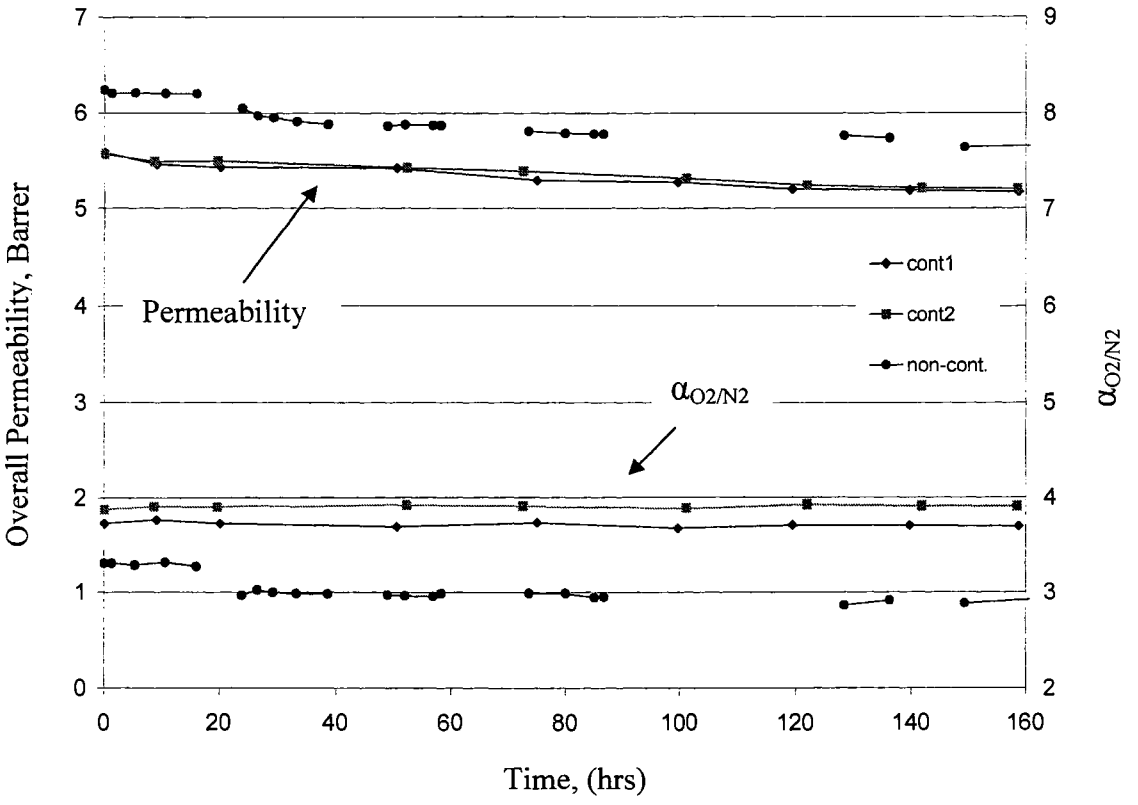

Figure 7.3 Changes in the overall permeability and permeability ratio, $\alpha_{O2/N2}$, with time. Membrane thickness, 5.35 μm; operating pressure, 25 psig

Hence, the remarkable reduction in the O_2 permeability of 2-C membrane (non-continuous routine) is responsible for the reduction in the selectivity of the membrane 2-C. Figure 7.4b shows the relative permeability for individual gases. Similar to Fig. 7.2b, O_2 in the non-continuous routine exhibited the steepest decrease in the relative permeability, and the decrease occurred in most cases during the period of pressure release. In the continuous routine, there was some difference in the speed of decrease of O_2 permeability between the membranes 2-A and 2-B, but N_2 permeability was almost the same for both membranes.

In Figs. 7.1 and 7.3, physical aging of membranes with different thicknesses under two routines is observed as the reduction in over all permeability. The reduction in the permeability is deeper and faster in thinner membranes. But more importantly, it is much deeper and faster in the non-continuous routine than in the continuous routine. A sudden and a steep reduction in permeability and in selectivity take place during pressure reduction periods. This reduction in the overall permeability is due to the much greater reduction in O_2 than N_2 (Figs. 7.2b and 7.4b). In fact, N_2 permeability in the non-continuous routine could be connected with a straight line through the pressure reduction periods. On the other hand, the reduction in O_2, in non-continuous routine, could not be represented by a straight line, especially in earlier stages. Figures 7.2b and 7.4b show the reduction in N_2 permeability is similar for both operational routines.

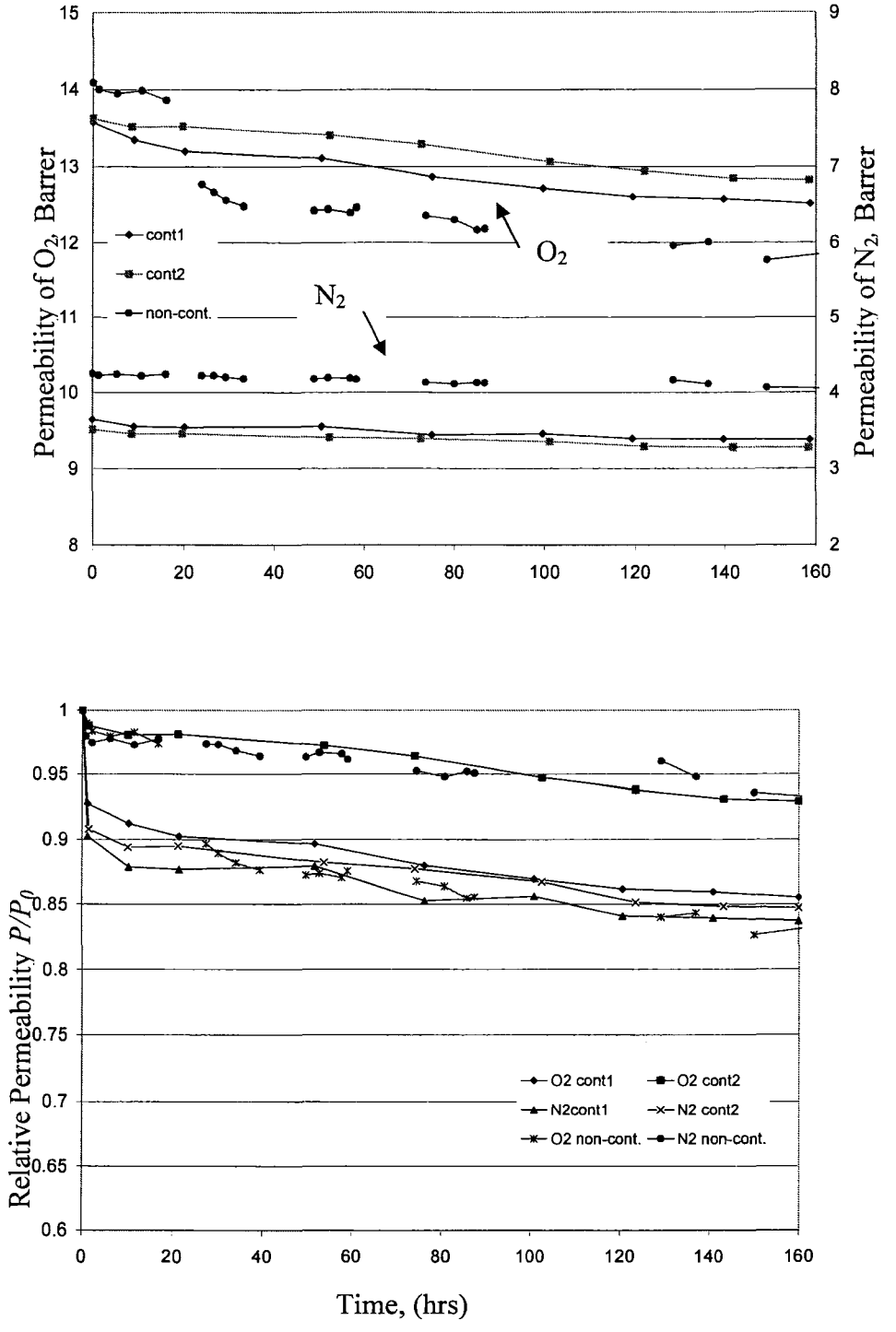

Figure 7.4 Time dependent changes of (a) the individual permeability of O_2 and N_2 (b) the relative permeability of O_2 and N_2. Membrane thickness, 5.35 μm ; operating pressure, 25 psig

7.4.1.2 Aging in continuous 50 psig pressure

Figure 7.5 shows the change in the overall permeability and the permeability ratio $\alpha_{O2/N2}$ change with time for two membranes with a thickness 3.7±0.2 μm. Both membranes (3-A and 3-B) were dried in the ambient air for 16 hours after casting. The gas permeation experiment was carried out under the feed gas (air) pressure of 50 psig for 150 hours. From the figure, the permeability of 3-A was lower than 3-B from the beginning to the end of the experiment. On the other hand, 3-A's permeability ratio was higher than 3-B. Similar to the overall permeability, the permeability ratio kept decreasing for 3-A from the beginning to the end, with the steepest decrease between the first and second measurements. Interestingly, unlike the permeability, the permeability ratio increased from the first to the second measurement for the membrane 3-B, followed by the steady decrease until the end of the experiment.

In Fig. 7.6a, the permeability of individual O_2 and N_2 component is shown. The O_2 permeability of membrane 3-A decreased while that of membrane 3-B increased from the first to the second measurement. For the second measurement, O_2 permeabilities of both 3-A and 3-B were equal. The N_2 permeability of membrane 3-B is much higher than 3-A, which is the reason for the low permeability ratio of 3-B. Figure 7.6b, shows the relative permeability of individual gases through 3-A and 3-B.

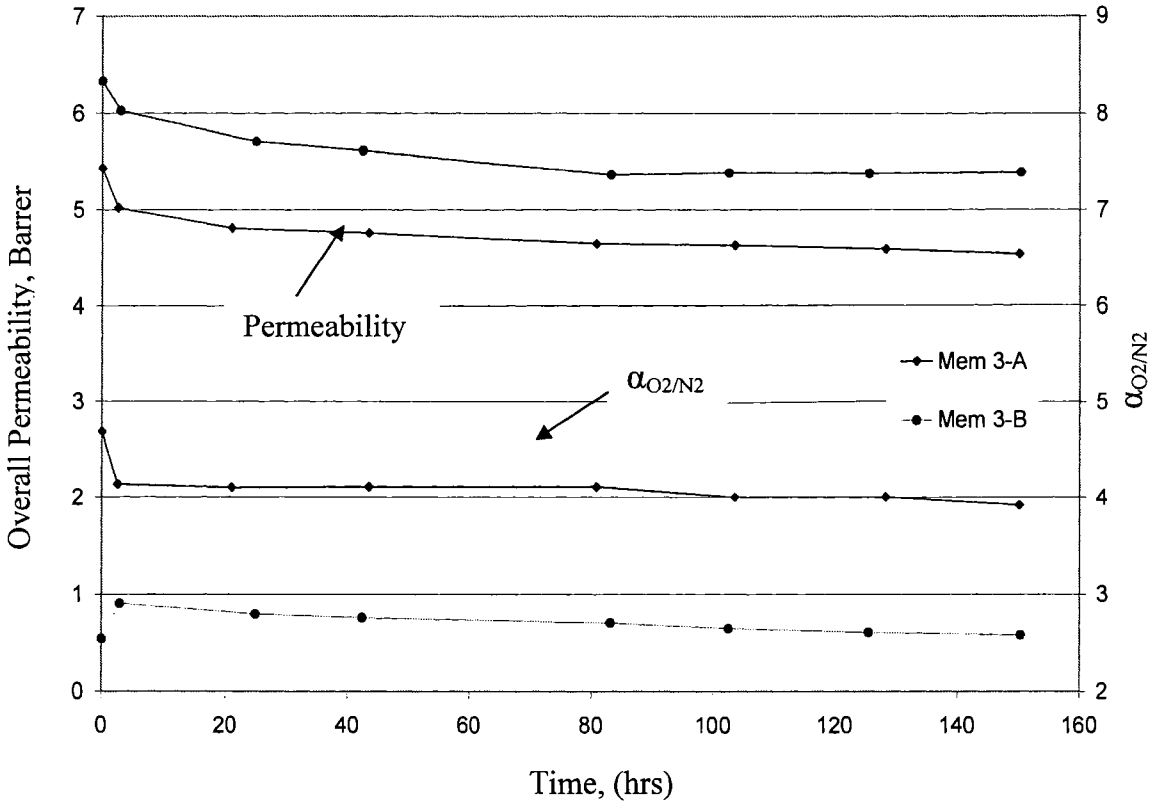

Figure 7.5 The changes in the overall permeability and permeability ratio, $\alpha_{O2/N2}$, with time. Membrane thickness, 3.7 μm; operating pressure, 50 psig; operation routine, continuous

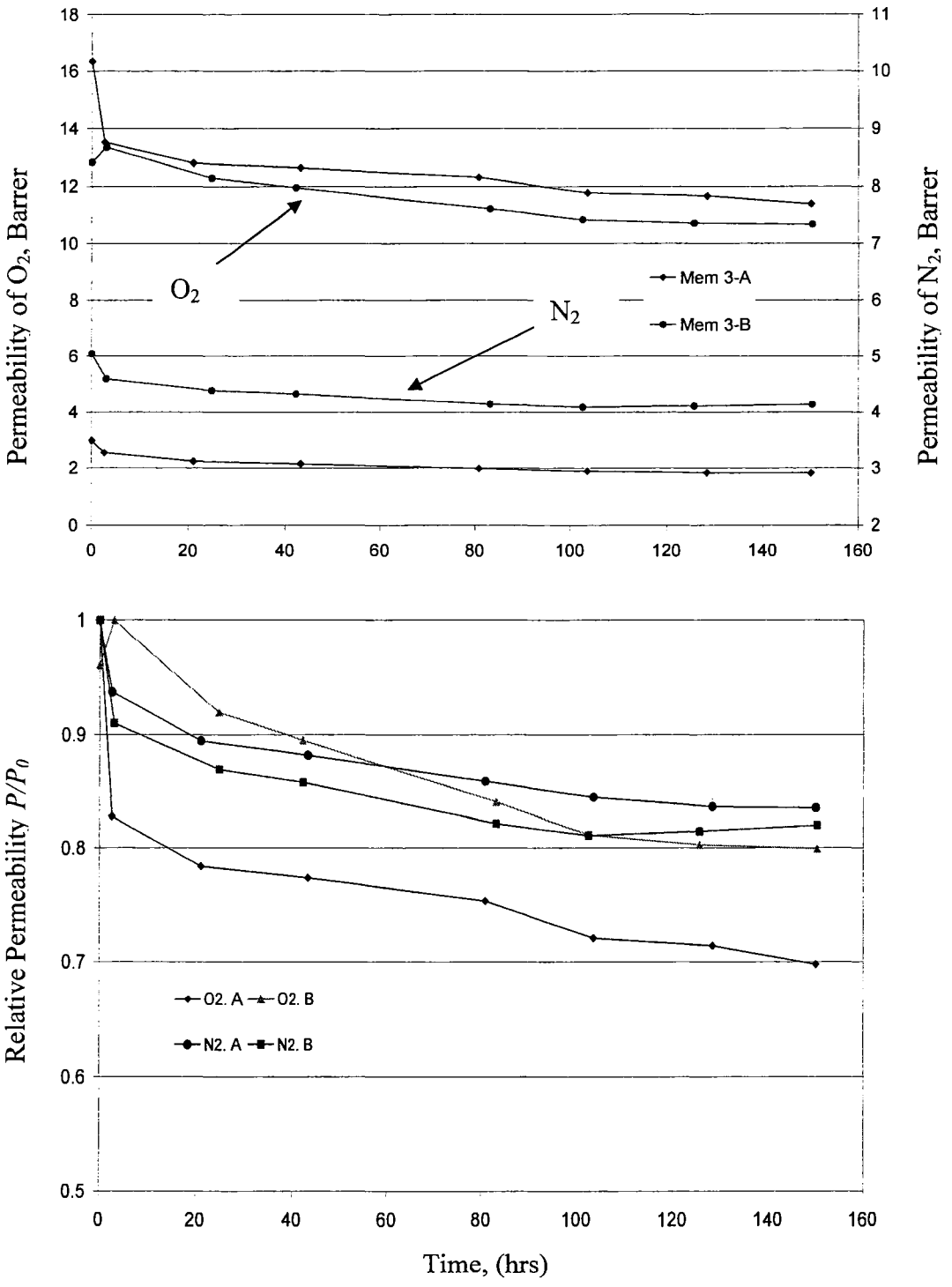

Figure 7.6 The time dependent changes of (a) the permeability of O_2 and N_2 (b) the relative permeability of O_2 and N_2. Membrane thickness, 3.7±0.2μm; operating pressure, 50 psig; operational routine, continuous

Figure 7.7, shows the change in the overall permeability and the permeability ratio, $\alpha_{O2/N2,}$ with time for two membranes with a thickness 6.45±0.25 μm. Both membranes (4-A and 4-B) were dried in the ambient air for 16 hours after casting. The gas permeation experiment was carried out under the feed gas (air) pressure of 50 psig for 160 hours. The permeability of 4-A was higher than 4-B from the beginning to the end of the experiment. On the other hand, the permeability ratio of 4-A was lower than 4-B. The overall time dependent changes of these membranes are less significant than those of the thinner 3-A and 3-B membranes.

In Fig. 7.8a, the permeability of individual O_2 and N_2 component is shown for the membranes 4-A and 4-B. The permeability of both gases in membrane 4-A is higher than those in membrane 4-B, which is due to the higher free volume in 4-A. Figure 7.8b shows the relative permeability of individual gases through membranes 4-A and 4-B. The decrease in O_2 permeability is more than N_2 permeability for both membranes. The permeabilities of O_2 and N_2 are more widely apart for membrane 4-A than 4-B. which shows, relatively, a higher difference between both gases final relative permeability.

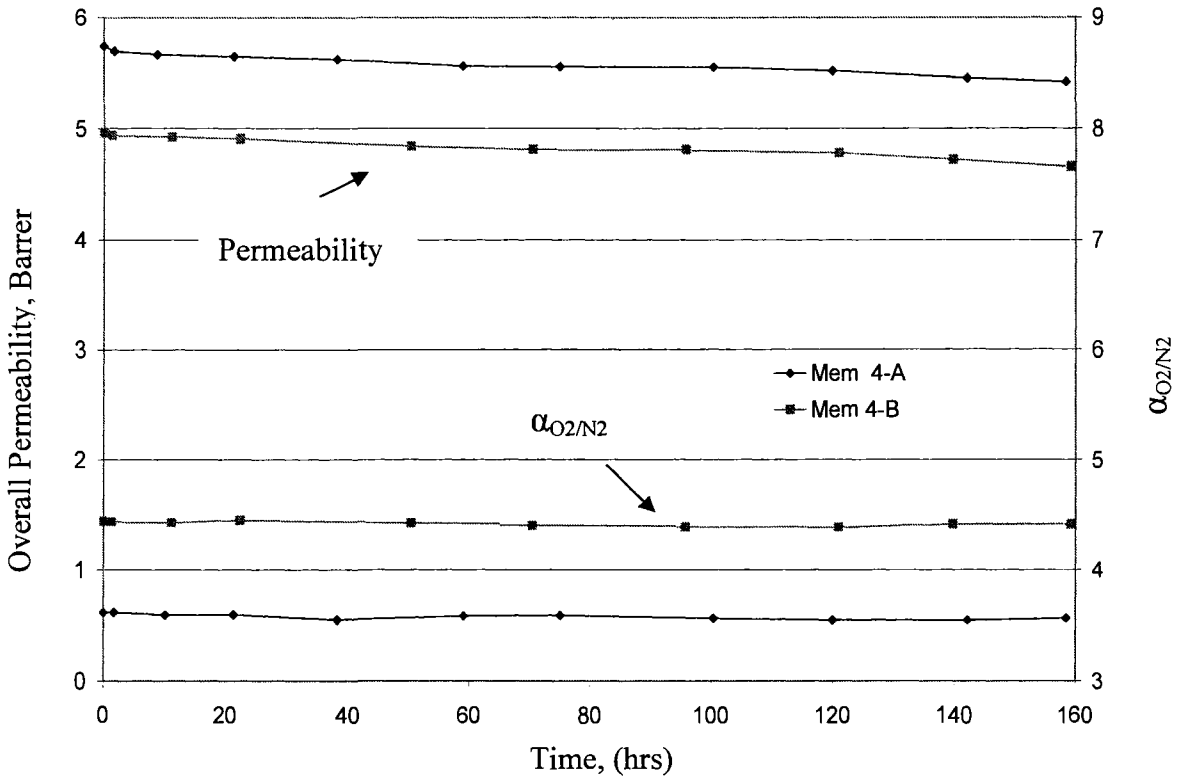

Figure 7.7 The changes in the overall permeability and permeability ratio, $\alpha_{O2/N2}$, with time. Membrane thickness, 6.45±0.25μm; operating pressure, 50 psig; operation routine, continuous

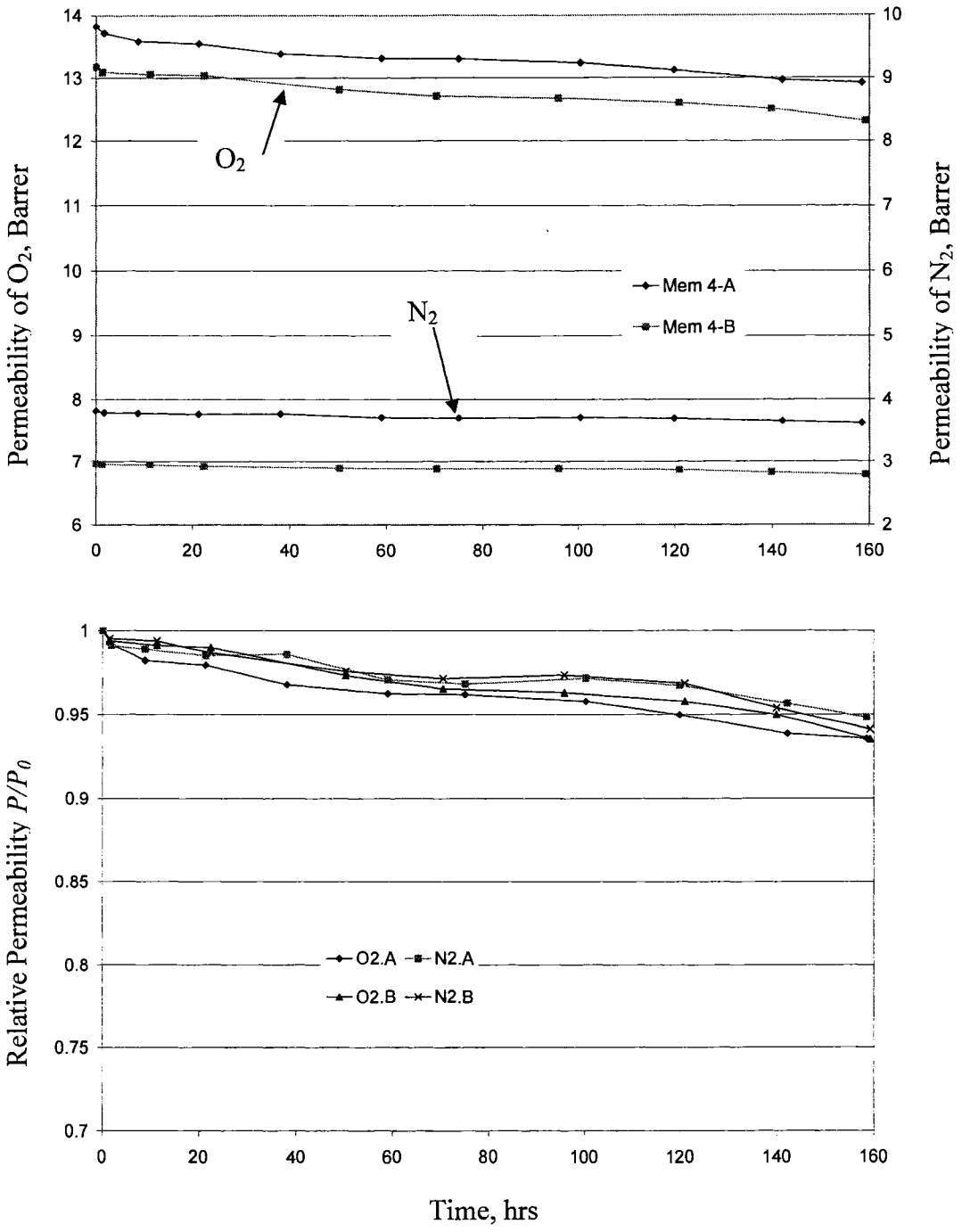

Figure 7.8 The time dependent changes of (a) the permeability of O_2 and N_2 (b) the relative permeability of O_2 and N_2. Membrane thickness, 6.45±0.25μm; operating pressure, 50 psig; operation routine continuous

7.4.2 Effect of Initial Free Volume

7.4.2.1 Aging in 25 psig air pressure

In Fig. 7.9, overall permeability $P_{overall}$ and the permeability ratio, $\alpha_{O2/N2}$, are plotted versus operational period for two experiments conducted using two membranes (5-A, thickness 5.5, and 5-B, thickness 7.25 μm). The drying time after casting in ambient air was 6 hours. The experiments were conducted under 25 psig feed pressure. The decrease in the overall permeability of the thinner membrane, 5-A, was more than the thicker membrane, 5-B. The thinner membrane started with a higher selectivity than the thicker membrane. The selectivity of the thicker membrane increased during the first hour, and then decreased all the way to the end of the experiment. On the other hand, the selectivity kept increasing with time for the thinner membrane.

Figure 7.10a shows the changes in the individual permeability of O_2 and N_2 through membranes 5-A and 5-B. O_2 permeability of 5-A is higher than 5-B. The permeability of N_2 is similar for both membranes in the earlier part of the experiment (up to about 25 hours), and then the decrease in permeability was faster for 5-A than 5-B. As a result, 5-B had a larger N_2 permeability in the end of the experiment. Figure 7.10b shows the change in the relative permeability of the individual gases with time. The fractional reduction in these membranes seems much higher than the ones dried for 16 hours (Compare with Fig. 7.4b continuous runs with membranes 2A and 2B). The relative permeabilities of the thinner membrane (5-A) were higher than the thicker membrane (5-B) in the earlier stage of the experiment but eventually became either nearly equal (for oxygen) or lower (for nitrogen) to those of 5-B at the end of the experiment.

Comparing Figs. 7.3 and 7.9, it is obvious the overall permeability of membranes 5A and 5-B are much higher than those of membrane 2-A and 2-B. This is because membrane 5-A and 5-B were dried for a much shorter period (6 hours) than 2-A and 2-B (16 hours). This indicates that there is a larger free volume in the membranes that were dried for a shorter period. As mentioned above, however, the fractional reduction of the permeability is severer for the membranes 5-A and 5-B than the membranes 2-A and 2-B, which means a higher initial free volume results in a severer aging. It is however interesting to note that the overall permeability obtained at 160 hours of operation is higher for 5-A and 5-B than 2-A and 2-B, even though the aging was severer for the former membranes.

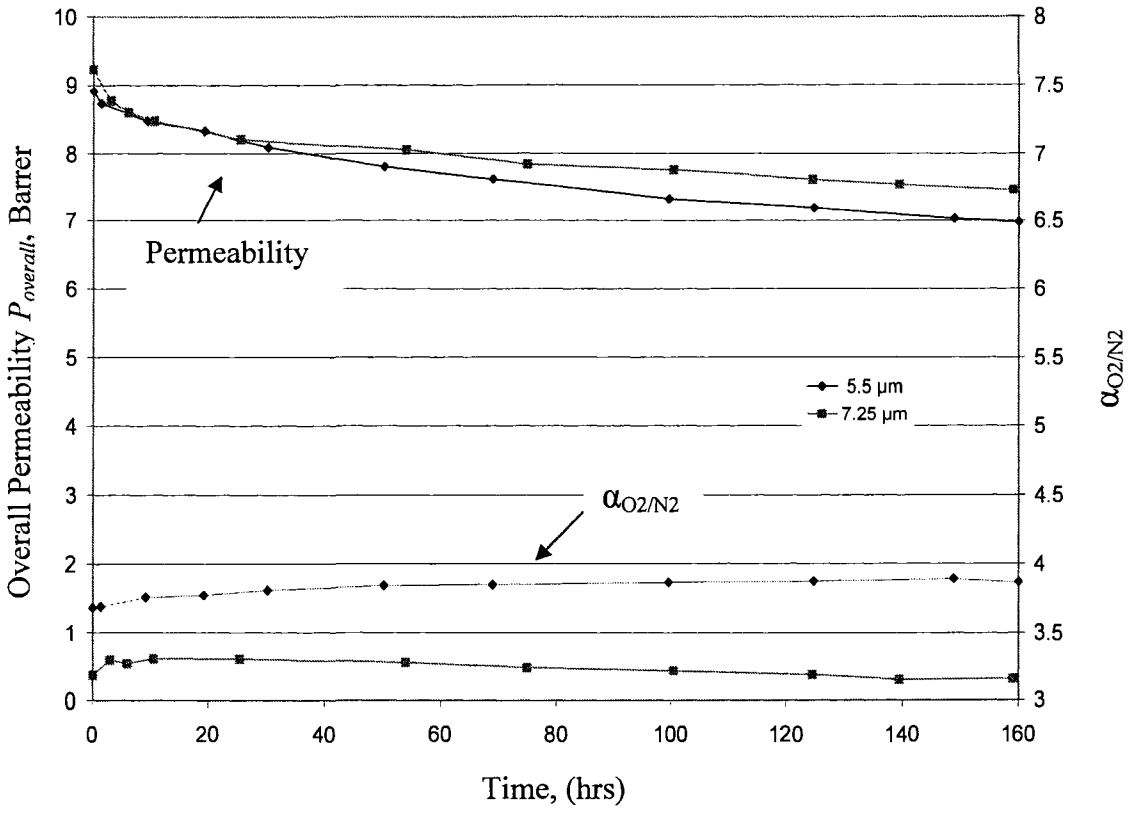

Figure 7.9 Changes in the overall permeability and permeability ratio, $\alpha_{O2/N2,}$ with time. Membrane thickness; 5.5 (5-A) and (5-B) 7.25 µm; membrane drying time, 6 hours; operating pressure, 25 psig; operational mode, continuous

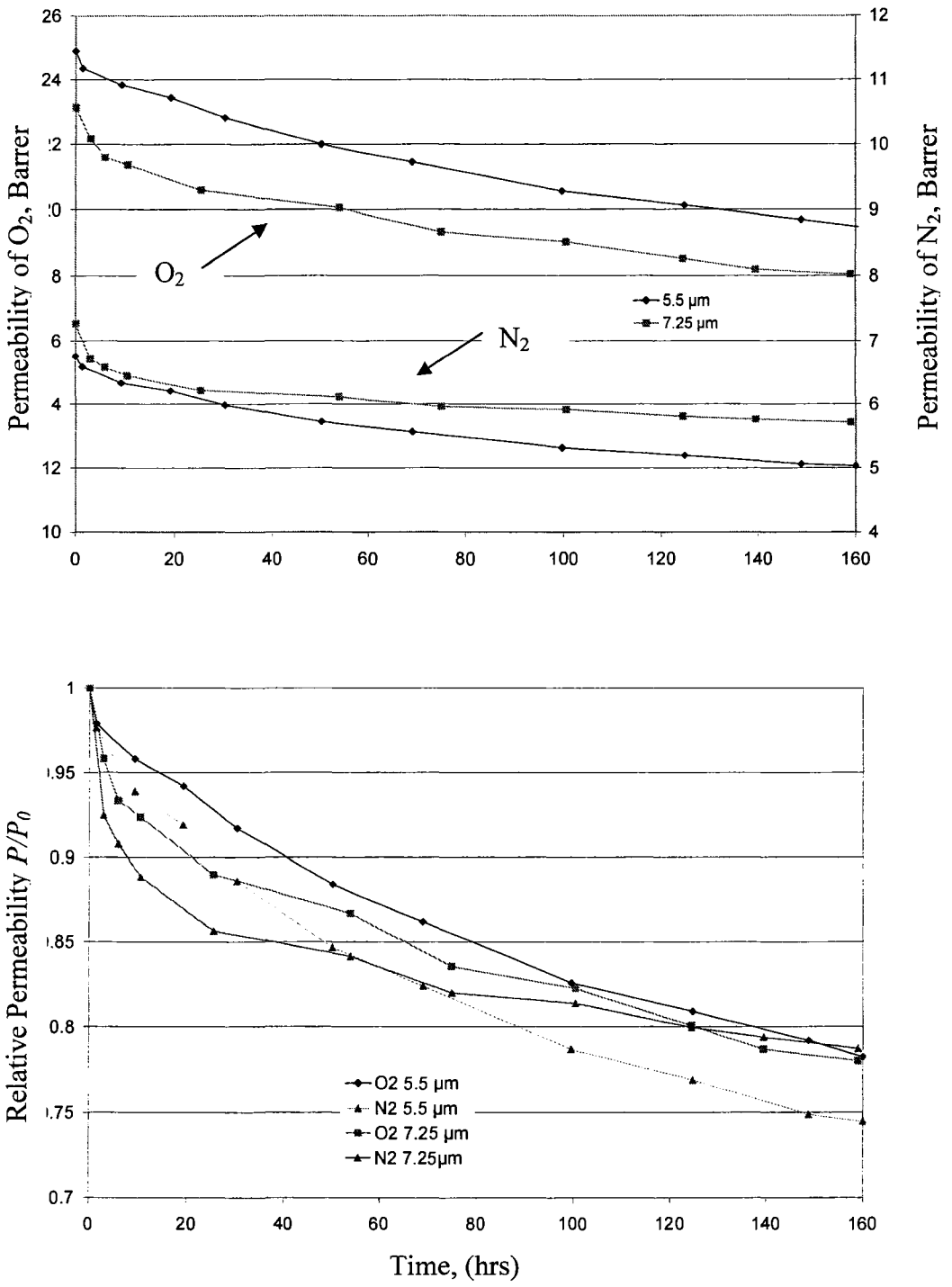

Figure 7.10 Time dependent changes of (a) the permeability of O_2 and N_2 (b) the relative permeability of O_2 and N_2. Membrane thickness, 5.5 (5-A) and 7.5 µm (5-B); membrane drying time, 6 hours; operating pressure, 25 psig; operational mode, continuous

7.4.2.2 Aging in 50 psig air pressure

In Fig. 7.11, overall permeability $P_{overall}$ and permeability ratio, $\alpha_{O2/N2}$, are plotted versus operational period for two experiments conducted with two membranes (6-A with a thickness 5.5μm and 6-B with a thickness 7.5μm). The drying time, after casting, in ambient air was 6 hours for both membranes. The air permeation experiments were conducted under the operating pressure of 50 psig in a continuous operational mode for 160 hours. The permeability ratio kept increasing for the thinner membrane (6-A), while it decreased for the thicker membrane (6-B) in the earlier stage. This behaviour has also been observed for the membranes 5-A and 5-B, when the membranes were subjected to the feed gas pressure of 25 psig (Fig. 7.9). In contrast to the data in Fig. 7.9, the selectivity of the thicker membrane (6-A) was slightly higher than 6-B at the start of the experiment. Further comparing Figs. 7.9 and 7.11, the overall permeability values in Fig. 7.11 are higher than in Fig. 7.9. Even after 160 hours of operation, permeabilities obtained at 50 psig (Fig. 7.11) were higher than those obtained at 25 psig (Fig. 7.9).

Figure 7.12a shows the individual permeability of O_2 and N_2 for these membranes. Figure 7.12b shows the relative permeability of individual gases versus the experiment time. It shows that more reduction in permeability occurred for 6-A than 6-B, particularly at the end of the run. The thinner membrane (6-A) started at lower permeability and selectivity than the thicker membrane (6-B). The difference in the selectivity is rather small. Similar to all previous observation, the reduction in the permeability of the thinner membrane is greater.

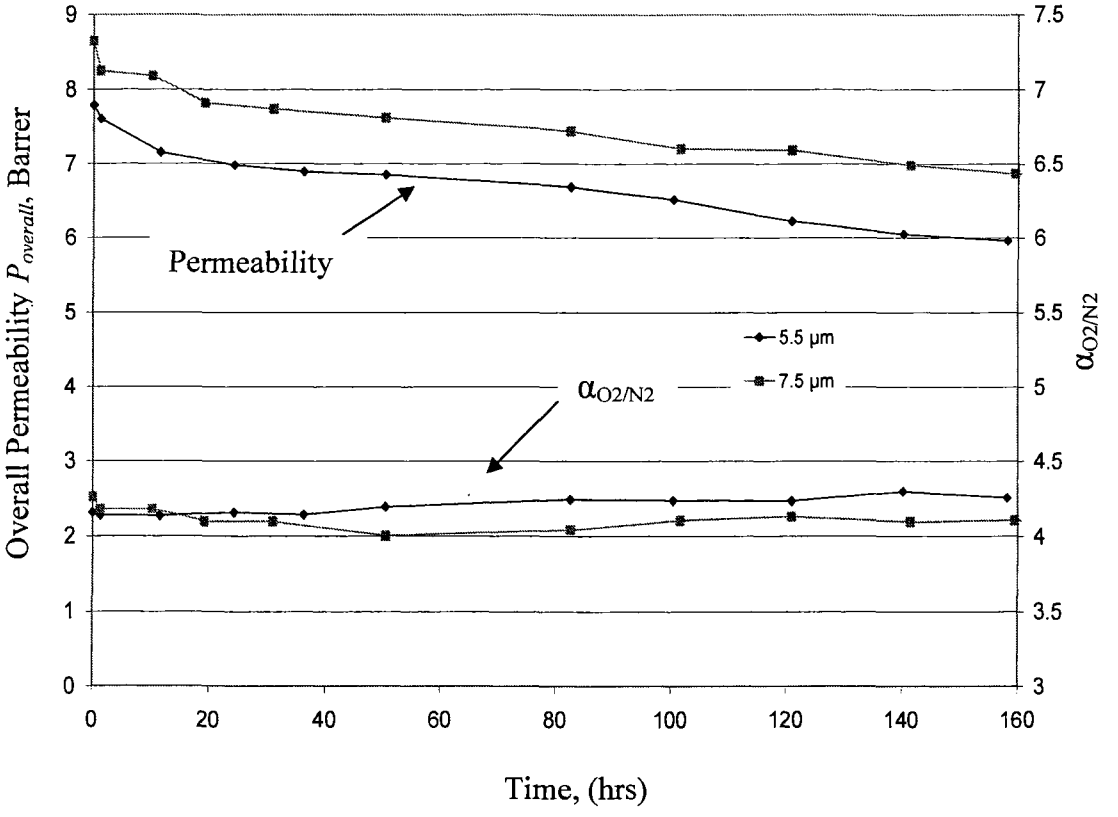

Figure 7.11 The changes in the overall permeability and permeability ratio, $\alpha_{O2/N2}$, with time. Membrane thickness, 5.5μm (6-A) and 7.5μm (6-B); drying time, 6 hours; operating pressure, 50 psig; operational mode, continuous

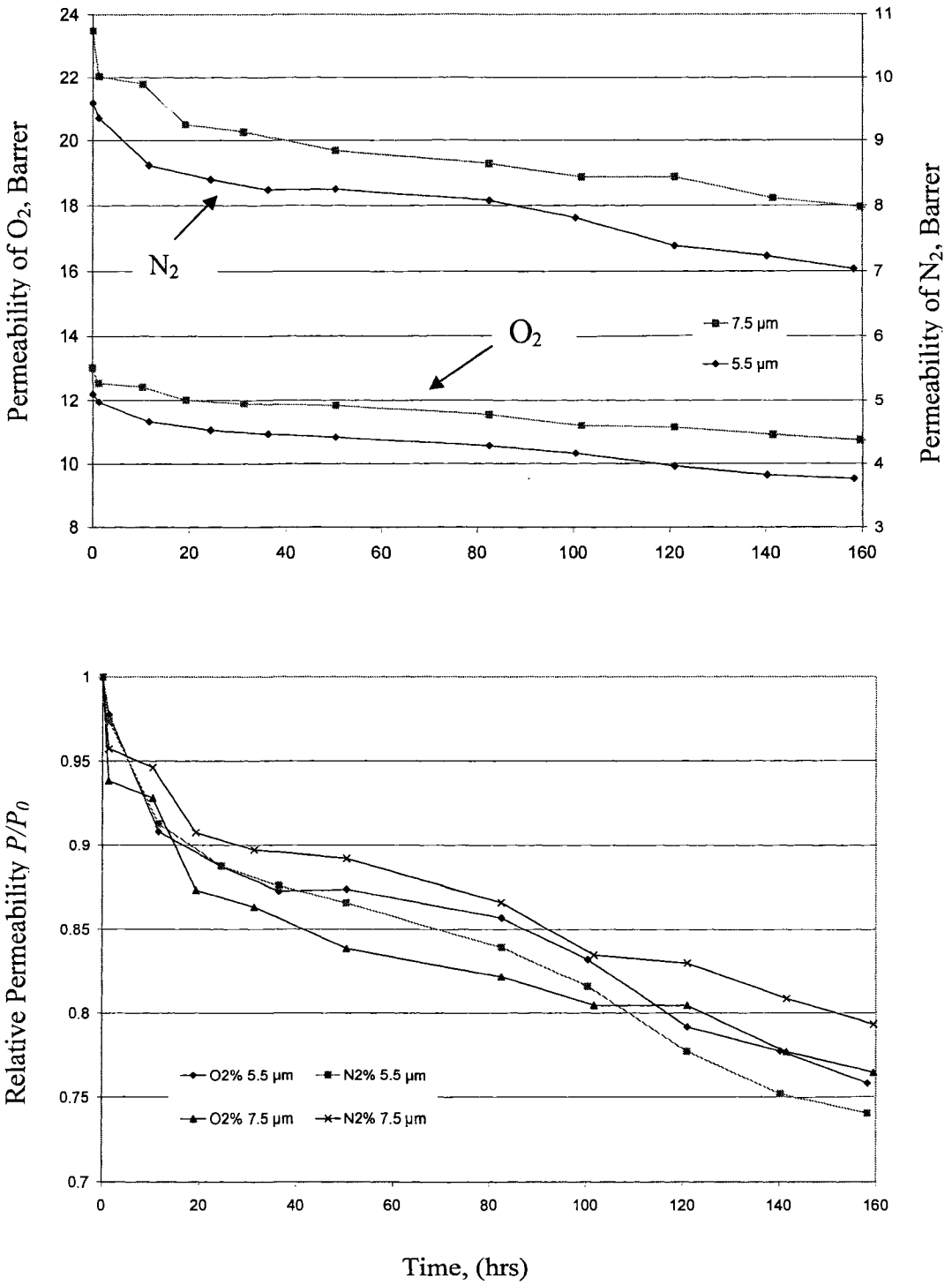

Figure 7.12 The time dependent changes of (a) the permeability of O_2 and N_2 (b) the relative permeability of O_2 and N_2. Membrane thickness, 5.5µm (6-A) and 7.5µm (6-B); drying time 6 hours, operational mode, continuous; Operating pressure, 50 psig

7.5 Discussion

In the above experiments, the effects of 1) operational mode (continuous or non-continuous) 2) membrane thickness 3) drying time (initial free volume) and 4) operating pressure on the aging were investigated. The effects of these 4 parameters are summarized in Table 7.2, together with the sets of supporting experimental data.

Table 7.2 Effect of operational mode, membrane thickness, drying time and operating pressure on the aging rate.

Parameters	**Effects**	**Supporting experimental data (Comparison of overall permeability)**
Operational mode	Aging is faster for non-continuous mode.	1-A(cont.) vs. 1-B(non-cont) (Fig. 7.1) 2-A and 2-B(cont.) vs. 2-C (non-cont)(Fig. 7.3)
Membrane thickness	Aging is faster for thinner membranes.	3-A and 3-B(3.7μm) (Fig. 7.5) vs. 4-A and 4-B(6.45μm)(Fig. 7.7) 5-A(5.5μm)vs. 5-B(7.25μm) (Fig. 7.9) 6-A(5.5μm) vs. 6-B(7.5μm) (Fig. 7.11)
Operating pressure[a]	Aging is faster at lower operating pressure.	5-A (5.5μm)(Fig. 7.9) vs. 6-A(5.5μm) (Fig. 11)
Drying time	Aging is faster for shorter drying time (larger initial free volume).	5-A (6 h)(Fig. 7.9) vs. 2-A and 2-B(16 h) (Fig. 7.3)

[a] This effect is not necessarily supported by comparison of 1-A vs. 3-A and 3-B

Although some data are simply confirmation of the phenomena observed in Chapter 6, Table 7.2 provides a more complete picture for the effects of the parameters on aging. The most interesting observation is, however, the change of selectivity (permeability ratio) in the aging process. As mentioned earlier the trade-off effect, i.e. selectivity increase with a decrease in permeability or vice versa, is generally accepted, except for few experimental data that have appeared in the literature. There are, however, many experimental data that are contradictory to the trade-off effect, as shown in Figs. 7.1 to 7.12. Table 7.3 summarizes the change in the permeability ratio in the aging process.

Table 7.3 Change in permeability ratio in the aging process

Change in permeability ratio	**Supporting data**
Continuous decrease in selectivity (Anti-trade-off effect)	1-B(non-cont) (Fig. 7.1), 2-C(non-cont) (Fig. 7.3), 3-A and 3-B (Fig. 7.5)
No significant change in selectivity throughout the aging process	2-A and 2-B(cont) (Fig. 7.3) 4-A and 4-B (Fig. 7.7)

*1-A(cont)(Fig. 7.1) does not belong to any category.

The above table shows that 4 cases showed no significant change in permeability ratio and 4 cases, including 1-B, 2-C and 3-A and 3-B showed a clear anti-trade-off effect, i.e. the permeability ratio kept decreasing throughout the aging process. Note that the first 4 membranes have lost the overall permeability only little, in other words, their aging effect was only marginal. Membranes dried for 6 hours showed a mixture of increase and decrease of permeability ratio throughout the experiment period.

The conventional explanation of the trade-off effect is as follows. As aging progresses, the inter-segmental distance in the polymer matrix decreases, rendering the macromolecular segments stiffer. The narrower inter-segmental space and less segmental motion both contribute to enhancement of the sieving effect. Larger molecules (in this work nitrogen) are separated from the smaller molecules (in this work oxygen) more effectively. At the same time, the gas permeation slows down as the inter-segmental space through which gas molecules diffuse becomes narrower. This mechanism explains the trade-off effect, but, obviously, can not explain the anti-trade-off effect observed in this work.

A novel concept is presented here to explain the anti-trade-off effect. According to the dual mode sorption theory given in Section 2.1.1 the gas sorption occurs at two sites, one at the Henry site and the other the Langmuir site. While the former site is present in the inter-segmental space in the continuous polymer matrix, the latter arises from the presence of the excess free volume, distributed as small holes in the polymer matrix. Gas molecules are often trapped in these holes and can leave the holes only by diffusion through the polymer matrix that surrounds the holes. The gas transport mechanism through the polymer matrix presented above to explain the trade-off effect is obviously applicable for the Henry site. However, we also have to consider the Langmuir site gas transport. When the total volume of the holes is larger, in other words excessive free volume is larger, so is the amount of gas molecules trapped in these holes; i.e. more gas molecules are sorbed in the polymer. This contributes to the increase in solubility, S, and consequently to permeability, P, according to the sorption-diffusion model. As aging progresses, the volume of the holes becomes smaller, lowering the solubility, S. Thus, the

permeability, P, should decrease. Hence, decrease in permeability with aging is predicted both by the Henry site and by the Langmuir site transport mechanism, which is quite natural. For the selectivity, the story might be different. It is reasonable to assume that more O_2 molecules are sorbed at the Langmuir site than N_2 molecules due to O_2's stronger affinity to the membrane polymer. Therefore, the O_2 sorption is affected more than N_2 sorption when the hole is squeezed. The permeability of O_2 molecules will be reduced much faster than N_2 permeability, leading to the decrease in the permeability ratio, $\alpha_{O2/N2}$. In other words, the Henry site transport and the Langmuir site transport will have opposite effects on the permeability ratio, as the aging progresses. These two effects are super-imposed. Depending on which effect is more dominant and at which stage of aging, the permeability ratio may increase, decrease, remain constant, show a maximum or show a minimum.

Let us now consider the cases, 1-B, 2-C, 3-A and 3B where the continuous decrease in permeability ratio, i.e. anti-trade-off effect was observed. According to the above discussion, these were the cases where the Langmuir site transport was dominant. Looking into the permeability data of individual gases in Figs. 7.2, 7.4 and 7.6, the oxygen permeability of 1-B, 2-C and 3-A decreases much faster than the nitrogen permeability, which is exactly expected to happen when the volume of the Langmuir holes gradually decreases during the aging process.

It should also be noted that the effects of various parameters on the overall permeability summarised in Table 7.2 also can be explained by the proposed transport mechanism. At present, however, focus is placed more on the selectivity change.

7.6 Conclusion

The effects of various parameters on aging are as follows. The aging is facilitated,

1) when the feed gas pressure is released,
2) when the membrane is thinner
3) when a low operating pressure is applied, and
4) when the membrane is dried for a shorter period.

These observed effects are confirmation of the observation made in chapter 6.

Contrary to the trade-off effect, the selectivity of the membrane decreased with a decrease in permeation rate during the aging process in many experiments. This observation as well as the effects of the various parameters on the permeation rate, mentioned above, can be explained by a novel dual gas transport model, one through the Henry site and the other through the Langmuir site. In particular, the Langmuir site occupied primarily by oxygen molecules plays a crucial role in the change of gas permeability and selectivity with aging.

CHAPTER 8

Summary of the Results and Recommendations

8.1 Summary of the Results

The general objective of this work was to understand the molecular mechanism of gas transport and physical aging in glassy polymers. The specific objective of this research was to investigate the effect of feed gas pressure on the permselective properties and the physical aging of PPO membranes. The gas-polymer system chosen to accomplish this objective was Air-PPO. A sweep-gas constant pressure system was built and used to carry out the gas permeation and separation experiments.

To begin with, the effect of feed gas pressure on the permselective properties of PPO membranes was studied under three pressures; 25, 50 and 100 psig. To investigate the effect of membrane morphology, membranes with different thicknesses were used in this study. Before they were subjected to the permeation experiments, the used membranes were stabilized. Stabilization was necessary to prevent any intervention from time dependent changes that might take place during the experiments under feed gas pressure. To confirm that the membranes were stabilized in a similar fashion, the stabilization process was carried in two different environments, one at the elevated temperature and the other at the elevated gas pressure.

The trends in the gas permeability were different for oxygen and nitrogen.. The response of the permeability to the pressure did not follow the solution diffusion model, according to which no pressure effect is expected. These novel observations were interpreted in thermodynamic terms and related to the change in enthalpy and entropy of the gases in the void volume. The performance of these membranes also depended on the membrane thickness, which was ascribed to the change of membrane morphology with thickness. The density of PPO membranes decreases from the top side to the bottom side of the membrane, causing the formation of asymmetric structure in the direction of gas permeation.

Realizing the fact that membrane morphology could suffer from some irregularities, the next step taken was to investigate the effect of these irregularities on physical aging process. Membranes with different thicknesses were thermally aged in vacuum after being prepared by the same method. The effects of pinholes and membrane asymmetry were investigated. It was found that the presence of pinholes would disturb

any physical aging observations by an increasing tendency of the permeability with time. On the other hand, observation of the aging of thick asymmetric membranes could be mistaken as support layer pressurization.

In the next step, the relative permeation rate of air was used to compare the effect of different experimental routines on the aging of PPO membranes with different thicknesses. In addition to the constant pressure system, a constant volume system was used to investigate the effect of vacuum on the aging process. A novel approach was adopted to close the gap between gas permeability and dynamic observations for physical aging. The response of the permeability with time was explained in accordance to the resemblance between the decay of permeability with time and the relaxation process of visco-elastic materials.

In this approach, viscosity is considered as a resistance to the elasticity (segment movement) which is the driving force to the relaxation process. The presence of gas molecules increases the viscosity of the gas-polymer mixture and decreases the elasticity of the polymer segments, causing slower aging process. Two different routines were used to investigate the effect of vacuum on the aging. It was found that membranes exposed to vacuum for a longer time aged faster. These results also support the observation that thinner membranes age faster than thicker membranes.

The last step to study the effect of gas pressure on the physical aging was to observe the changes in the permselective properties of PPO membranes. The trade-off relationship is usually considered to occur during the aging process, i.e. permselectivity increases as aging proceeds. A decrease in the free volume is expected to cause a

decrease in the permeability and an increase in the permselectivity. However, many of our experiments resulted in contrary observations, i.e. the permselectivity decreased as aging proceeded. These new observations were made possible by using air, the mixture of oxygen and nitrogen, instead of single gasses for the permeation and separation experiments.

This observation was explained by the following two factors: 1) the larger size of nitrogen than oxygen molecule 2) the higher affinity of oxygen to the polymeric material than nitrogen molecule.

The selectivity of oxygen (small molecule) over nitrogen (large molecule) is enhanced as the aging proceeds by the decrease in the distance between the macromolecular segments that constitute the Henry site of gas sorption. On the other hand, oxygen molecules occupy the hole-like Langmuir site more than nitrogen molecules due to the stronger affinity of oxygen to the polymer. As the hole size shrinks during the aging, the amount of oxygen in the Langmuir site decreases, leading to the decrease in oxygen permeability and also the decrease in the selectivity of oxygen over nitrogen. The latter mechanism can explain the anti-trade-off effect.

8.2 Recommendations

This work could successfully answer some questions concerning the effect of gas pressure, membrane thickness etc. on aging. More research is however needed to generalize the conclusions obtained by this research. Some of the recommendations to help in reaching this goal are:

1- The conclusions obtained in this work should be examined by other gas-polymer systems.

2- To investigate the effect of vacuum more in details, permeation and separation experiments with gas mixtures should be conducted using a constant volume system

3- Membranes of different free volumes and free volume distributions should be prepared under different conditions, e.g. changing the solvent to prepare the polymer dope, changing the solvent evaporation rate etc. The conclusions obtained by the present work should be examined by conducting the gas permeation and separation experiments using those newly prepared membranes.

References:

Acharya, M., Foley, H.C.; Transport in nanoporous carbon membranes: experiments and analysis; *A.I.Ch.E J.*, **46**, 911-921 (2000).

Aguilar-Vega, M., Paul, D. R.; Gas transport properties of polyphenylene ethers; *J. Polymer. Sci.:Part B: Polymer physics,* **31,** 1577-1589 (1993).

Alfrey, T., Goldfinger, G., Mark, H.; The apparent second-order transition point of polystyrene; *J. Appl. Phys.,* **14**, 700-705 (1943).

Alntiev, A., Drioli E., Gokzhaev, M., Golemme, Illinich, O., Lapkin, A., Volkov, V., Yampolskii, Yu.; Gas permeation properties of phenylene oxide polymers; *J. Membr. Sci.,* **138**, 99-107, (1998).

Andrews, R.D.; Transition phenomena and solid state structure in glassy polymers; *J. Polymer. Sci.:Part C.,* **14,** 261-265 (1966).

Balik, C.M., Said, M.A.; Residual porosity and relaxation in polymeric latex films studied by CO_2 diffusion; *Mat. Res. Soc. Symp. Proc.,* **215**, 199-204 (1991).

Bondi, A.; Physical properties of molecular crystals, liquids, and glasses, Wiley, New York, 1968.

Callister Jr, W.D.; Material science and engineering: An introduction; John Wiley and son. Inc. New York; (1997).

Capitani, D., Clericuzio, M., Fiordiponti, P.,Lillo, F., Segre, A.L.; Oxygenadsorption on poly (2'6-dimethyl) phenyleneoxide. A solid state H-NMR study; *Eur. Polym. J.*, **29**, 1451-1456 (1993).

Chang Geng-Wen, Jamieson, A. M., Zhibin YU, McGervey, J. D.; Physical Aging in the Mechanical Properties of Miscible Polymer Blends; *J. Appl. Polym. Sci.,* **63,** 483–496 (1997).

Chartoff, R.P. In Thermal characterization of polymeric materials, Turi, E.A., Ed.; Academic Press: New York, p 548-573 (1997).

Coady, A.B., and Davis, J.A.; CO2 recovery by gas permeation; *Chem. Eng. Prog.,* **78,** 45 (1982)

Chow, T.S.; Molecular kinetic theory of the glass transition; *Polym. Eng. Sci.,* **24** (14) 1079-1085 (1984).

Chung, T., Teoh, S. K.; The aging phenomenon of polyethersulphone hollow fiber membranes for gas separation and their characteristics, *J. Memb. Sci.*, **152**, 175-188 (1999).

Costa, G., Iurilli, C., Cavazza, B., Turturro, A; Physical aging phenomena in poly(*tert*-butylacetylene) solvent cast films: Influence of operating conditions; *ACS Symposium,* **733**, 85-94 (1999).

Curro, J.G., Lagasse, R. R., Simha, R; Use of a theoretical equation of state to interpret time-dependent free volume in polymer glasses; *J. Appl. Phys.,* **52**, 10, 5892-5897 (1981).

Curro, J. G, Lagasse, R. R., Simha, R.; Diffusion model for volume recovery in glasses; *Macromolecules,* **15,** 1621-1626 (1982).

Deng, Q., Jean, Y.C.; Free volume distribution in an epoxy polymer probed be positron annihilation: Pressure dependence; *Macromolecules,* **26**, 30-34 (1993).

DiBenedetto, A. T., Paul' D. R.; Diffusion in Amorphous Polymers; *J. Polymer Sci.: Part C.,* **10**, 17 (1965).

Dietz, W. A.; Response Factors for Gas Chromatographic Analyses; *J. Gas Chromatography, 5, 68-71* (1967)

Dolittle, A.; Studies in Newtonian flow. II. The dependence of viscosity of liquids on free space; *J. Appl. Phys.,* **22**(12), 1471-1475 (1951).

Dorkenoo, K.D., and Pfromm, P.H.; Experimental evidence and theoretical analysis of physical aging in thin and thick amorphous glassy polymer films; *J. Polym. Sci.:Part B: Polym. Phy.* **37,** 2239-2251 (1999).

Dorkenoo, K.D., and Pfromm, P.H.; Accelarated aging in thin poly[1-(trimethylslilyl)-1-propyne] films; *Macromolecules.* **33,** 3747-3751 (2000).

Fang., S. M., Stern, S. A., Frisch, H. L.; A "Free Volume" Model of Permeation of Gas and Liquid Mixtures through Polymeric Membranes, *Chemical Engineering Series,* **30**, 773 (1975).

Felder, R. M., Huvard, G. S.; Permeation, Diffusion, and Sorption of Gases and Vapors, *Methods of Experimental Physics,* 16c, Chapter 17, Academic Press, NY (1980).

Hay, A.S.; "High performance polymers: Their origin and development" in proceeding of the symposium on the history of high performance polymers at American Chemical Society Meeting, Elsvier, New York NY, 1986.

Hiarai, N., Eyring, H.; Bulk viscosity of liquids; *J. Appl. Phy.*, **29**(5), 810-816 (1958).

Hodge, I.M.; Physical aging in glassy polymer glasses; *Science*, **267**, 1945-1947 (1995).

Huang, Y., Paul, D. R.; Physical aging of thin glassy polymer films monitored by gas permeability; *Polymers*, **45**, 8377-8393 (2004).

Huang, Y., Paul, D. R.; Effect of Temperature on Physical Aging of Thin Glassy Polymer Films; *Macromolecules*, **38**, 10148-10154 (2005).

Hutchinson, M.J.; Physical aging of polymers; *Prog. Sci.*, **20,** 703-760 (1995).

Hutchinson, M. J., Kovacs, A. J.; A simple phenomenological approach to the thermal behavior of glasses during uniform heating or cooling; *Polym. Sci. Eng.*, **14,** 1575-1590 (1976).

Hutchinson, M. J., Kovacs, A. J.; Effect of thermal history on structural recovery of glasses during isobaric heating; *Polym. Sci. Eng.*, **24**(14), 1087-1103 (1984).

Ilinitch, O. M., Fenelonov, V.B., Lapkin, A.A., Okkel, L.G., Terskikh, V. V., Zamaraev, K.I.; Intrinsic microporosity and gas transport in polyphenylene oxide polymers; *Microporous and Mesoporous materials,* **31**, 97 (1999).

Kamiyu, Y., Hirose, T., Mizoguchi, K., Terada K.; Sorptive Dilation of Poly(vinylbenzoate) and Poly(vinyl butyral) by Carbon Dioxide, *J. Polymer Sci:Part B: Polymer Physics,* **26**, 1409 (1988).

Kapure, S., Rogers, C. E.; Gas transport properties of glassy polymers; *J. Polym. Sci:Part B: Polymer Physics,* **10**, 2107 (1972).

Kauzmann, W.; Nature of the glassy state; *Chem. Rev.*, **43,** 219-256 (1948).

Kawakami, H., Mikawa, M., Nagaoka, S.; Gas transport properties of asymmetric polyimide membrane with an ultrathin surface skin layer; *Macromolecules*, **31**, 6636-6638 (1998).

Kesting, R. E., Fritzsche, A. K.; Polymeric Gas Separation Membranes, John Wiley & Sons, Inc.,1993.

Kim, J. H., Jang, J., Lee, D., Zin, W.; Thickness and Composition Dependence of the Glass Transition Temperature in Thin Homogeneous Polymer Blend Films; *Macromolecules*, **35**, 311-313 (2002).

Koros, W. J. and Fleming, G. K.; Membrane-based Gas Separation; *J. Memb. Sci,* **83**, 1-80, (1993)

Koros, W. J. Chern, R. T.; Separation of Gaseous Mixtures using Polymer Membranes; *Handbook of Separation Process Technology,* edit. R. W. Rousseau, (1987).

Kruczek, B., Matsuura, T.; Limitations of a constant pressure type testing system in determination of gas transport properties of hydrophilic films; *J. Memb. Sci.*, **177**, 129-142 (2000).

Khulbe, K.C., Matsuura, T., Noh, S.H.; Effect of thickness of the PPO membranes on the surface morphology; *J. Memb. Sci.*, **146**, 243-251 (1998).

Lee, W. M.; Selection of Barrier Materials from Molecular Structure, *Poly. Eng. and Scie,* **20**(1), 65 (1980).

Lin, W., Chung, T.; The physical aging phenomenon of 6FDA-durene polyimide hollow fiber membranes; *J. Memb. Sci.,* **38**, 765-775 (2000).

McCaig, M.S., Paul, D.R.; Effect of UV crosslinking and physical aging on the gas permeability of thin polyaryalat films; *Polymer,* **40,** 7209-7225 (1999).

McCaig, M.S., Paul, D.R.; Effect of film thickness on the change in gas permeability of a glassy polyarylate due to physical aging: part I. Experimental observations; *Polymer,* **41,** 629-637 (2000).

McCaig, M.S., Paul, D.R., Barlow, J.W.; Effect of film thickness on the change in gas permeability of a glassy polyarylate due to physical aging: part II. Mathematical model; *Polymer,* **41,** 639-648 (2000).

G. B. McKenna, Y. Leterrier, C. R. Schultheisz,; The evolution of material properties during physical agibg; *Polym. Eng. Sci.*, **35**, 403 (1995).

Morisato, A., He, Z., and Pinnau, I.; Mixed-gas properties and physical aging of poly(4-methyl-2-pemtyne); *ACS Symposium,* **733**, 56-67 (1999).

Nagai, K., Freeman, B.D., Hill, A.J.; Effect of physical aging of poly(1-trimethylsilyl-1-propyne) films synthesized with $TaCl_5$ and $NbCl_5$ on gas permeability, fractional free volume, and positron annihilation lifetime spectroscopy parameters; ; *J. Polym. Sci.:Part B: Polym. Phy.* **38,** 1222-1239 (2000).

Nagai, K., Higuchi, A., and Nakagawa, T.; Gas permeability and solubility of poly(1-trimethylsilyl-1-propyne-*co*-phynyl-1-propyne) membranes; *J. Polym. Sci.:Part B: Polym. Phy.* **33,** 289-298 (1995).

Nagai, K., Watanabe, T., and Nakagawa, T.; Effects of aging on molecular motion of poly(1-trimethylsilyl-1-propyne) membranes synthesized using various catalysts; *Polymer. J.,* **28**(10) 933-935 (1996).

O'reilly, J.M., Physical aging and enthalpy relaxation of amorphous polyesters; *J. Polym. Sci.:Part B: Polym. Phy.*, **38** 495-499 (2000).

Park, J.Y., and Paul, D.R.; Correlation and prediction of gas permeability in glassy polymer membrane materials via a modified free volume based group contribution method; *J. Memb. Sci.*, **125**, 23-39 (1997).

Paul, D. R., and Koros, W. J.; Design considerations for Measurement for Gas Sorption in Polymers by Pressure Decay; *J. Poly. Sci: Poly. Phy. Ed.*, **14**, 1903 (1976).

Percec, S., Li, G.; Chemical modification of poly(2,6-dimethyl-1,4-phenylene oxide) and properties of resulting polymers; *ACS Symposium Series*, vol. 364, American Chemical Society, Washington, DC, 1988.

Petropoulos, J. H.; Quantitative Analysis of Gaseous Diffusion in Glassy Polymers, *J. Poly. Sci.: Part A-2*: **8**, 1797 (1970).

Perera, D.Y., Schtyser, P., de Lame, C., Eynde, V.; Film formation and physical aging in organic coatings; *ACS Symposium,* **733**, 210-221 (1999).

Persson, K.M., Gekas, V., Tragardh, G.; Study of membrane compaction and its influence on ultrafiltration water permeability; *J. Memb. Sci.* **100,** 155-162 (1995).

Pfromm, P.H., and Koros, W.J.;Accelarated physical aging of thin glassy polymer films: evidence from gas transport measurements; *Polymer,* **36**, 2379-2387 (1995).

Pinnau, I.; Cassilas, C. G.; Morisato, A.; Freeman. B. D. Long-term permeation properties of poly(1-trimethylsilyl-1-propyne) membranes in hydrocarbon—vapor environment. *J. Polym. Sci.: Part B: Polym. Phys.*, ***35***, 1483-1490 (1997).

Polotskaya, G. A. S. A. Agranova, T. A. Antonova, G. K. Elyashevich; Gas Transport and Structural Features of Sulfonated Poly (phenylene oxide); *J. Polym. Sci.* **66,** 1439-1443(1997).

Prasada, R., and Shaner; "Comparison of gas separation technology" in polymer gas separation membranes, Paul, D. R.; Yampol'skii, Yu, CRC Press, London 1994.

Ramos, A. R., Kovacs, A.J., O'Reilly, J.M., Greener, J.; Effect of combined pressure and temperature changes on structural recovery of glass-forming materials: 1extension of KAHR model; *J. Appl. Polym. Sci.* **26**, 501-513 (1988).

Rezac, M.E., Pfromm, P.H. Costello, L.M. Koros, W.J.; Ageing of thin polyimide-ceramic and polycarbonate-ceramic composite membranes; *Ind. Eng. Chem. Res.* **32** 1921 (1993).

Robertson, R.E.; Effect of free volume fluctuation on polymer relaxation in the glassy state: II. Calculated results; *J. Polym. Sci.:Polym. Phy.*, **17,** 597-613 (1979).

Robertson, C.G., Wilkes, G.L.; Physical aging behavior of miscible blends containing atactic polystyrene and poly(2,6-dimethyl-1,4-phenylene oxide); Polymer, **41** 9191–9204 (2000).

Robeson, L. M.; Correlation of Separation Factor versus Permeability forPolymeric Membranes, *J. Memb. Sci.,* **62**, 165 (1991).

Robeson, L.M., Smith, C.D., Langsam, M.; A group contribution approach to predict permeability and permselectivity of aromatic polymers; *J. Memb. Sci.*, **132**, 33-54 (1997).

Ruden, Alfred "The Elements of Polymer Science and Engineering" 2nd Ed, Academic Press, San Diego (1999).

Simha, R., Curro, J.G., Robertson, R.E.; Molecular dynamics of aging in the glassy state; *Polym. Eng. Sci.,* **24**(14) 1071-1078 (1984).

Sperling, L. H.; "Introduction to physical polymer science" 3rd ed.; Wiley-interscience; New York; (2001).

Stern, S. A.; Polymers for Gas Separations: the Next Decade, *J. Memb. Sci.*, **94**, 1 (1994).

Struik, L.C.E.; Physical aging in amorphous polymers and other materials; Elsevier scientific publishing company:New York; (1978).

Tabe, M.A.; Matsuura, T.; Sourirajan, S. Design and construction of gas permeation system for the measurement of low permeation rates and permeate compositions; *J. Memb. Sci.*, **98,** 281-286 (1995).

Takada, K., Matsuya, H., Masuda, T., Higashimura, T.; Gas permeability of polyacetylenes carrying substituents; *J. Polym. Sci.,* **30**, 1605-1616 (1985).

Tiemblo, P., Guzman, J., Riande, E., Mijangos, C., Reinecke, H.; Effect of physical aging on the gas transport properties of PVC and PVC modified with pyridine groups; *Polymer*, **42,** 4817-4823 (2001).

Toi, Keio; Diffusion and sorption of gases in poly(ethylene Terephtalate); *J. Poly. Sci.: Poly. Phy. Ed.,* **11**, 1829-1839 (1973).

Toi, K., Morel, G., Paul, D.R.; Gas sorption and transport in poly (phenylene oxide) and comparison with other glassy polymers; *J. Polym. Sci.* **27,** 2997 (1982).

Tribone, J.J., and O'reilly, J.M.; Pressure-jump volume-relaxation studies of polystyrene in the glass transition region; *J. Polym. Sci. Part B:Polym. Phy.,* **27,** 837-857 (1989).

Van Krevelen, D. W.; Properties of Polymers, Their correlation with chemical structure; their numerical estimation and prediction from additive group contributions, Third Ed, Elsevier, NY, 1990.
Vieth, W.R., Sladek, K.J.; A model for diffusion in glassy polymers; *J. Coll. Sci.*, **20**, 1014 (1965).

Vieth, W. R., Howell J. M., Hsieh, J. H.; Dual Sorption Theory: Review Paper; *J. Membr. Sci.*, **1**, 177 (1976).

Vrentas, J.S., Duda, J.L.; Diffusion of small molecules in amorphous polymers; *Macromolecule*, **9**(5), 785-790 (1976).

Vrentas, J.S., Duda, J.L.; Diffusion in polymer-solvent systems. I. Reexamination of the free volume theory; *J. Polym. Sci.*, **15**, 403-416 (1977).

Yampol'skii, P.Y., Shishatskii, S.M., Shantorovich, V.P., Antipov, E.M., Kuzmin, N.N., Pykov, S.V., Khdjaeva, V.L., Plate, N.A; Transport characteristics and other physiochemical properties of aged poly(1-trimethylsilyl-1-propyne); *J. Appl. Polym. Sci.* **48**, 1935-1944 (1993).

Yang, A. C. M., Wang, R. C., Lin, J. H.; Ductile-brittle transition induced by aging in poly(phenylene oxide) thin films; *Polymer*, **37**, 5751-5754 (1996).